Chapter 4
Organic Porous Polymer Materials: Design, Preparation, and Applications

Liangxiao Tan, Kewei Wang, Qingyin Li, Yuwan Yang, Yunfei Liu and Bien Tan

Abstract The synthesis of porous organic polymer materials with nanoscale range has long been an important science subject and received an increasing level of research interest owing to their essential properties merging both of the porous materials and polymers such as low skeleton density, processability, easy functionality, and diverse synthetic methods. In this chapter, several porous polymer materials including covalent organic frameworks (COFs), hypercrosslinked polymers (HCPs), conjugated microporous polymers (CMPs), polymers of intrinsic microporosity (PIMs), and macroporous polymers from high internal phase emulsions (HIPEs) will be introduced as well as their diversiform synthetic methods and potential applications including gas storage, carbon capture, separation, catalysis, sensing, energy storage and conversion.

4.1 Introduction

Design, construction, and utilization of advanced functional materials with special porous architectures in micro- and nanoscale range have long been an important science subject. Porous polymers especially have attracted a large amount of research attention owing to their unique characteristics that combine both porous materials and polymers [1]. First of all, porous polymers are able to be designed and prepared with high surface area and well-controlled pore structure [2–4]. Secondly, porous polymers are processable due to their polymer chain essence. For instance, they can be easily synthesized with various micromorphology such as hollow nanosphere [5–7], thin film [8–10], and monolithic form [11–15]. Some kinds of porous polymers may even be dissolved in common organic solvents for further solvent-based process technology, however, without losing their porosity [16–18].

L. Tan · K. Wang · Q. Li · Y. Yang · Y. Liu · B. Tan (✉)
School of Chemistry and Chemical Engineering, Huazhong University of Science and Technology, Wuhan 430074, China
e-mail: bien.tan@mail.hust.edu.cn

Z. Lin et al. (eds.), *Polymer-Engineered Nanostructures for Advanced Energy Applications*, Engineering Materials and Processes,
DOI 10.1007/978-3-319-57003-7_4

Furthermore, a wide range of optional organic building blocks as well as multitudinous synthesis methods enable the resulting porous polymers facile to incorporate multiple chemical functionalities within networks or pore surface which is far different from inorganic porous materials such as zeolite, carbon, and silica [4, 19–22]. Besides, porous polymer frameworks are composed of light elements which provide a weight advantage in many applications.

For the porous polymers, surface area and pore size are the two most important factors that affect their performance. According to the IUPAC recommendation, pores can be divided into the following three species: micropores with pore size less than 2 nm; mesopores with pore size between 2 and 50 nm; and macropores with pore size larger than 50 nm [23]. Usually, smaller pore size contributes larger adsorption amount of sorbate molecules at lower pressures which results in a higher surface area [24]. To introduce micropore into the polymer matrix, rigid aromatic building blocks are necessary to be adopted directly linking together or by other rigid groups such as alkynes [25] or alkenes [26] in order to construct a fixed rigid structure which prevent the polymer chains from collapsing. After the removal of solvent, the space that solvent filled previously will be permanent pore [27].

According to the synthetic methods and the chemical structure, microporous organic polymers (MOPs) can be roughly classified as covalent organic frameworks (COFs) [3, 28], hypercrosslinked polymers (HCPs) [29, 30], conjugated microporous polymers (CMPs) [31, 32], polymers of intrinsic microporosity (PIMs) [33, 34], covalent triazine-based frameworks (CTFs) [35, 36], porous aromatic frameworks (PAFs) [2, 37], and so on. Among them, COFs are a class of crystalline networks with well-ordered structures and uniform pore size that related to their monomers. COFs are usually formed via reversible bond-forming chemistry such as boronic acids' self-condensation or with diols to form bromine rings by which the most thermodynamically stable structure can exist [27].

Some other polymers possess rather amorphous networks with disordered structure and normally a wider pore size range [38]. Amorphous networks always require metal-catalyzed high-yielding reactions to achieve entire condensation as possible. For example, Lewis acid catalytic Friedel–Crafts alkylation reaction is usually for HCPs synthesis [29], and CMPs are prepared by noble metal catalytic Sonographer–Ghaghara coupling, Yamamoto coupling, Suzuki coupling reactions, and so on [32].

In this chapter, we mainly discuss the following microporous organic polymers including covalent organic frameworks, hypercrosslinked polymers, conjugated microporous polymers and polymers of intrinsic microporosity as well as some macroporous polymers based on polymerization of high internal phase emulsions (polyHIPEs). Not only the design and synthetic strategies, but also the potential applications of these porous polymers will be introduced in detail including gas storage, carbon capture, separation, catalysis, sensing, energy storage, and conversion.

4.2 Covalent Organic Frameworks

Covalent organic frameworks are a new class of porous covalent crystalline organic networks based on dynamic covalent chemistry which leads to the process of forming, broking, and reforming covalent bonds [39]. Generally, linking organic molecules by covalent bonds into extended networks typically generates amorphous, disordered solid materials. The ability to develop strategies for obtaining crystals of such solids is of interest because it opens the way for precise control of the geometry and functionality of the extended structure, and the stereochemical orientation of its constituents. The attainment of crystals is done by several techniques in which a balance is struck between the thermodynamic reversibility of the linking reactions and their kinetics. This success has led to the expansion of COFs including organic units linked by these strong covalent bonds: B–O, C–N, B–N, and B–O–Si. Compared to the amorphous porous organic polymers (PIMs, CMPs, and HCPs), COFs have permanent geometry, and it is possible to predict the structures of the resulting COFs using powder X-ray diffraction (PXRD) techniques. For this advantage, it can be directed to the synthesis of COFs structures by design and for their formation with desired composition, pore size, and aperture, which make COFs an attractive class of new porous materials. In 2005, Yaghi and co-workers demonstrated the utilization of the topological design principle in their synthesis of covalent-linked crystalline porous organic frameworks [28]. Since this seminal work, the chemical synthesis of COFs has progressed significantly, and been used in gas storage, solid supports for catalysis, and optoelectronic devices. In this account, we outline how this chemistry was used to prepare crystalline COFs and highlight their synthesis, characterization, and applications.

4.2.1 Design and Synthesis

The synthesis of COFs could be designed through the principles of reticular chemistry [40–44]. Normally, the basic concerns for design mainly focus on the porosity and the structural regularity. In this regard, much experience has been obtained from the synthesis of metal-organic frameworks (MOFs). However, the crystalline framework of MOFs via the coordination bonds is much easier formed than to fabricate crystalline COFs via the covalent bonds. In order to form the crystalline solid, the formation of linkages should be well reversible and the reaction rate must be on a timescale that allows for self-correction of defects [45].

4.2.1.1 Design Principles

Crystalline COFs are synthesized in condensation reactions of organic building blocks, with geometry shape. The structure of the building blocks must meet two

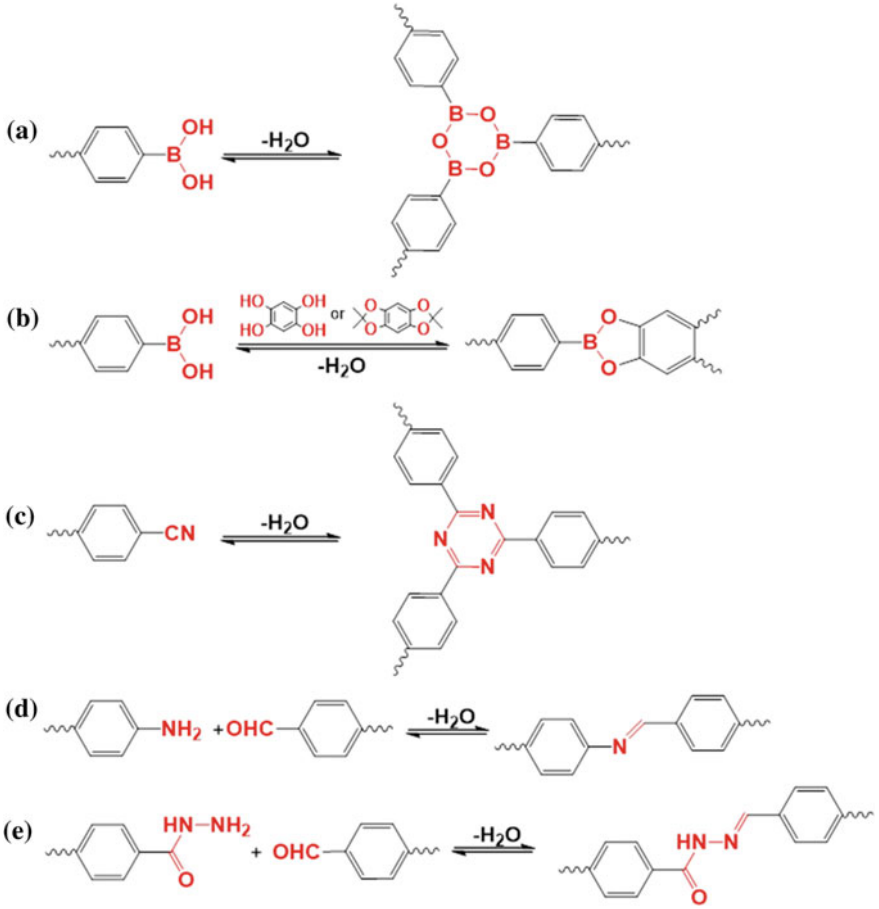

Fig. 4.1 Reversible reactions that have been successfully developed for the construction of COFs [36, 47–49, 70]

requirements: (1) the formation reaction should be reversible, and (2) the geometry of the building blocks should be well preserved in the COFs [46]. Figure 4.1 summarizes the synthetic reactions successfully applied for the COFs synthesis. The reaction A is based on the reversible formation of boronate anhydride from the dehydration of boronic acid. The synthesis of COF-1 was led by Yaghi and co-workers via this reaction [47]. An analogous dehydration reaction (reaction B) between boronic acid and (acetonide-protected) catechol results in the reversible formation of boronate esters by which a series of boron-containing COFs have been successfully obtained [47, 48]. The synthesis of triazine-based frameworks has been prepared via the nitrile cyclotrimerization under ionothermal condition, which represents a unique method (reaction C) [36, 49]. CTFs simultaneously provide high thermal, chemical, and mechanical stabilities along with a high degree of

conjugation; however, they typically possess low crystallinity as a result of the poor reversibility of the trimerization reaction. The reactions D and E are based on the imine bonds structure (–C=N–), by which several COFs have been synthesized with the new networks. The dehydration of aldehyde and amine gives rise to the Schiff base-type linkage (reaction D), while the reaction E between aldehyde and hydrazide affords the hydrazine structure.

As mentioned above, the rigid conformation of the building blocks enables the topological design of the COFs. Figure 4.2 summarizes the building units used, the general features of which are rigid in structure and symmetric multiconnective so as to meet the requirement for constructing the regular pores of COFs. For clarity, these building blocks are classified based on functional groups such as ($-B(OH)_2$, –OH, –CHO, $-NH_2$, and –CN). The synthetic strategies for COFs are based on diversity of building blocks, which endows the COFs with high flexibility in their molecular design.

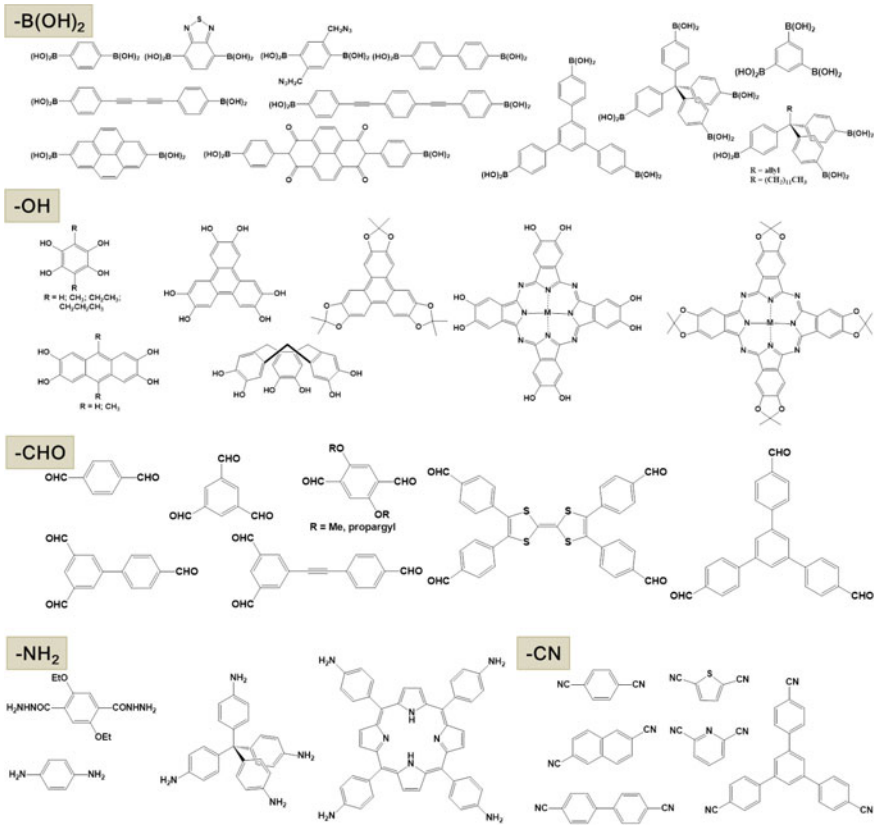

Fig. 4.2 Building units that have been successfully utilized for the synthesis of COFs [36, 47–49, 70]

4.2.1.2 Synthetic Methods

Since Yaghi and co-works exploited the solvothermal method to achieve the first successful COF-1 in order to construct the skeleton of COFs, many research groups have attempted to expand the synthetic possibility in different ways. We summarize the solvothermal, ionothermal, and microwave methods applied for the COFs synthesis below. Compared to bulky methods, surface or film COFs have been developed via reactions on substrates, such as metal surface and graphene sheet.

Solvothermal Synthesis

Initial studies were carried out in Pyrex tube via the solvothermal synthesis method which was degassed using several freeze–pump–thaw cycles, sealed, and heated to a desired temperature for 2–9 days. The precipitate was obtained, washed with suitable solvents, and dried under vacuum to yield the COFs powder. Issues such as the solubility, reaction pressure, crystal growth rate, and reversibility are the important points to be considered when selecting the reaction media and conditions. For example, whether fully soluble or completely insoluble building blocks can lead to the synthesis of COFs needs further experimental investigations [50, 51].

Moreover, solvent combination and ratio are the important factors for the highly crystalline COFs synthesis. As an example, Jiang and co-workers discussed the influence of solvents on the crystallinity of COFs [51]. When the ratio of mesitylene and dioxane is 19/1 or 9/1(v/v), COFs with high crystallinity could be obtained. At the same time, a suitable temperature and optimal inside pressure ensure the reversibility of the reaction. Generally, COFs have been prepared at temperatures ranging from 85 to 120 °C which is dependent on the chemical reactivity of the building blocks.

Microwave Synthesis

Microware-assisted reactions have been widely adopted in chemistry and material synthesis [52, 53]. 2D COF-5 and 3D COF-102 were obtained via the microwave heating by Cooper and co-workers [54, 55]. Compared to the solvothermal methods, microwave synthesis provides several advantages, such as rapid reaction, without sealed vessel, and more efficient.

Ionothermal Synthesis

Thomas and co-workers exploited the ionothermal synthesis method to produce crystalline porous CTFs [36]. Cyclotrimerization of nitrile building units in molten $ZnCl_2$ at 400 °C affords crystalline CTFs. The molten $ZnCl_2$ plays important roles in this system, not only as the solvent and catalyst but also as the template for the reversible cyclotrimerization and crystallization. However, most synthesized CTFs are amorphous materials, a probable reason is that this method seems to be partially reversible [46].

Synthesis of Monolayer COFs on Substrates

Forming the monolayer COFs on surface takes a further step for real applications. So far, Ag, highly ordered pyrolytic graphite (HOPG), and graphene have been used to prepare monolayer COFs. Condensation of the building blocks onto a metal surface formed monolayer of COF-1 and COF-5 [5]. The molecular arrays were obtained by the sublimation of 1,4-benzenediboronic acid (BDBA) and 2,3,6,7,10,11-hexahydroxytriphenylene (HHTP) under ultrahigh vacuum (UHV) from two heated molybdenum crucible evaporators onto a clean Ag(111) surface. Images of molecular layers were conducted using scanning tunneling microscopy (STM) at room temperature [56] (Fig. 4.3). The preparation of defect-free monolayer may require fine-tuning reaction conditions, highly purified building blocks, and employing a suitable single-crystal metal substrate to direct the building block alignment.

Subsequently, a HOPG surface was adopted instead of a metal surface to prepare monolayer COFs [57]. In this experiment, biphenyldiboronic acid, 1,4-benzenediboronic acid, and 9,9-dihexylfluorene-2,7-diboronic acid were deposited onto a HOPG surface from their THF solutions, and $CuSO_4 \cdot 5H_2O$ as a water "reservoir," followed by heating in a sealed autoclave at 150 °C for 1 h to form COFs monolayer. Structural analysis of the network showed a uniform pore spacing of 2.3 nm, which was in excellent agreement with the 2.27 nm size predicted by density functional theory (DFT) calculations and thus confirming the covalent formation of boroxine-linked SCOF-1. To achieve the reliable interface of electrodes or incorporate into real devices, Dichtel and co-workers reported the synthesis and characterizations of layered oriented COF-5 films onto single-layer graphene (SLG on SiO_2) surface (Fig. 4.4) [58–60]. Then, TP-COF, NiPc-COF, HHTP-DPB-COF, and ZnPc-PPE-COF were successfully prepared on graphene surfaces, and their thicknesses can be tuned by controlling the reaction time.

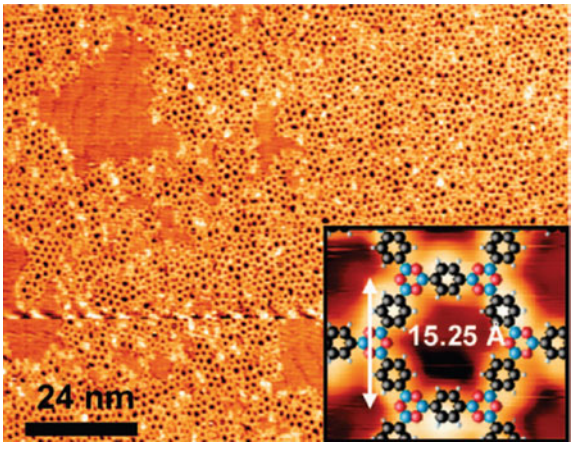

Fig. 4.3 STM image of the near-complete monolayer of SCOF-1 film synthesized from the deposition of 1 on Ag (111). The inset shows the proposed chemical structure for SCOF-1. Reproduced from Ref. [56] with kind permission of © 2008 American Chemical Society

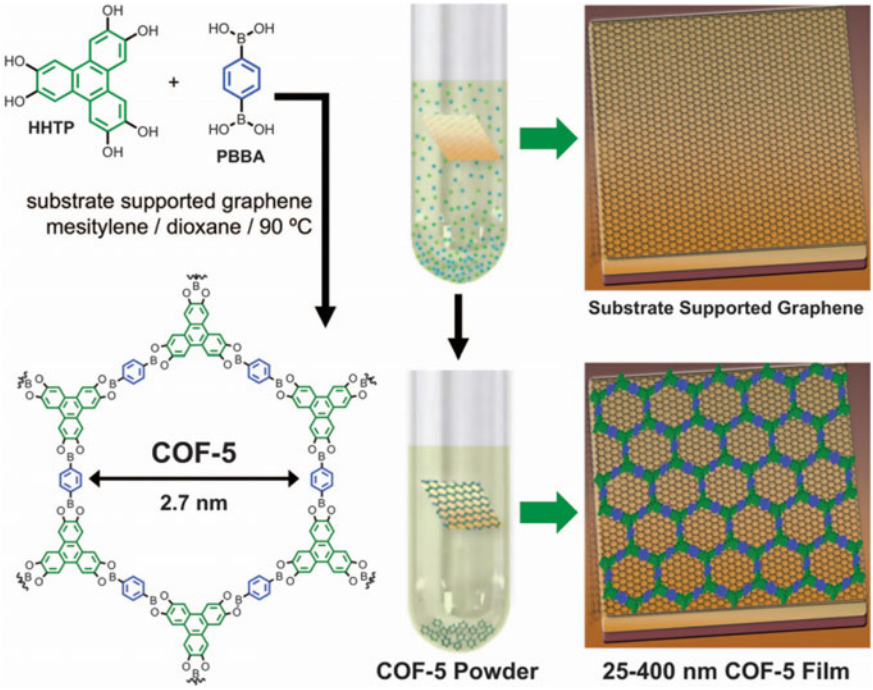

Fig. 4.4 Solvothermal synthesis of HHTP and PBBA on a single-layer graphene surface, affording COF-5 as the film on the graphene surface and as the powder precipitated around the bottom of the tube. Reproduced from Ref. [58] with kind permission of © 2011 The American Association for the Advancement of Science

4.2.1.3 Structural Studies

Due to the highly crystalline structure, COFs with special architecture can be characterized by PXRD techniques. The structural simulation provides an important tool in revealing COFs' stacking structures. Besides, the structural regularity, composition, and atomic linkage of the COFs can be characterized by infrared spectroscopy, solid-state NMR spectroscopy, elemental analysis, and X-ray photoelectron spectroscopy. In molecular perspective, COFs can be classified into three categories: boron-containing, triazine-based, and imine-based COFs.

Boron-containing COFs

In 2006, COF-1 was synthesized as a crystalline material by the self-condensation of 1,4-phenylenediboronic acid (BDBA) which resulted in a structure consisting of extended layers stacked in staggered form and gave hexagonal pores with 1.5 nm diameter and BET surface area of 711 $m^2\ g^{-1}$. It has also been applied for the synthesis of three-dimensional COFs by condensation of molecules with tetrahedral structure, such as tetra(4-dihydroxyborylphenyl)methane (TBPM) and tetra

(4-dihydroxyborylphenyl)silane (TBPS) [3]. Subsequently, Lackinger and co-workers used para-diboronic acids, in which the size of the organic backbone varied from phenyl to quaterphenyl incrementally, to synthesize a series of isoreticular 2D COFs [61]. These networks ranged from 1.5 to 3.8 nm, and the corresponding pore sizes increased from 1.0 to 3.2 nm. Scanning tunneling microscopy was employed for structural characterization of the covalent networks as well as non-covalent self-assembled structures that were formed on the surface prior to the thermally activated polycondensation reaction. Recently, Fischer and co-workers developed a novel synthesis strategy for COF-1 at room temperature which was suitable for multigram scale synthesis [62]. This methodology shifts COF synthetic chemistry from sealed tubes to open beakers.

In addition to self-condensation, boronic acids can also react with catechols to form five-membered C_2O_2B boronate esters. And the mechanistic studies of COF-5 formation have been done from initial homogenous conditions (Fig. 4.5) [63]. The obvious advantage of this co-condensation strategy is the diverse combination of boronic acids and diols as building units, by which a series of COFs could be constructed with different properties and functionalities. For example, via the co-condensation of monomers 2,3,6,7,10,11-hexahydroxytriphenylene (HHTP) and pyrene-2,7-diboronic acid (PDBA), a 2D COF material (TP-COF) was successfully obtained [64]. TP-COF is a highly blue luminescent and electrical conductive material. Moreover, the functionality of COFs could be tailored with more versatile building units. For instance, via the co-condensation of donor and acceptor monomers, COFs with segregated donor–acceptor heterojunctions were synthesized [59, 65, 66]. Meanwhile, photoresponsive structurally dynamic COFs [67], polygonal shape-persistent macrocycles COFs [68], and star-shaped COFs [69] were also successfully synthesized using this strategy.

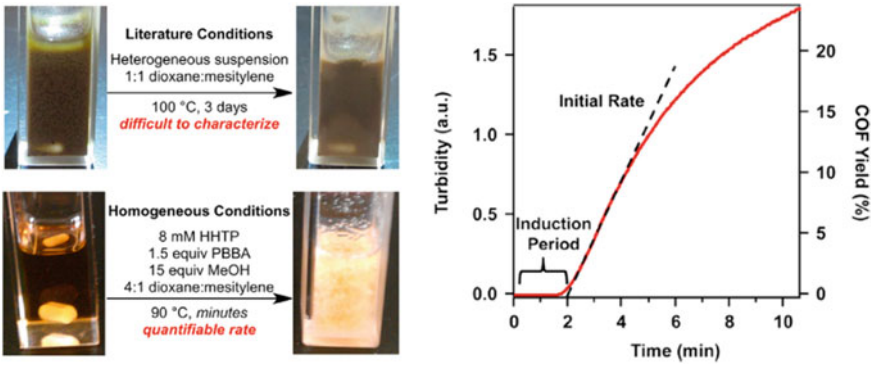

Fig. 4.5 A comparison of heterogeneous and homogeneous growth conditions for COF-5 and turbidity measurement of COF-5 formation as a function of time (8 mM HHTP, 1.5 equiv of PBBA, 15 equiv of MeOH, 4:1 dioxane/mesitylene, 90 °C). Reproduced from Ref. [63] with kind permission of © 2014 American Chemical Society

Based on the methods above, three-dimensional COFs were synthesized by condensation or co-condensation of molecules with tetrahedral geometry, such as TBPM or TBPS, TBPM, and HHTP [3].

Imine-based COFs

Similarly, C=N bond formation reaction has been applied to synthesize COFs with imine linkages [70]. One category is the "Schiff base"-type COFs formed via the co-condensation of aldehydes and amines (reaction D in Fig. 4.1). The first imine-based COF (COF-300) was synthesized via the dehydration reaction of tetra-(4-anily)methane and terephthaldehyde [70]. Subsequently, many scientists involved in this field. Jiang [71–76] and Rahul [77–81] are the best of them. Jiang and co-workers used this method mainly to focus on porphyrin-containing COFs synthesis [71, 73, 76]. By tuning the size and length and by introducing specific functional groups of the building blocks, photochemical active COFs [73], chiral COF catalysts, [75], adsorbents [73, 76], and chemical probe [82] can be produced. Rahul and co-workers designed a series of COFs based on the 1,3,5-triformylphloroglucinol (TP) units [77, 79–81, 83]. More recently, 3D imine-based COFs were synthesized via the Knoevenagel condensation reaction, showing excellent catalytic activity [84]; the other one was 3D pyrene-based COF, which was constructed through [4+4] imine condensation reactions. The novel 2D COFs with two different pores were recently developed.

Zhao and co-workers designed a dual-pore COF, which possessed both micopores and mesopores (7.1 and 26.9 Å) (Fig. 4.6a) [85]. Zhang and co-workers successfully synthesized two COFs with heterogeneous pore structures through the desymmetrized vertex design strategy [86]. Pore size distribution analysis revealed that two types of micropores (1.06 and 1.96 nm) were incorporated into the resulting COFs (Fig. 4.6b).

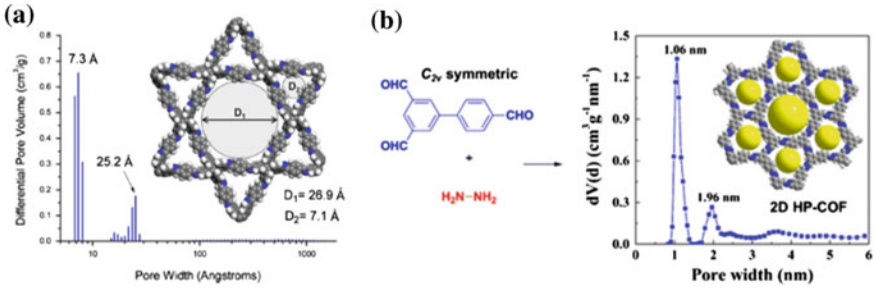

Fig. 4.6 **a** Schematic representation for the synthesis of TpBDH and TfpBDH [one unit of a space filling model of TpBDH and TfpBDH is shown in the inset of the chemical drawing model]; **b** syntheses of HP-COF-1 and PSDs of HP-COF-1. Reproduced from Ref. [85] with kind permission of © 2014 American Chemical Society, Reproduced from Ref. [86] with kind permission of © 2015 American Chemical Society

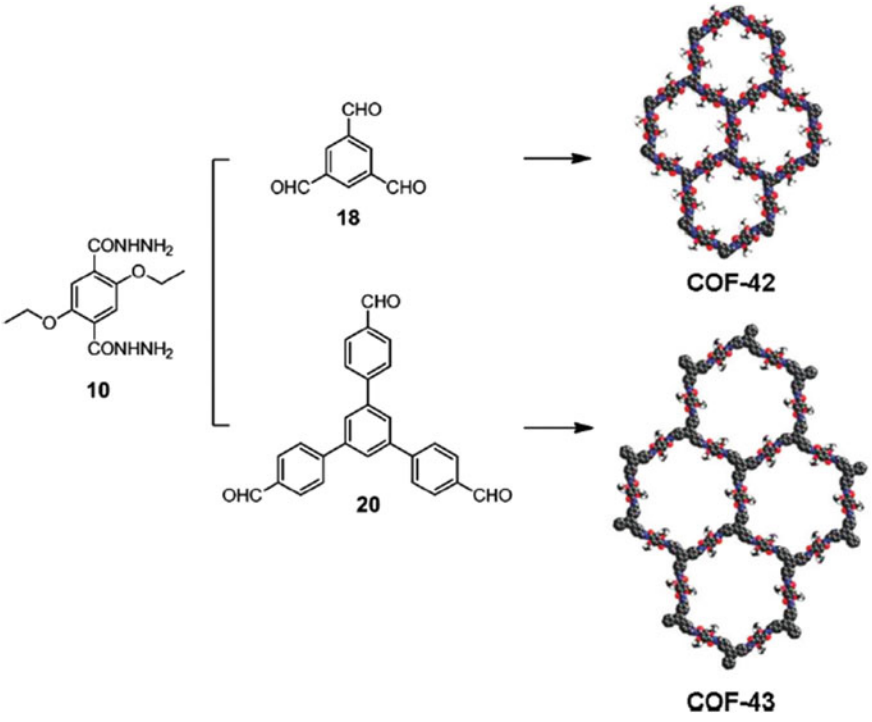

Fig. 4.7 Building units and the extended structures of COF-42 and COF-43. Reproduced from Ref. [87] with kind permission of © 2011 American Chemical Society

Another type of imine-based COFs is hydrazone-linked COFs synthesized by pioneer Yaghi and co-workers via the co-condensation reaction of aldehydes and hydrazides (Fig. 4.7). By employing 2,5-diethoxyterephthalohydrazide and 1,3,5-triformylbenzene or 1,3,5-tris(4-formylphenyl)benzene as the building units, COF-42 and COF-43 were successfully synthesized [87]. The existence of abundant hydrogen bonds within the hydrazone units is beneficial for the formation of the eclipsed structure. More recently, Wang and co-workers designed fluorescent COFs (COF-LZU8) by introducing the thioether groups into COF-42 for efficient detection and removal of Hg^{2+} ions [88].

Triazine-based COFs

Covalent triazine-based frameworks were firstly developed by Thomas and co-workers [36]. The CTFs synthesis was based on cyclotrimerization of aromatic nitrile building units in molten $ZnCl_2$ at 400 °C (reaction C in Fig. 4.1). Interestingly, the ratio of $ZnCl_2$ to monomer is the key to the CTFs synthesis. The higher ratio (10:1) would lead to an amorphous polymer but with higher surface area (1123 $m^2\ g^{-1}$). Compared to the two types of materials above, the CTFs are

usually of lower crystallinity. The reaction for CTFs is partially reversible reaction. To date, only two crystalline CTFs have been successfully synthesized [36, 49].

Other COFs

Polyimide-COFs (PI-COFs) were designed by Yan and co-workers using the imidization reaction. The resulting PI-COFs possessed large pore sizes that can be tuned by extending the building units, and in particular, PI-COF-3 displayed the largest size (5.3 nm) among the results reported to date [89]. Subsequently, 3D porous PI-COFs with non- or fourfold-interpenetrated diamond networks were synthesized which represented the first kind of COFs ever to be employed in controlled drug delivery with high loading and good release control [90]. Novel COFs with two types of covalent bonds have been developed using orthogonal reactions. This strategy can be adapted not only in binary systems but also in more complicated systems. For example, the first multiple-component NTU-COF-2 showed both high BET surface area and large H_2 uptake capacity [91].

4.2.2 Application Exploration

The applications of COFs are derived from their porosity and functional unit skeleton. With tunable porous architecture, these COFs are new candidates for further applications, such as gas storage, catalyst, and photoelectric device.

4.2.2.1 Gas Storage

Hydrogen Storage

Fossil fuels such as oil, natural gas, and coal contain carbon and produce CO_2, CO gases including a higher ratio of nitrogen oxides (NO_x) and sulfur dioxide (SO_2) which lead to pollution and global warming. Moreover, coal and fuel oil are available in limited supply. However, hydrogen is a clean, highly abundant, and non-toxic renewable fuel, and it is viewed as a promising clean fuel in the future which only generates water vapor after burning. The major problem with this fuel is its storage since it needs to be stored like other compressed gases. Hydrogen is usually stored in three different ways, viz. compression, liquefaction, and in a solid material [92, 93]. COFs have generated much interest in the study of the hydrogen storage materials.

Normally, COFs with larger surface areas possess higher hydrogen uptake capacities under the same condition. For example, 3D COF-102 with a higher BET surface area of 3620 $m^2\ g^{-1}$ showed the highest hydrogen uptake up to 7.2 wt% at 1 bar and 77 K [94]. This capacity is comparable to that of MOF-177 (7.5 wt%, S_{BET}: 4500 $m^2\ g^{-1}$) [95], MOF-5 (7.6 wt%, S_{BET}: 3800 $m^2\ g^{-1}$) [96], and PAF-1

(7.5 wt%, S_{BET}: 5600 m^2 g^{-1}) [2]. For 2D COFs, COF-10 (S_{BET}: 1760 m^2 g^{-1}) showed the highest hydrogen uptake of 3.92 wt% at 1 bar and 77 K compared to the other 2D COFs [94]. Recently, Zhao and co-workers developed a high BET surface area (1619 m^2 g^{-1}) NTU-COF-2, with two types of covalent bonds using orthogonal reaction. Its hydrogen uptake is 1.55 wt% at 1.0 bar and 77 K [91]. However, the exceptional COF-11 Å with the lower BET surface area (105 m^2 g^{-1}) showed hydrogen uptake of 1.22 wt% at 1.0 bar and 77 K [94]. The DOE road map target for hydrogen storage is set to be 9 wt% and 81 kg H_2 m^{-3} at 253–323 K with a pressure of 100 atm by the year 2015. Rooting on this purpose, the practical employment of COFs toward hydrogen uptake seems remoted.

Carbon Dioxide Storage

The emission of CO_2 due to the combustion of fossil fuels is one of the major sources for the accumulation of CO_2 in the atmosphere. To stabilize atmospheric CO_2 level, it is necessary to develop CO_2 capture and storage/sequestration technologies [94]. The storage of CO_2 has been extensively studied using a wide range of porous materials, for example, porous carbons, silicas, and MOFs [42, 97, 98]. Yaghi and co-workers achieved a very high CO_2 uptake of COF-102 reaching 120 wt% at 55 bar and 298 K [94]. However, COF-102 showed higher adsorption at low pressures than COF-108 because of their compact atomic packing; on the contrary, at high pressures, higher CO_2 uptake value (422.4 wt%) was obtained for COF-108. Compared with other porous materials (for example, ZIFs) [43, 99], COFs via reasonable design might become good candidates for CO_2 storage.

Methane Storage

Natural gas has been demonstrated to be potential as an alternative fuel for vehicular application due to its abundance and low price. Much effort has been focused on reaching the DOE target (180 cm^3) of storing methane at 35 bar, because this is the pressure in natural gas pipelines. Similar to the cases of hydrogen storage, the capability of methane storage is based on surface areas of COFs. The adsorption capacity of methane at 35 bar and 298 K in 3D COF-102 (18.7 wt%, 3620 m^2 g^{-1}) is higher than that of 3D COF-103 (17.5 wt%, 3530 m^2 g^{-1}) [94]. For 2D COFs, COF-5 has a lower value (8.9 wt%). Although the capacities of methane storage are similar in some COFs, decreasing the costs and efforts in synthesizing COFs still remain a big challenge toward the practical employment.

Ammonia Storage

Boron-containing COFs with abundant boron element (electron-deficient element) are useful for adsorbing ammonia. Among the series of boron-containing COFs, COF-10 has the highest ammonia uptake (15 mol kg^{-1}) at 1 bar and 298 K [100]. Moreover, COF-10 has a good circulation property. However, the stability of boron-containing COFs restrains their application.

4.2.2.2 Heterogeneous Catalysis

Organocatalysis in homogeneous systems is problematic because of the difficulty of separating expensive catalysts for repeated use [101–103]. Most heterogeneous organocatalysts are based on linear polymer supports; however, such catalysts exhibit low activity owing to the inefficient access to the catalytic sites. To overcome this issue, crystalline MOF-based organocatalysts have been developed. However, their stability, enantioselectivity, and diastereoselectivity need to be improved [75]. Imine-based COFs, due to containing abundant C=N (basic group), are useful for organic catalysis. Jiang and co-workers developed π-electronic COFs as a new type of metal-free heterogeneous catalyst, which enabled the high-performance catalysis of Diels–Alder reactions in neat water and ambient condition. Meanwhile, they prepared the mesoporous COFs with two distinct chiral segments by post-synthetic functionalization. The resulting crystalline metal-free catalysts displayed high activity, enantioselectivity, and recyclability for Michael reactions. On the other hand, imine-based COFs can incorporate metal ions into its pores via the coordination reaction with nitrogen atoms in the COFs. In 2011, Wang and co-workers realized the first application of metal COFs (Pd/COF-LZU1) for highly efficient Suzuki-Miyaure coupling catalysis reaction [104]. Recently, Vaidhyanathan and co-workers reported an amphiphilic triazine COF and the facile single-step loading of Pd(0) nanoparticles. The 18–20% of nano-Pd loading gave highly active composite working in open air at low concentrations (Conc. Pd (0) < 0.05 mol%, average TON 1500) catalyzing simultaneous multiple site Heck couplings and C–C couplings using "non-boronic acid" substrates, and exhibited good recyclability with no sign of catalyst leaching [105].

4.2.2.3 Photoelectric Applications

COFs with the photoelectric performance (PPy-COF) were firstly synthesized via the self-condensation of PDBA under solvothermal condition by Jiang and co-workers [106]. Remarkably, PPy-COF possessed 2D eclipsed structures with a higher BET surface area of 868 $m^2\ g^{-1}$, and showed a fluorescence shift compared to its monomer PDBA. PPy-COF is electrically conductive, displaying photoconductivity with a quick response to light irradiation, and is capable of repetitive on–off photocurrent switching with a large on–off ratio (Fig. 4.8).

Phthalocyanines (Pcs) have received considerable attentions due to their unique optical and electronic properties which give rise to the application of Pcs in various domains, such as organic field-effect transistor, optical information storage, organic solar cell, photodynamic therapy, and nonlinear optical material. Phthalocyanine-based polymers combine the excellent physical and chemical properties of Pcs as well as good solubility and processability, which are becoming one of the research hot spots. Spitler and Dichtel synthesized an eclipsed 2D COF (PC-PBBA-COF) containing metal-free phthalocyanine groups using phthalocyanine tetra(acetonide) and BDBA [48]. At the same time, Jiang and co-workers synthesized nickel

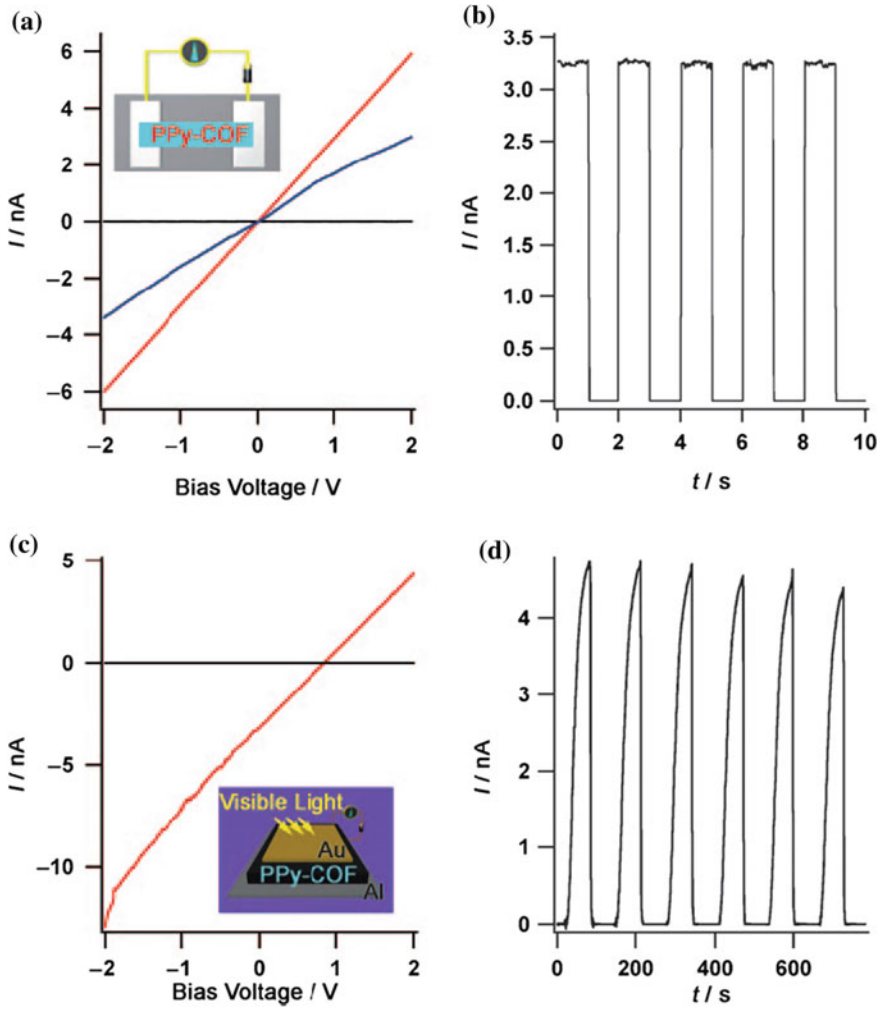

Fig. 4.8 **a** I–V profile of PPy-COF between two Pt electrodes 10 mm apart (*black curve*: without PPy-COF; *blue curve* with PPy-COF; *red curve* with iodine-doped PPy-COF). **b** Electric current when the 2 V bias voltage was turned on or off. **c** I–V profile of PPy-COF between sandwich-type Al/Au electrodes (*black curve* without light irradiation; *red curve* upon light irradiation). **d** Photocurrent when the light was turned on or off. Reproduced from Ref. [106] with kind permission of © 2009 Wiley-VCH (color figure online)

phthalocyanine-based COFs (NiPc COF and 2D-NiPc-BTDA COF) via the boronate esterification reaction of (2,3,9,10,16,17,23,24-octahydroxyphthalocyaninato) nickel(II) with BDBA or benzothiadiazole diboronic acid (BTDADA) [50, 51]. Both NiPc COF and 2D-NiPc-BTDA COF possessed eclipsed structures with BET surface areas of 624 and 877 $m^2\ g^{-1}$, respectively. Due to 2D eclipsed structure,

NiPc COF showed an enhanced light-harvesting capability in the visible and near-infrared regions. And NiPc COF revealed highly photoconductive property, exhibiting a panchromatic light response and exceptional sensitivity to visible and near-infrared photons. Subsequently, they synthesized 2D tetragonal metallophthalocyanine by introducing electron-withdrawing blocks at the edges of *n*-channel 2D COFs. 2D-NiPc-BTDA COF turned to be an *n*-type semiconductor and exhibited great changes in the carrier transport mode with a broad and enhanced absorbance of light up to 1000 nm. Moreover, this COF exhibited panchromatic photoconductivity and was highly sensitive to near-infrared lights. Recently, they developed a new donor–acceptor strategy to construct COFs with various skeletons and pore for charge separation and photoenergy conversion. For example, using a three-component topological design diagram in conjunction with click chemistry, they developed a method for converting the open lattice of COFs into photoelectric structures. Most recently, they reported the design and synthesis of a photoresponsive COF with anthracene units as the photoresponsive π-building blocks. The COF is switchable upon photoirradiation to yield a concavo-convex polygon skeleton through the interlayer[4p+4p] cycloaddition of anthracene units stacked in the π-columns [67].

Porphyrins possess extensive π-conjugated systems which contribute to electron transfer from donor unit to acceptor unit, and high molar absorption coefficient in light absorption, and their properties can be easily tuned via synthetic modifications for the periphery or by metal insertion into the cavity of porphyrin. In recent years, porphyrins have been applied in the synthesis of porous materials such as MOFs [47, 107, 108], CMPs [109], and COFs [76]. Jiang and co-workers reported the porphyrin-based COF (ZnP-COF) constructed via the boronate esterification reaction of zinc(II) 5,10,15,20-tetrakis(4-(dihydroxyboryl)phenyl) porphyrin and 1,2,4,5-tetra-hydroxybenzene. ZnP-COF revealed a tetragonal 2D eclipsed structure with a large BET surface area of 1742 $m^2\ g^{-1}$ and an average pore size of 2.5 nm. Subsequently, the photoelectronic properties of ZnP-COF and other two porphyrin-based COFs (H_2-COF and CuP-COF) have been studied [46]. Compared to H_2-COF, ZnP-COF and CuP-COF showed high-rate ambipolar and electron conduction, respectively. CuP-COFs have been investigated in a recent work, in which fluoro-substituted and non-substituted arenes at different molar ratios were integrated into the edge units that stack to trigger self-complementary π-electronic interactions in the COFs. These interactions also showed a prominent effect on changing the π-electron distribution in the framework and lowering the HOMO-LUMO gap (Fig. 4.9) [71].

4.2.3 Summary

COFs have emerged as an important class of materials because their backbone is built entirely from light elements (thus far, C, N, O, B, Si) held together by strong covalent bonds (B–O, C–N, B–N, and B–O–Si) to make robust porous materials

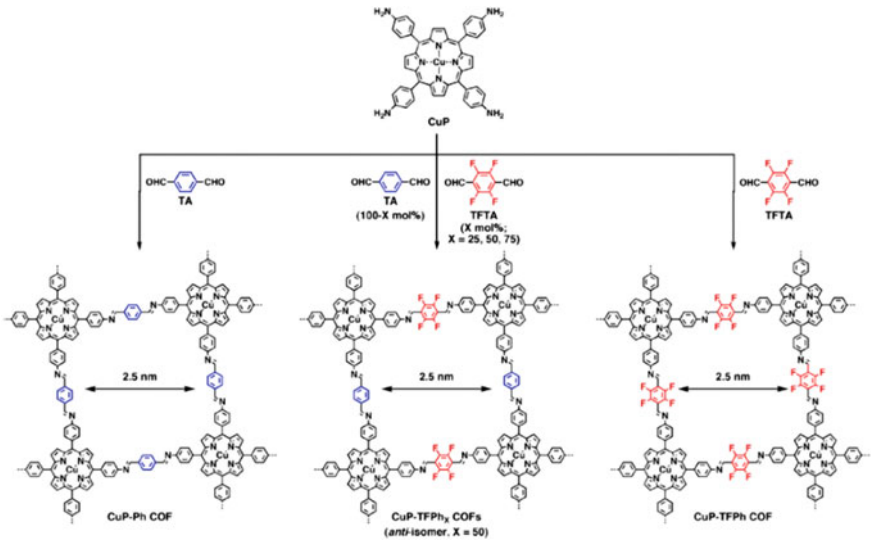

Fig. 4.9 Schematic representation of the synthesis of COFs integrated with self-complementary π-electronic interactions (CuP-TFPh$_X$, X = 25, 50, and 75 mol%) and the CuP-Ph and CuP-TFPh Controls. Reproduced from Ref. [71] with kind permission of © 2013 American Chemical Society

including the advantages of predictable structures and tunable pore functionality and metrics. The crystallization problem has been overcome in COF chemistry except CTFs, and a large variety of COF structures have been made and will continue to evolve in their diversity and complexity. However, the development of new synthetic methods is the key to broaden the COFs family. Formability is another important issue for the practical application of COFs. Finally, both the introduction of functional groups and post-modification are the critical subjects according to the practical application of COFs.

4.3 Hypercrosslinked Polymers

Hypercrosslinked polymers represent a novel class of porous polymer materials containing abundant microporous structure [29, 30]. These polymers are mainly prepared by the Friedel–Crafts chemistry and developed by taking the concepts of "crosslinking" which, however, is further extended [110]. The obtained polymer networks are usually cross-linked with highly rigidity linkages which prevent the polymer chains from collapsing. Therefore, these resulting polymer materials contain permanent micropore, high surface area, and large pore volume. According to the difference between the synthetic methods, hypercrosslinked polymers are mainly prepared by the following three approaches: (1) post-crosslinking polymer precursors, (2) direct one-step polycondensation of functional monomers, and

(3) knitting rigid aromatic building blocks with external crosslinker. In this part, we will introduce the development of hypercrosslinked polymers in detail as well as compare the merits between various synthetic methods. Networks with specific functionalities and controlled micromorphology which can be applied in broad practical and potential applications such as gas storage, adsorption, separation, catalysis, sensing are also discussed.

4.3.1 Post-crosslinking Procedure

"Davankov-type" resins are commonly regarded as the first category of hypercrosslinked polymers which were initially discovered and investigated in the early 1970s [111]. These hypercrosslinked polymeric networks can be generated by further crosslinking of either dissolved linear polystyrene or swollen gel-type styrene-divinylbenzene copolymer precursors [112]. The representative reaction scheme is provided in Fig. 4.10. The polymer precursors are dissolved or swollen in solvents which separate the polymer chains, and then, a crosslinking step was carried out immediately to lock these chains forming a rigid intensive network. After removing the solvent, the rigid linkage units prevent the chains from collapsing thus resulting in interconnected pores in the polymer matrix [113].

As pioneers in this field, Davankov with his colleagues has done a large amount of research in preparing various kinds of hypercrosslinked materials as well as exploring the reaction conditions [110, 112, 114–116]. An intermolecular hypercrosslinked soluble material was obtained from the linear polystyrene using monochlorodimethyl ether (MCDE) as the crosslinking agent in the presence of $SnCl_4$ catalyst [114]. A series of surface areas up to 680–1000 $m^2\ g^{-1}$ can be obtained with materials showing potential applications in chromatography, separation of contaminants from liquid solutions, and adsorption of organic vapors.

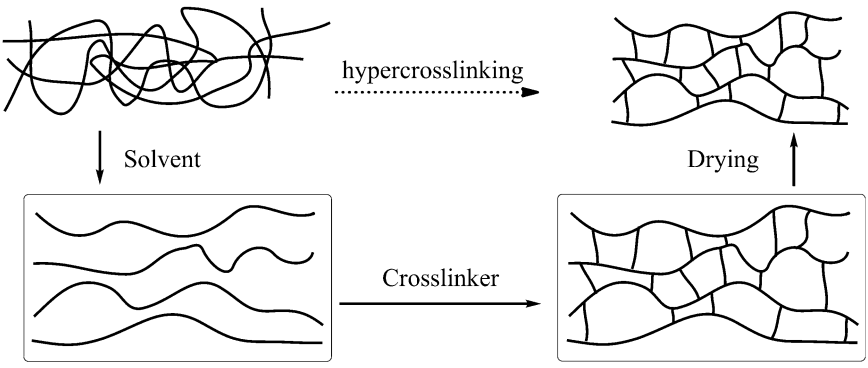

Fig. 4.10 Scheme of the representative hypercrosslinking reaction. Reproduced from Ref. [113] with kind permission of © 2007 Royal Society of Chemistry

Low-cost CCl_4 is a good crosslinker with less toxicity compared with monochlorodimethyl ether. By post-crosslinking styrene-divinylbenzene copolymer precursors, a series of 1000 $m^2\ g^{-1}$ surface area hypercrosslinked resins were produced via Friedel–Crafts reaction with CCl_4 as the crosslinker as well as aluminum or ferric chloride as the catalyst [117].

With similar linear structure as polystyrene, polyDVB-VBC (which is short for polydivinylbenzene-co-vinylbenzyl chloride) can be efficient precursors for hypercrosslinking which convert the chloromethyl groups into methylene bridges thus creating stronger crosslinking linkages (Fig. 4.11) [118, 119]. Sherrington and co-workers [119] synthesized a variety of hypercrosslinked polymers based on polyDVB-VBC precursors and investigated the porosity discrepancy affected by different synthetic conditions including the monomer ratio, solvent, catalyst, and reaction time. The resulting surface areas ranged from 300 to 2000 $m^2\ g^{-1}$ of different precursors with tiny structure variation using Lewis acid catalysts. For example, a gel-type precursor containing 2 mol% DVB yielded a surface area of $\sim$1200 $m^2\ g^{-1}$ within only 15 min initiating crosslinking which rose steadily to 2090 $m^2\ g^{-1}$ after 18 h.

Despite various synthetic strategies, hypercrosslinked polymers with controllable pore size and size distribution were also studied. Tan group [120] chose the typical poly(DVB-VBC) copolymer as the precursor to investigate the influence of the precursor structure on porosity. By increasing the DVB content, the pore size of the obtained hypercrosslinked poly(divinylbenzene-co-vinylbenzyl chloride) (HCP-DVB-VBC) can be efficiently adjusted from macropore to micropore size showing a more uniform and narrower microporous structure. When the DVB concentration is higher than 7%, a typical type I nitrogen adsorption/desorption isotherm was observed indicating a pure microporous polymer network. Gas adsorption properties of these materials were also investigated indicating that the smaller micropore size and higher microporous volume are beneficial for H_2 and CO_2 uptakes.

Recently, polystyrene-base block copolymers exhibited attractive advantages in designing microporous materials with hollow structure [121, 122]. By adopting the self-assembly of PMMA-b-PS copolymer, Wu et al. [122] synthesized uniform

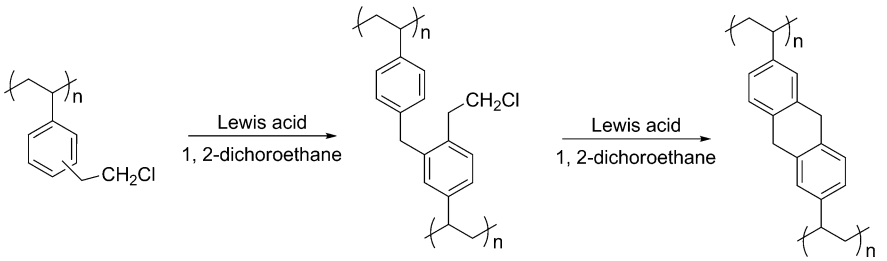

Fig. 4.11 Post-hypercrosslinking of DVB-VBC polymer precursors. Reproduced from Ref. [119] with kind permission of © 2006 American Chemical Society

PMMA@PS core–shell micelles in a selected mixed solvents, followed by hypercrosslinking to produce microporous hollow spheres. Precise control over the nanostructures can be achieved by the variation of the molecular composition of PMMA-b-PS. After carbonization into carbon hollow spheres, these as-prepared nanoscale materials showed good CO_2 capture and supercapacitance properties.

4.3.2 *Direct One-Step Self-polycondensation*

In recent years, "Davankov-type" resins displayed a rapid development in the synthetic strategies. However, their post-crosslinking essences resulted in limited applications because of the tedious reaction process as well as restricted optional precursors. What if hypercrosslinked polymer synthesized directly from small molecule monomers which contain functional groups such as chloromethyl group? Early researches were started by Cooper and co-workers [123]. Via a simple one-step condensation polymerization process, three kinds of bis(chloromethyl) aromatic monomers (Fig. 4.12) including dichloroxylene (DCX), bis(chloromethyl) biphenyl (BCMBP), and bis(chloromethyl) anthracene (BCMA) linked together with the elimination of functional groups and formed a highly crosslinked network. By changing the monomer ratio among the monomers as well as Lewis acid catalyst amount, surface area and porous structure of the resulting materials can be easily tuned. According to the N_2 adsorption/desorption analysis, these materials were predominantly microporous and exhibited apparent highest BET surface areas of up to 1904 $m^2\ g^{-1}$. Owing to their high surface area and permanent microporosity, these materials also showed outstanding performance in hydrogen adsorption [123], methane storage [13], and CO_2 capture [124] indicating their potential applications in energy and environment field.

This one-step condensation polymerization of small monomers highly extended the range of optional building blocks. Moreover, multifunctional polymer materials can be easily obtained by a simple copolymerization with other functional monomers.

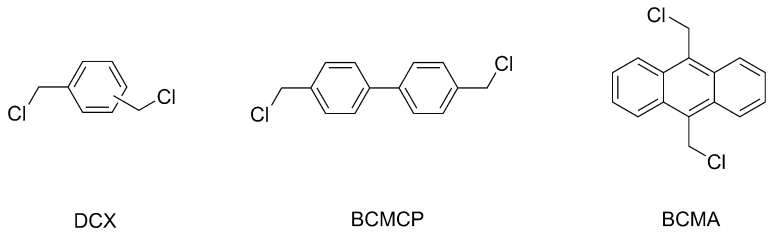

Fig. 4.12 Three typical monomers used in self-condensation polymerization. Reproduced from Ref. [123] with kind permission of © 2007 American Chemical Society

Yang et al. [125] synthesized a series of microporous copolymers from triphenylamine and p-DCX using $FeCl_3$- promoted oxidative polymerization and Friedel–Crafts alkylation. The BET specific surface areas ranging from 318 to 1530 $m^2\ g^{-1}$ were obtained with the increasing content of p-DCX. These nitrogen-functionalized materials exhibited an enhanced CO_2 uptake of 4.60 mmol g^{-1}, which was comparable with the best reported results for MOPs, activated carbon, and MOFs under the same conditions. Following investigation about hydrocarbons/water separation properties was also made using BCMCP as the crosslinker [126]. By changing the monomer ratio, hypercrosslinked polymers with apparent BET surface areas of 1362 and 1338 $m^2\ g^{-1}$ were obtained which showed benzene/water vapor selectivity as high as 53.5 and 63.6, respectively. Moreover, a monolithic polymer was also prepared to show potential application in oil spill cleanup.

Except for the traditional chloromethyl groups, Tan group [127] has explored two kinds of aromatic hydroxymethyl monomers such as 1,4-benzenedimethanol (BDM) and benzyl alcohol (BA) that can also be prepared into self-condensation microporous polymers (Fig. 4.13). N_2 adsorption/desorption isotherms of the polymers indicated a predominantly microporous network with high surface areas of up to 847 and 742 $m^2\ g^{-1}$, respectively. Polymer networks based on BA monomers can store a significant amount of CO_2 up to 8.46 wt% at 273 K/1 bar and H_2 up to 0.97 wt% at 77.3 K/1 bar. This research has enlarged the optional building blocks that even monofunctional compounds can be involved in the construction of hypercrosslinked polymers.

Following this study, Tan group [21] has recently demonstrated that rigid aromatic monomers and derivatives can also be utilized for a novel one-step self-polycondensation reaction (Fig. 4.14). This strategy is based on the Lewis acid catalytic Scholl reaction [128], which involves the elimination of aryl-bound hydrogen atoms accompanied by the formation of new aryl-aryl bonds. Due to the universality of this strategy, a wide variety of monomers are suitable including monomers with both high or low electron density, acidic or alkaline functional group containing monomers, aryl or fused ring-based monomers, as well as heterocyclic ring containing monomers. A series of microporous organic polymers with surface areas ranging from 636 to 1421 $m^2\ g^{-1}$ were synthesized according to the N_2 sorption analysis. Moreover, the porous structure and functionalities of the resulting networks can be easily modulated by adopting different functional building blocks indicating potential applications in gas storage, catalyst, optoelectronic sensing, and semi-conducting.

Zhu group [129] introduced several three-dimensional monomers such as triphenylamine, tetraphenylmethane, tetraphenylsilane, and tetraphenylgermane for the construction of spatial hypercrossslinked networks via the Scholl coupling reaction. With moderate surface areas reaching up to 1119 $m^2\ g^{-1}$, the resulting polymer networks exhibited relatively high CH_4 and CO_2 sorption capacity of 1.04 and 3.52 mmol g^{-1}, respectively (at 273 K/1.13 bar).

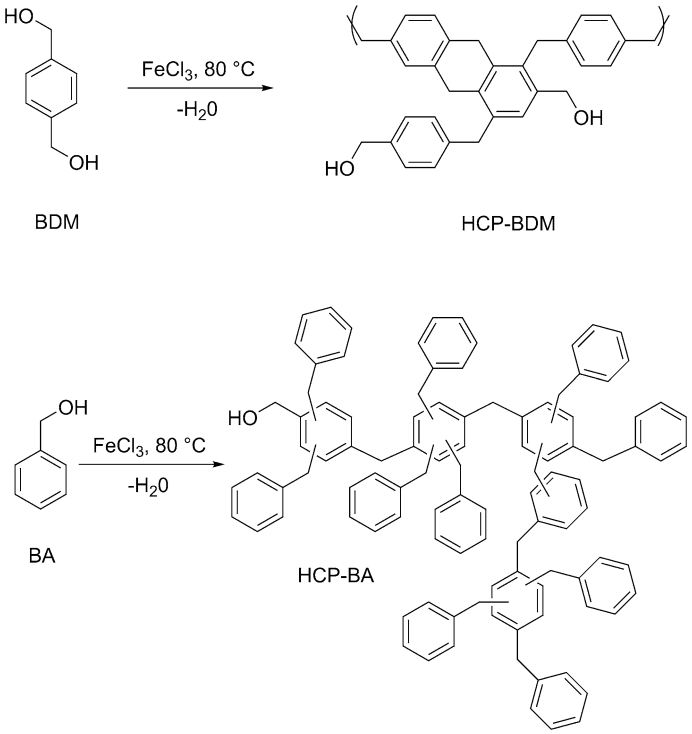

Fig. 4.13 Synthesis route of HCP-BDM and HCP-BA. Reproduced from Ref. [127] with kind permission of © 2013 American Chemical Society

4.3.3 External Crosslinking Strategy

Although this one-step self-polycondensation strategy has extended the optional building blocks boundary, there are still limitations for the synthetic routes. For example, the preparation of functional group containing monomers like chloromethyl group or hydroxymethyl group is difficult and is of high cost. Moreover, the hydrogen chloride generated from chloromethyl group also will do damage to fabrication facilities in large-scale industrial production and the environmental issues also need to be considered.

Considering these problems, a new strategy was proposed by Tan group [130] that using formaldehyde dimethyl acetal (FDA) external crosslinker to knit low functionality rigid aromatics via a simple Friedel–Crafts reaction in which anhydrous $FeCl_3$ acts as catalyst. This strategy is gentle, facile, flexible, and is of low cost that a wide variety of building blocks can be involved resulting in materials with predominantly microporous structure and high surface area (Fig. 4.15). By adjusting the ratio of monomer and the crosslinker, surface areas as well as the porous structure of the resulting networks can be roughly controlled and a high

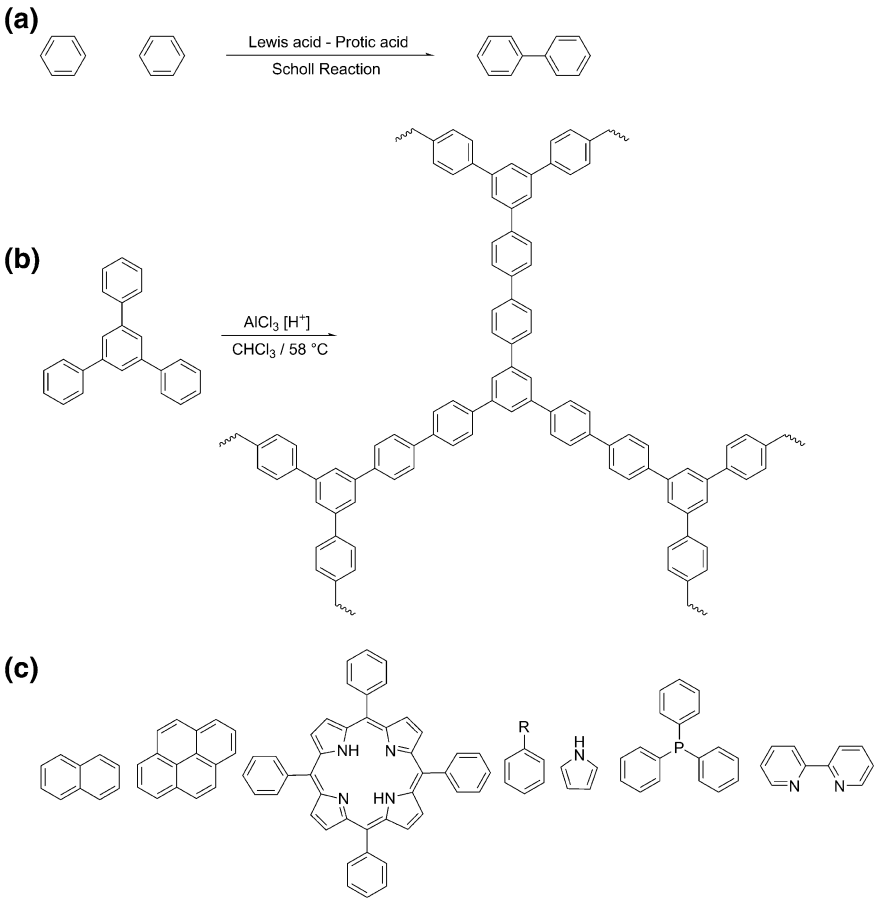

Fig. 4.14 **a** Typical Scholl reaction, **b** polymer networks form 1,3,5-triphenyl benzene, **c** other monomers. Reproduced from Ref. [21] with kind permission of © 2014 Royal Society of Chemistry

BET surface area of 1391 $m^2\ g^{-1}$ was obtained for benzene-based network. In addition, the functionality of the polymer networks can be easily modulated by introducing functional monomers. This knitting strategy demonstrated evident advantages compared with previous methods: (1) a large amount of monomers can be adopted even without specific functional groups, (2) facile synthesis conditions and low cost are easy to scale up, (3) result in materials with abundant microporosity and high surface area, and (4) modulation of microporous structure and functionality networks is simple, thus providing a novel pathway for the construction of functional polymers or materials with unique micromorphology.

The environmental issues are always the human concerns. The change in a global climate caused by excessive CO_2 emissions has attracted widespread public attention in recent years [131]. CO_2 capture and storage (CCS) technology is a

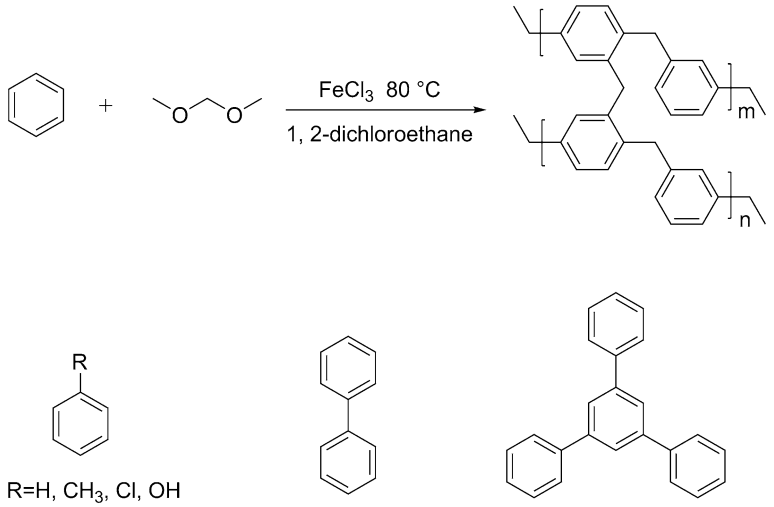

Fig. 4.15 Knitting rigid aromatic building blocks with FDA crosslinker. Reproduced from Ref. [130] with kind permission of © 2011 American Chemical Society

promising method using MOPs as physical adsorption material in which high adsorption capacity should be the key factor [132]. Enormous research has shown that the introduction of functional groups such as carboxyl and amine may enhance the CO_2 adsorption and selectivity for CO_2/N_2 by increasing the interactions between adsorbent and adsorbate [133–135].

Prof. Cooper thought highly of this strategy which extended the approach to a wide range of low functionality aromatic monomers, and these materials possessed more promising CO_2 uptakes at the higher pressures that are relevant to precombustion CCS [136]. By employing this knitting method, firstly they successfully synthesized a series of amino group containing polymer networks by the copolymerization of aniline and benzene [137]. Varying the monomer ratio leaded to a highest BET surface area of up to 1100 $m^2\ g^{-1}$ as well as an improved CO_2/N_2 selectivity up to 49.2; however, the entire benzene network only showed a CO_2/N_2 selectivity of 15.9. Polymerization of alcohol-containing monomers using knitting process produced microporous networks with surface areas of up to 1015 $m^2\ g^{-1}$ [138]. Moreover, synthesis of chiral networks without any complex monomer involvement is also successful. The investigation of CO_2 adsorption performance for these materials in "wet" condition showed that hydrophobicity endures a much smaller drop in CO_2 capacity which could be an important point to consider in the future design of sorbents for CO_2 capture. To move forward one step, they tested the CO_2 adsorption behaviors for several different kinds of microporous materials including carbon, zeolite 13x, ZIF-8, HKUST-1, and FDA knitting polymers [136]. The results showed that unlike other polar adsorbents, the hydrophobic FDA knitting polymers are hardly affected by the water vapors and adsorb CO_2 in a different way by physical swelling thus giving rise to a higher CO_2 capacity and

much better CO_2 selectivity. As a result, these knitting polymers have superior function as a selective gas adsorbent as would be required for materials preparation on the large industrial scale required for carbon capture.

By adopting this knitting method, some other researches focus on the development of constructing polymer networks using novel building blocks with special functional groups such as amino, hydroxyl, carbazole, and triptycene.

Zhu group [139] successfully prepared highly porous materials derived from amino and hydroxyl containing tetrahedral monomers with apparent surface areas up to 1230 and 1608 $m^2\ g^{-1}$, respectively. According to their functionality, the corresponding polymer networks revealed enhanced CO_2 adsorption capacities and higher heats of adsorption than the non-functionalized materials.

Dai and co-workers produced triazine- and carbazole-bifunctionalized task-specific porous polymers via the Friedel–Crafts reaction with surface areas of 563 and 913 $m^2\ g^{-1}$, respectively [22]. The resultant porous framework exhibits a comparable 18 wt% CO_2 uptake (273 K, 1 bar) and 38 selectivity for CO_2 over N_2. In addition, a series of novel carbohydrate-based microporous polymers were synthesized by knitting various hydroxyl-functionalized carbohydrate monomers [140]. BET surface areas around 800 $m^2\ g^{-1}$ were obtained as well as a considerable amount of CO_2 adsorption of 12 wt% with a 42 CO_2/N_2 selectivity at 273 K. Several factors including the quantity and reactivity of hydroxyl groups and the structure of the carbohydrate monomers that contributed to CO_2 adsorption were discussed indicating these microporous polymers' promising applications in carbon capture.

Han group [141] also selected two carbazole-based building blocks for constructing knitting porous materials via $FeCl_3$-promoted one-step oxidative coupling and Friedel–Crafts reaction. N_2 adsorption analysis confirmed that these networks were permanently microporous with BET specific surface areas around 1190 $m^2\ g^{-1}$. Besides the H_2 and CO_2 storage, these microporous networks also exhibited potential application in eliminating harmful small molecules from the environment such as toluene and formaldehyde.

Jiang group reported several kinds of knitting microporous organic polymers synthesized from a series of functional monomers containing hydroxyl, carbazole, and silole. The polymer networks based on tetraphenylethylene (TPE) and/or 1,1,2,2-tetraphenylethane-1,2-diol (TPD) [20] displayed surface areas ranging from 1980 to 618 $m^2\ g^{-1}$ with a decrease in CO_2 adsorption capacities. However, the CO_2/N_2 selectivity enhanced to the highest 119 with the TPD content increase. The carbazole-based knitting polymers [142] showed a comparatively performance in CO_2 storage and separation with 1845 $m^2\ g^{-1}$ high surface area. Novel silole-containing monomers were also used for building knitting aromatic polymers with similar surface areas around 1200 $m^2\ g^{-1}$ [143]. The introduction of silicon atom enhanced the binding affinity between the adsorbent and CO_2 molecules, thus resulting in a slight higher CO_2/N_2 selectivity compared with other non-functionalized MOPs. The activated carbon materials with high surface area of 2065 $m^2\ g^{-1}$ were obtained directly by potassium hydroxide-activated carbonization of a nitrogen-rich knitting polymer based on *N*,*N*,*N*′,*N*′-

tetraphenylbiphenyl-4,4′-diamine (DTPA) monomer [144]. An extreme high CO_2 uptake up to 6.51 mmolg^{-1} (1.13 bar/273 K) was obtained with a comparable 57 CO_2/N_2 selectivity. Considering the high surface area and good gas sorption performance, these knitting polymers are promising for CO_2 capture industrial applications.

Triptycene and its derivatives have earned a large amount of attention in supramolecular chemistry and materials science fields due to their specific three-dimensional rigid structure and easy functionalization. Zhang group has synthesized two series of triptycene-based knitting microporous polymers from hexaphenylbenzene-based triptycene [145] and tricarbazolyltriptycene building blocks [146]. According to the N_2 adsorption/desorption analysis, the obtained surface areas were 569 and 893 m^2 g^{-1}, respectively. With high thermal stability and comparable high surface area, these porous polymers are promising candidates for H_2 storage and carbon capture. In addition, triptycene monomer can be knitted with FDA crosslinker directly which resulted in high surface area reaching 1426 m^2 g^{-1} [147]. With hierarchical porosity, this kind of knitting polymer could be used as adsorbent for organic solvents and dyes in water treatment application.

The knitting strategy can also be directly used for crosslinking heterocyclic aromatic building blocks. Tan group [148] synthesized heteroatom-decorated knitting polymers using three typical heterocyclic molecules pyrrole, thiophene, and furan as monomers (Fig. 4.16). The BET surface areas were about 437–726 m^2 g^{-1} which were much lower compared to the benzene-knitted polymer network. However, the introduced heteroatoms provided excess lone electron pairs on the network skeleton which enhanced the binding affinity to CO_2 molecules by dipole–dipole interaction. As a result, Py-1 shows an extraordinarily high selectivity of CO_2/N_2 about 117 at 273 K which was the highest among all the microporous materials reported at that time.

Saleh et al. [149] explored more heterocyclic monomers including indole (IN), benzothiophene (BT), benzofuran (BF), carbazole (CBZ), dibenzofuran (DBF), and dibenzothiophene (DBT) for the construction of heteroatom-functionalized knitting polymers. Based on the N_2 sorption analysis, the synthesized polymer networks showed diversified surface areas in the range of 391–1022 m^2 g^{-1}. By attributing to

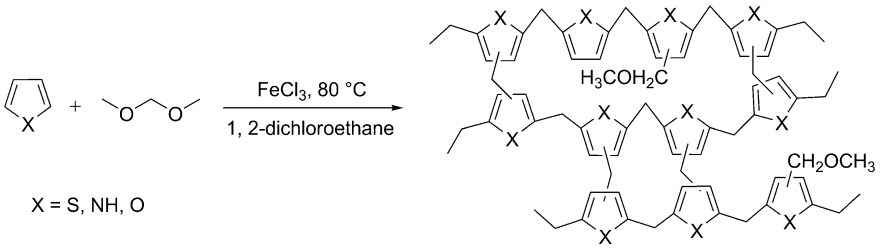

Fig. 4.16 Synthesis of aromatic heterocyclic microporous polymers via the knitting strategy. Reproduced from Ref. [148] with kind permission of © 2012 Wiley-VCH

their electron-rich electronic essence, these materials not only displayed high selective adsorption of CO_2/N_2 but also exhibited stable selective adsorption of CO_2/CH_4.

For organic chemistry field, the cheap and renewable CO_2 is an ideal carbon source. As a result, the incorporation of CO_2 capture and storage as well as the CO_2 utilization is an attractive potential application. In this respect, functionalized porous materials with both adsorption property and catalytic sites for CO_2 conversion could be promising materials.

Zhang et al. [150] developed a novel series of knitting porous polymers with phosphonium salt incorporated into the networks. By copolymerization triphenylphosphane (PPh_3) salts with benzene monomer, high surface area of 1168 $m^2\ g^{-1}$ was obtained with a moderate CO_2 uptake. These knitting microporous polymers can be used as catalysts for the conversion of CO_2 with propylene oxide into propylene carbonate which revealed a higher catalytic activity than the PS-supported phosphonium catalyst.

As is mentioned above, this knitting strategy via the Friedel–Crafts alkylation reaction proposed a simple and efficient synthetic route forming cost-effective porous materials with special functionality which can be promising solid sorbents for practical application in CCS technologies.

Moreover, the knitting strategy was also adopted for the preparation of heterogeneous catalyst [151–155]. Tan group [154] synthesized a phosphorus-decorated knitting polymers by crosslinking PPh_3 with benzene and then Pd was banded with PPh_3 groups to form KAPs(Ph–PPh_3)–Pd catalyst. The BET surface area was found to be 1036 $m^2\ g^{-1}$ for the knitting polymer network, which however showed no obvious decrease after binding with Pd (1025 $m^2\ g^{-1}$). The resulting networks showed a uniform dispersion of Pd nanoparticle owing to their refined microporous structure, and the heterogeneous nature improved the reactant diffusion of small molecules. As a result, the KAPs (Ph–PPh_3)–Pd exhibited excellent activity and selectivity for the Suzuki-Miyaura cross-coupling reaction of aryl chlorides in an aqueous ethanol solution under mild conditions. Following this study, three N-heterocyclic carbenes were successfully integrated into the skeleton of the knitting polymer for Pd loading [155]. BET surface area as high as 1229 $m^2\ g^{-1}$ was achieved. Due to the substantial porosity and individual pore structure, the catalyst afforded rapid conversion for the Suzuki-Miyaura cross-coupling reactions including various aryl halides and arylboronic acids in aqueous media. In particular, it can be used for 5 times without obvious inactivation.

The knitting methods can also be used for the synthesis of metal-free heterogeneous photocatalysts which contain photoactive-conjugated organic semiconductor units such as 4,7-diphenylbenzo [1, 2, 5] and thiadiazole (BT-Ph_2) [156]. The resulting photocatalysts were directly employed for a visible light-promoted, highly selective bromination reaction using HBr as a bromine source and molecular oxygen as a clean oxidant, however, without transition metal. High catalytic efficiency and good reusability were observed within the materials. The utilization of the simply prepared knitting microporous polymer photocatalyst opens new opportunities toward a sustainable and efficient material design.

The knitting microporous polymers were also prepared into electron sensor devices. Zhang et al. [157, 158] investigated the humidity sensing properties of the 3-hydroxybenzoic acid monomer-based knitting porous polymers. After loading LiCl salt [157], the sensors revealed good humidity sensing properties that the impedances dropped with the increase of relative humidity which is attributed to the interaction between the loaded LiCl and water molecules. In addition, the enhanced humidity sensing properties can be obtained when the knitting materials were loaded with lithium hydroxide [158]. Therefore, the lithium-modified knitting polymers could be a new category of humidity-sensitive materials.

In general, the utilization of this simple and efficient knitting strategy has greatly expanded the variety of hypercrosslinked polymers as well as application range by incorporating different functional monomers. In addition, this strategy was also adopted for the preparation of microporous materials with precisely controlled micromorphology such as nanoparticles [159], hollow microcapsules [5–7], two-dimensional polymeric membranes [8, 9, 160], and monolithic blocks [14, 15].

Hollow microporous organic capsules (HMOCs) combining the advantages of microporosity and nanocapsule were fabricated via the hard templating methods in which nano-SiO_2 was used as core template (Fig. 4.17) [7]. SiO_2@PS-DVB precursors with core–shell structure were prepared via a simple traditional emulsion polymerization process. After the knitting and etching approach, the HMOCs were obtained with specific hollow morphology and high surface areas up to 1129 $m^2\ g^{-1}$. By adjusting the DVB concentration, the resulting surface areas can be easily controlled which revealed a decreasing trend with the increasing DVB content. With hollow cavity inside, these HOMCs showed a much higher ibuprofen adsorption compared with the solid nanoparticles. Moreover, the controlled microporous structure made HOMCs to possess zero-order drug release kinetics demonstrating their attractive applications in medical field.

Compared to hollow capsule model, two-dimensional polymeric membranes have greater superiority for molecular level separation applications in industrial-scale chemistry, energy, and environment fields. Dai and co-workers [9] developed a facile one-pot approach for the synthesis of polymeric molecular sieve membranes by using non-porous polystyrene membrane as precursor via an in situ knitting process (Fig. 4.18). The resulting knitting polymeric membrane showed a sandwich porous structure comprising a dense microporous layer with an inner

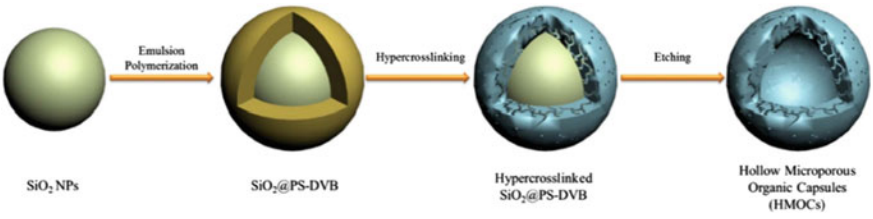

Fig. 4.17 Preparation of hollow microporous organic capsules. Reproduced from Ref. [7] with kind permission of © 2013 Macmillan Publishers Limited

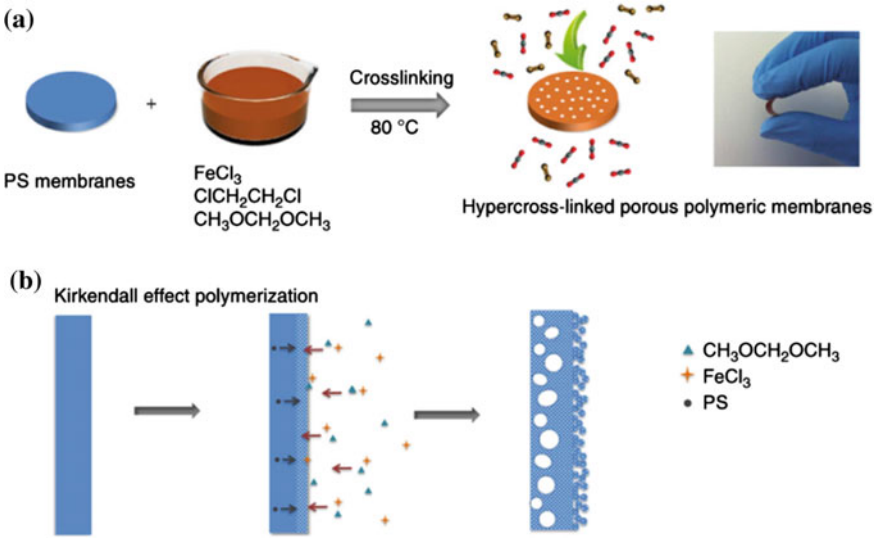

Fig. 4.18 **a** Synthesis of knitting microporous polystyrene membranes, **b** Mechanism for the formation of hierarchical porous structure. Reproduced from Ref. [9] with kind permission of © 2014 Macmillan Publishers Limited

macroporous core and outer mesoporous surface formed by small polymer particles. N_2 sorption analysis demonstrated the hierarchical porous structure showing type 1 reversible sorption isotherms with a slight hysteresis loop at relative high pressures. The BET surface areas varied from 218 to 618 $m^2\ g^{-1}$ with the crosslinking time increasing, while the CO_2 permeability increased from 222.2 to 5261 barrer. On the contrary, the CO_2/N_2 selectivity decreased to 18.5 from 30. The high permeability and good selectivity indicated the promising potential applications in gas separation.

Based on this novel in situ concept, Kim et al. synthesized the knitting microporous polystyrene ionic liquid membranes via an in situ crosslinking of polystyrene membrane precursors [8, 160]. The 1-allyl-3-methylpyridinium bromide ionic liquid was incorporated into polymer matrix directly by dissolving in DMF solvent with polystyrene. Followed by a casting process, the polystyrene ionic liquid membranes were obtained. After coordinating with ferric [8] and nickel salts [160], these membranes were applied for the catalysis of H_2 generation from sodium borohydride and 4-nitrophenol reduction, respectively.

Compared with other specific micromorphology, three-dimensional macroscopic hierarchical porous monolith forms have attracted significant attention due to the rapid mass transport driven by convection through the internal connecting pores. Svec and co-workers reported the preparation of porous polymer monoliths by knitting styrene-type polymers involving three external crosslinkers BCMBP, DCX, and FDA [15]. Polymeric monoliths with surface areas reaching up to 900 $m^2\ g^{-1}$ were obtained using BCMBP as crosslinker in only 2.5 h knitting

process. Owing to the high surface area and interconnecting hierarchical porous structure, the monoliths as the stationary phase for liquid chromatography delivered a significant improvement in efficiency in the reversed phase separation of small molecules. Tan group [14] also synthesized hierarchical porous polystyrene monoliths by knitting poly(styrene-divinylbenzene) high internal phase emulsions. BET surface areas of 196–595 $m^2\ g^{-1}$ were obtained by N_2 sorption analysis with interconnecting well-defined macroporous, mesoporous, and permanent microporous structure. Owing to the interconnected cellular structure as well as the hydrophobicity in the skeleton, these monoliths exhibited a fast equilibrium and high adsorption capacity for organic solvents.

In summary, the knitting strategy using FDA as external crosslinker has become a very practical method for the preparation of hypercrosslinked polymer with multifunctionality and special micromorphology, while the surge to expand the synthesis strategy never stops.

4.3.4 Summary

Hypercrosslinked polymers have experienced an extended exploration in the design, synthetic strategy and potential applications since the discovery by Davankov. According to the development, there are mainly three synthetic routes: (1) post-crosslinking polymer precursors, (2) direct one-step polycondensation of functional monomers, and (3) knitting rigid aromatic building blocks with external crosslinker. Among them, the external knitting strategy has been proved to be a facile and efficient method and widely adopted for the synthesis of functional polymers or materials with unique micromorphology.

Even though, there also exists some challenges for developing HCPs. For example, the polymer networks of HCPs are highly irregular due to their fast dynamical character of the Lewis acid catalytic reaction. The huge amount heats generated by hypercrosslinking and hydrogen chloride released from unavoidable catalyst hydrolysis are also intractable problems for large-scale industrial production. Looking for new synthetic approaches for higher surface area HCPs which can be more than 3000 $m^2\ g^{-1}$ is always highly desired. HCPs with controllable structure and new function will be a prolonged research hot spot with broad applications in photoelectricity, sensors, and semi-conducting devices.

4.4 Conjugated Microporous Polymers

CMPs, firstly reported in 2007 [25], are a class of microporous organic polymers consisting of π-conjugated segments totally bonded by covalent bonds, which inherently combine π-conjugated skeleton with microporous structure.

Porous architecture of CMPs can be controlled by molecular design, for instance, the surface areas and pore volumes can be easily tuned by using different monomers with various molecular lengths. Moreover, employment of diverse functional modules is feasible to construct CMPs. By selecting proper monomers, CMPs usually can be synthesized by conventional metal-catalyzed reactions, such as Sonogashira–Hagihara coupling [161], Suzuki coupling [162], Yamamoto couplings [163], oxidative polymerizations [164], and Schiff base reaction [165]. CMPs materials are always prepared by irreversible reactions, so they are usually amorphous and show short range of structural order. The pores are accessible to various guest molecules and metal ions, which allow the construction of supramolecular structures and organic–inorganic hybrids. Compared with crystalline COFs and MOFs, amorphous CMPs can be synthesized more easily by linking the appropriate organic building units to achieve functionalization and the functional groups can be fully exposed. The incorporation of new functional groups into CMPs has generated numerous new functional materials.

Although most of the works focus on developing new strategies, tuning the pore size distribution and surface area of CMPs, some efforts have already been made to control morphology, such as quasi-zero-dimensional (0D) microspheres [162], one-dimensional (1D) nanofibers and nanotubes [166], two-dimensional (2D) nanosheet structures [167], as well as three-dimensional (3D) monoliths [168]. What's more, the development of soluble CMPs also remains to be well explored [169].

CMPs have attracted tremendous attention and become one of the fastest developing types of porous materials. These kinds of material allow the complementary utilization of π-conjugation and porosity, which are unique and usually not available in other porous materials. Such structural features bring CMPs a large number of exciting properties and potential applications, such as gas storage [170], catalysis [171], sensors [163], and anode materials [172].

4.4.1 Synthesis and Modification

Typically, linear polymers are created with two end groups monomers ($A_2 + B_2$). As for three-dimensional CMPs, one or more monomers with more than two end groups ($A_x + B_y$, $x > 2$, $y > 2$) are needed.

4.4.1.1 Synthesis Method

Laybourn et al. [173] studied the framework formation mechanism of CMPs. The results showed that monomer concentration, solvent, temperature, and building block structure would affect the network formation in complex situations (Fig. 4.19). Firstly, oligomers are formed in solution, which resulted in clusters. And then, these clusters precipitate from solution and continue to react in solid state

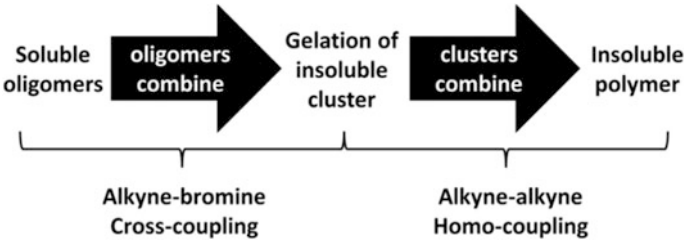

Fig. 4.19 Proposed reaction mechanism for the formation of CMP networks. Reproduced from Ref. [173] with kind permission of © 2014 American Chemical Society

by crosslinking, which lead to the formation of CMPs frameworks at last. The initial precipitated material exhibits a low degree of microporosity and significant interparticulate mesoporosity; true microporous materials are only formed at longer time upon fusion of the clusters and further crosslinking within the particles. Xu et al. [174] disclosed that the linkage geometry plays a vital role in the control over the porosity, gas adsorption, π-conjugation, exciton migration, and luminescence of CMPs. Works from Dawson et al. [175] and Tan et al. [176] showed that the choice of the reaction solvent is also important.

Many CMPs have been synthesized with miscellaneous polymerization, including Suzuki coupling reactions [177], Sonogashira coupling [25], Yamamoto coupling reaction [178], oxidative coupling polymerization [179], Schiff base chemistry [180], and electropolymerization (EP) [181] etc.

Suzuki cross-coupling reaction is one of the most powerful one-step pathways for the formation of carbon-carbon bonds [162] (Fig. 4.20a). Typically, Suzuki coupling reactions are performed under homogeneous conditions using a variety of phosphine ligand/palladium catalytic complexes. However, oxygen will cause the formation of homocoupling and deboronation by-products. Consequently, the Suzuki reaction often needs to be performed under highly oxygen free condition. Sonogashira coupling reaction which introduces acetylenyl groups in CMP frameworks is one of the most studied reactions among all the synthetic methods for the fabrication of CMPs [161] (Fig. 4.20b). Moreover, triple bonds may lead to a more rigid and extended network structure and can be used to adjust the porosity [182], and pore size and surface area [183]. At the same time, the final properties of CMPs can also be affected by the reaction conditions. Yamamoto coupling reaction is a C–C coupling of aryl-halogenide compounds mediated by transition metal complexes [163] (Fig. 4.20c). Only halogen-functionalized monomers are involved, while on the other hand, stoichiometric quantities of the nickel complexes are also important. Oxidative coupling polymerization has cost-effective advantages in the preparation of CMPs. CMPs materials can be prepared in large scales by oxidative coupling polymerization which shows advantages of adopting cheap catalyst, with low room temperature and only need single monomers [164] (Fig. 4.20d). Catalyst can be completely removed by easy purification [184]. Schiff base chemistry is a novel synthetic strategy for CMPs, which is a catalyst-free and

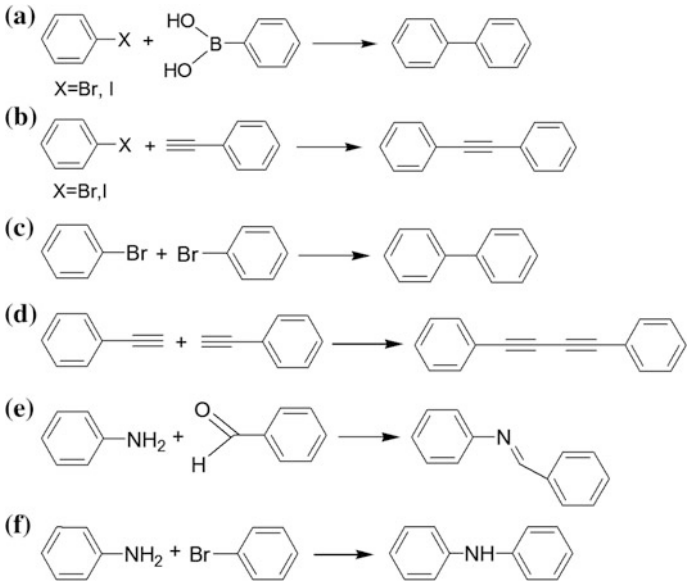

Fig. 4.20 Reactions have been successfully used for the construction of CMPs [161–165, 185]

one-pot reaction. Schiff base chemistry can build nitrogen-rich CMPs networks with high surface areas [165] (Fig. 4.20e). Buchwald–Hartwig (BH) coupling is utilized for the generation of C–N bonds via the palladium-catalyzed cross-coupling of amines with aryl halides [185] (Fig. 4.20f). The BH coupling approach allows the expansion of repertoire of possible C–N bond formation through the facile synthesis of aromatic amines. This useful method also provides a simple route to nitrogen-containing redox-active systems.

Direct arylation polymerization is a new method for synthesizing CMPs [186]. However, CMPs synthesized by direct arylation polycondensation are only limited to monomers containing two-arm fluoroarenes and nitrogen-free tri- or tetra-bromoarenes (Fig. 4.21).

Electropolymerization has been proven to be a useful method for fabricating electroactive CMPs films, which is an in situ polymerization of CMPs precursors or monomers [197]. The precursors are dissolved at first, and then, the coupling reaction occurs on the electrode surface. At last, the CMPs films depose on the electrode (Fig. 4.22). This strategy is of low cost, without catalyst, and controlled thickness of the film can be obtained.

4.4.1.2 Modification

The incorporation of metal sites into CMPs opens up the second-generation porous materials. Porphyrin which possesses macrocyclic cavity basic pyrroles is widely

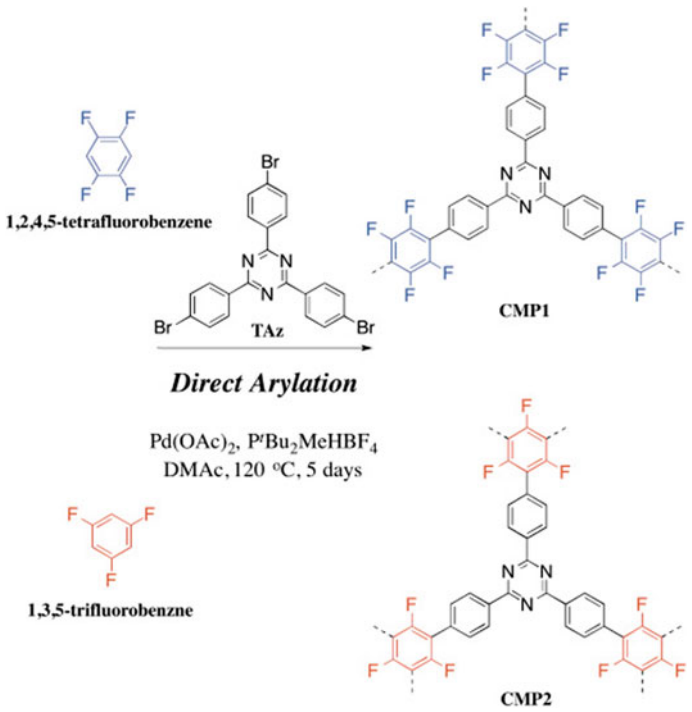

Fig. 4.21 Direct arylation polycondensation of fluoroarene monomers with TAz into CMPs. Reproduced from Ref. [186] with kind permission of © 2016 Elsevier

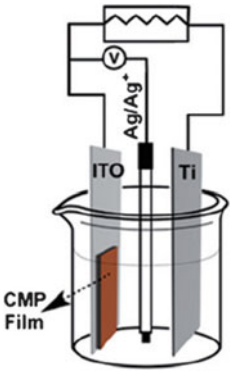

Fig. 4.22 Setup of the three-electrode electrochemical cell for the polymerization of monomers and the deposition of CMPs films on ITO. Reproduced from Ref. [197] with kind permission of © 2015 Wiley-VCH

used in CMPs to form modified CMPs. Some metal-porphyrin CMPs using metal-porphyrin (metal: Zn, Co, Cu, Fe, Ni, etc.) as monomer have shown combined chemical and physical properties for applications in catalysis [187–190], supercapacitor [191], photosensitizer [192], and adsorption [89]. Metal ions (Fe and Al) can also be introduced into porphyrin-based CMPs and show good performance

in adsorption [184] and CO_2 capture [193]. Some other methods are also used to introduce metals into CMPs framework. Jiang et al. [194] prepared MO-CMP by two methods: post-treating bipyridine-functionalized CMPs with metal complexes (Re, Rh, and Ir) and the direct Sonogashira–Hagihara cross-coupling of halogenated metal-organic monomers. Fischer et al. [195] copolymerized $Li[B(C_6F_4Br)_4]$ with 1,3,5-triethynylbenzene using Sonogashira coupling $[Mn^{II}(bpy)]^{2+}$ complex and then immobilized in the CMP networks which is a promising catalyst for the aerobic oxidation of alkenes. Xie et al. [196] reported a class of Co/Al-coordinated CMPs which exhibit outstanding CO_2 capture comparable to MOFs.

Lee et al. [198] prepared CMPs by Sonogashira coupling and then prepared CMP-Co_3O_4 composites via organometallic complexation of cobalt carbonyl with microporous organic networks (MONs) and the successive oxidation. The materials showed the enhanced stability as anode materials.

Some organic molecules are also used as modifiers. For example, thiolyne can be introduced into CMPs networks [199–201]. Ratvijitvech et al. [202] reported the post-synthetic modification of amine-functionalized CMPs by anhydrides to build a series of amide-functionalized networks.

4.4.2 Control of Morphology

Morphology is an important factor in CMPs properties. Many efforts have been focused on the morphology control. Normally, template strategy and stepwise method have been used to control CMPs morphology.

4.4.2.1 Template Strategy

Template strategy is a straightforward method to build CMPs with specific morphology similar to the template. Zhuang et al. [203] reported a graphene-inspired synthetic approach for the preparation of sandwich-like CMP. Furthermore, they demonstrated a series of heterostructures CMPs with 0D, 1D, or 2D morphology, by using bromo-functionalized carbon nanospheres (0D CSs), single-walled carbon nanotubes (1D SWNTs), and reduced graphene oxide (2D RGO) as templates. The resulting CMPs showed nanosphere, nanotube, and nanosheet morphologies, and then carbonized. They found that the performance of these nanocarbon-based zinc-air batteries using nanocarbon as air electrode was affected by morphology (2D > 1D > 0D) [204]. Son group studied the synthesis of new functional MONs based on Sonogashira coupling by template strategy. SiO_2 [205, 206], Fe_3O_4 [187, 207], zeolites [208], and MOF [209] were used as templates, and the resulting materials showed good performances as catalysts [187, 206], precursor of inorganic materials [205, 207], and adsorbents [208, 209]. Tan et al. [210] reported a one-step synthesis of nanoscale CMP (NCMP) capsules by using PMAA microspheres as

self-sacrificial templates. The morphology, nanostructure, and shell thickness can be precisely controlled.

4.4.2.2 Stepwise Method

By controlling reaction conditions, CMPs with different morphology can be obtained. Tan et al. [176, 211] found that reaction solvents and the structure of monomers would influence the morphologies of the polymers (sphere, tubular, and plate). Ma et al. [212] illustrated the design principle and the synthesis of CMPs nanoparticle (Fig. 4.23).

Chun et al. [166] studied the mechanism of the formation for tubular CMPs synthesized by Sonogashira coupling (Fig. 4.24). Briefly, the formation of three types of structures (1D connection, interconnection of 1D chains to 2D networks, and 3D networking) occurred at the same time in which competition happened among them. The kinetic differences in these competitions may lead to morphology anisotropy. At last, tubular CMPs were formed. In order to optimize CMPs performance, thin films play a crucial role. The method to fabricate CMPs films mainly focuses on surface-initiated [167], layer-by-layer crosslinking [213, 214], casting soluble CMPs [169, 215], and electropolymerization [181, 191, 197, 216, 217]. First investigated by Cooper's group [169], efforts have been focused on the solubility of CMPs (SCMP). Hu's group demonstrated a "catalyst@pore" method to synthesize SCMPs by utilizing a well-defined silica-supported carbon nanomembranes as the nanoreactors by which the SCMPs particle size can be controlled by tuning the pore size of the nanoreactor [218, 219].

Up to now, the development of general and effective methods for the preparation of high-performance CMPs monolithic materials is still remained a huge challenge. Du et al. [220] reported CMPs aerogels derived from drying the gel matrix (Fig. 4.25). At the same time, high internal phase emulsion (HIPE) polymerization has been proved to be an efficient technique in building CMPs monolithic materials [221].

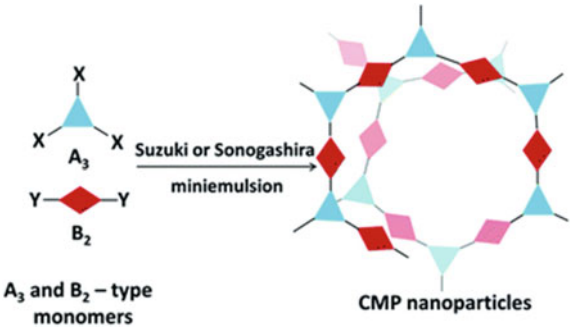

Fig. 4.23 Synthetic route to CMP NPs via (A_3 + B_2)-type Suzuki-Miyaura or Sonogashira–Hagihara cross-coupling polycondensation reactions in an oil-in-water miniemulsion system. Reproduced from Ref. [212] with kind permission of © 2015 Royal Society of Chemistry

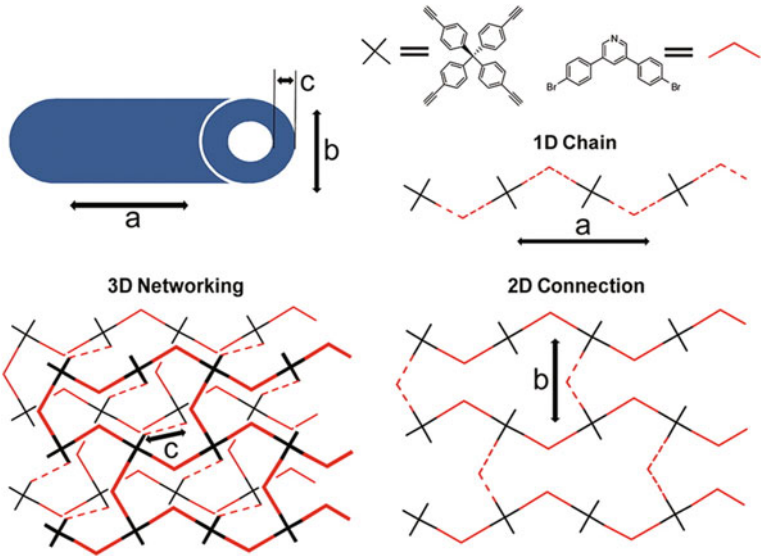

Fig. 4.24 Suggested mechanistic aspects of tubular CMPs. Reproduced from Ref. [166] with kind permission of © 2012 American Chemical Society

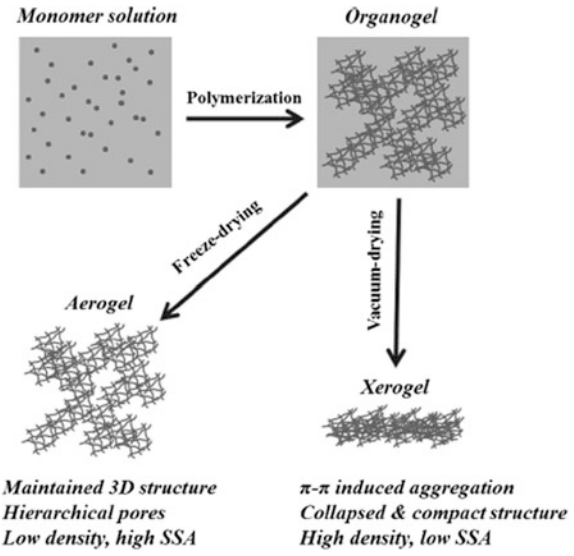

Fig. 4.25 Schematic illustration of the structure and preparation procedures for the PTEB aerogel and xerogel. Reproduced from Ref. [220] with kind permission of © 2014 Wiley-VCH

4.4.3 Application

4.4.3.1 Absorbent and Gas Storage

CMPs with structural tunability and high porosity have great potential to be developed as efficient absorbents. In the past few years, most studies have focused on the synthesis of CMPs with specific chemical and physical properties for chemical capture, sequestration, and separation. CMPs have been provided as efficient absorbents absorbing toxic chemicals such as amines [208, 222], iodine [89, 223], toluene [184, 209], benzene [224], and oil [168, 225].

CMPs possess π-conjugation along the main chain, which provides CMPs the potential in gas storage. It is known that gas adsorption performances of CMP materials depend on the character of building blocks. By introducing N, S, O elements into CMPs structure, CO_2 adsorption performance will be improved due to the strong interactions with CO_2 molecules [164, 182, 226–229]. What's more, Fischer et al. [230] fabricated CMPs with weak coordinating cations in their backbone. The material presented a CO_2 uptake of 2.49 mmol g^{-1} at 273 K and 1 bar and 2.85 mmol g^{-1} after ion exchange with chloride. A class of Co/Al-coordinated CMPs reported by Xie et al. [196] exhibited outstanding CO_2 capture comparable to metal-organic frameworks.

4.4.3.2 Battery and Supercapacitors

Considering environmental problem, clean and sustainable energy systems have been investigated. With a high degree of π-conjunction, homogeneous microporous structure, high surface area, and flexibility in the molecular design, CMPs have enormous potential as electrode materials for energy storage devices. Lee et al. [198] reported MON-Co_3O_4 composites and studied its applications as anode materials in lithium-ion batteries. Zhang et al. [231] synthesized CMPs from 4,7-dicarbazyl-[2,1,3]-benzothiadiazole (PDCzBT) by $FeCl_3$ oxidation coupling polymerization which exhibited excellent electrochemical performance for Li and Na storage including high specific capacity, outstanding cycle stability, and superior rate performance.

As material with 2D morphology can be benefit for energy storage, CMPs films now are studied as potential electrode materials in supercapacitors [191, 232, 233]. The reported materials all had high specific capacity, superior cycle stability, and remarkable rate capability. What's more, CMPs also can be carbonized as efficient supercapacitor materials due to its conjugated structure [204, 207, 234].

4.4.3.3 Catalyst

CMPs, combining the photoactive π-electron backbone and porous surface properties, have been recently introduced as stable heterogeneous photocatalysts for organic synthesis [235], such as oxidative coupling [206, 212, 236, 237], and oxidative hydroxylation of arylboronic acid [238]. Metal CMPs possess catalytic activities to reactions including carbene insertion into N–H bonds [187], carbon dioxide conversion to cyclic carbonates [190], Suzuki coupling reactions [239], and oxygen reduction reaction [189].

Furthermore, Zhang et al. [164] synthesized carbazole-based multifunctional CMPs which act as an efficient heterogeneous organocatalyst for Knoevenagel condensation with high activity, wide substrate adaptability, and good recyclability. Wang et al. [240] envisioned that chiral organometallic catalysts could be introduced into the structure of CMPs for the first time.

4.4.3.4 Fluorescence Property and Sensor

Large surface areas of CMPs provide a broad interface for interaction between analyte and sensor materials. Liu et al. [163] reported the first example of a chemosensing CMPs, which allow the material to achieve rapid responses and dramatically enhanced detection sensitivities. In sensing applications, solution-processible fluorescent porous materials based on CMPs are useful. Wu et al. [241] succeeded in developing solution-dispersible CMPs which exhibited a selective and sensitive fluorescence quenching response to 2,4,6-trinitrotoluene (TNT). Up to date, attentions have been paid to prepare fluorescence films. CMPs are possible to tune their electronic and photophysical properties by modifying the optical band gap. Cooper's group introduced different comonomers and varied the monomer distribution to tuned CMPs photophysical properties by controlling optical band gaps in CMPs [242, 243]. Ma et al. [244] obtained dendrimer films by EP method, which were verified to be rapid response, highly sensitive, and excellent reusable fluorescence probes for TNT vapor, Fe^{3+}, and benzene vapor.

4.4.3.5 Others

Jin et al. [245] studied the entrapment and release behavior of hollow CMPs spheres toward guest molecules, which can be controlled by media. At the same time, by using an appropriate solvent, guests could be entrapped into the cavity of the hollow structure. Based on the controlled release behavior of the guest-entrapped CMPs materials, a fluorescent alert system for organic solvent existence in water can be developed.

Tan et al. [210] synthesized nanoscale CMPs capsules by using PMAA microspheres as self-sacrificial templates. The resulting material showed a tunable absorption ability and shape-dependent photothermal conversion efficiency. Upon

exposure to 808 nm light, these materials rapidly generated heat and caused thermal ablation of HeLa cells with less than 10% viability.

4.4.4 Summary

CMPs are a class of MOPs that combine π-conjugation structure with porosity. A wide variety of chemical reactions are used to build CMPs with different structures and functionalities. The flexibility of molecular design and the tunable structure make CMPs extensive applications in various fields. However, the synthesis of CMPs with controlled morphologies and functionalities is still a challenge.

4.5 Polymers of Intrinsic Microporosity

Over a long period of time, tremendous efforts of porous materials have been devoted to the research of macroporosity and mesoporosity [246, 247]. However, it was largely unexplored for preparing pure organic microporous networks within polymeric materials [248]. It has been known that active carbon is used in various aspects as adsorbents, catalyst supports, and deodorizers [249, 250]. Considering its vast commercial value while with the limited quantities for systematic chemical and structural modification, researchers were inspired to imitate the structure of active carbon, and thus, a wide range of PIMs were developed.

The main chains of PIMs are constructed with rigid and contorted molecular structures, which cannot fill space efficiently [16]. Unlike conventional microporous materials, PIMs are soluble and can be processed readily for enormous applications. It is worth noting that microporous structure of PIMs will maintain either in solid state or in liquid state, which offers wide applications in gas separation, heterogeneous catalysis, hydrogen storage, and so on.

4.5.1 Preparation of Polymers of Intrinsic Microporosity

Initially, the Pc macrocycle was selected as the basic unit by Mckeown and co-workers owing to its extended planarity and unique property [251]. The structural diversity of Pc-containing polymers and their optical and electronic properties made them suitable for a wide range of applications. However, due to strong non-covalent interactions (predominantly π–π interactions), the prepared Pc-containing polymers showed a strong tendency that the aromatic units tend to aggregate into columnar stacks, leading to non-porous solids, which failed to form microporous architecture. Hence, it is essential to introduce a highly rigid and nonlinear linking group between the phthalocyanine subunits to ensure the

space-inefficient packing, thus avoiding structural relaxation and consequent loss of microporosity. To fulfill these requirements, they introduced microporous structure into phthalocyanine subunits, and obtained the first Pc-containing PIMs in the later 2002 [252]. A nonlinear linking group derived from the commercially available 5,5′,6,6′-tetra-hydroxy-3,3,3′,3′-tetramethyl-1,1′-spirobisindane (**A1**) was designed to connect phthalocyanine subunits and provided the nonlinear shape by means of efficient dioxane-forming reaction between **A1** and 4,5-dichlorophthalonitrile (**B1**), to produce a rigid phthalocyanine microporous polymer network (Fig. 4.26). They also confirmed that the spirocyclic crosslinking prevents a compact packing of the phthalocyanine components, which resulted in an amorphous microporous structure. Nitrogen adsorption measurements showed that the materials possessed high surface areas in the range of 450–950 $m^2\ g^{-1}$, with significant adsorption at low relative pressure ($p/p_0 < 0.01$) indicating microporosity.

Following on the progress of these phthalocyanine-based polymers of intrinsic microporosity (Pc-network-PIMs), other rigid structures are also investigated to determine whether they are suitable components for constructing microporous organic materials. Due to the potential heterogeneous catalysis properties, metal-containing porphyrins are treated as desirable components of microporous organic materials. Nevertheless, the preparation of porphyrins is a low-yielding process, which is unsuitable for polymer network assembly. To conquer this difficulty, rigid spirocyclic linking groups were introduced directly into preformed porphyrin subunits by means of the efficient dioxane-forming reaction between the mesotetrakis(pentafluorophenyl) porphyrin (monomer **B2**) and the monomer **A1** [253]. A number of useful applications were obtained for heterogeneous catalysis by supporting porphyrins within or on the surface of materials matrix. A synthetic strategy based on the reaction of preformed porphyrin **1** was devised. For the

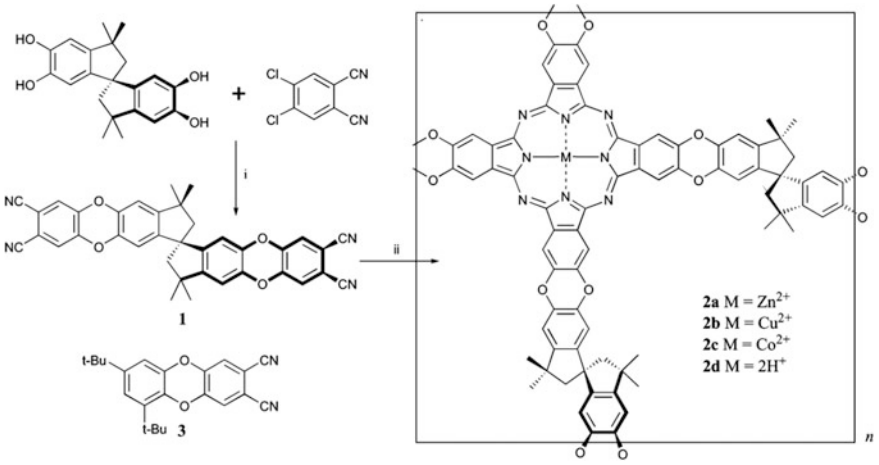

Fig. 4.26 Synthetic route of Pc-network-PIMs. Reproduced from Ref. [252] with kind permission of © 2002 Royal Society of Chemistry

preparation of the bis(phthalonitrile) precursor into the phthalocyanine network polymers, a facile reaction between 5,5′,6,6′-tetrahydroxy-3,3,3′,3′-tetramethyl-1,1′-spirobisindane **2** and 4,5-dichlorophthalonitrile was used. Porphyrin network polymers were directly prepared from **1** and **2** via dibenzodioxane formation, and the resulting porphyrin-network-PIM demonstrated to show high surface areas around 1000 $m^2\ g^{-1}$.

It offers a general reaction from the formation of Pc-network-PIMs and Porphyrin-network-PIMs by dioxane formation reaction which links planar aromatic macrocycles with a rigid spirocyclic spacer [33]. It can be concluded that for microporosity, at least one of the monomers must contain rigid contorted structure, which may be a spirocentre (e.g., **A1** and **B8**), a non-planar rigid skeleton (e.g., **A2**, **A4**, and **A6**), or a single covalent bond around which rotation is hindered (e.g., **A7**, **B1** and **B7**). If reaction occurs between two planar monomers (e.g., **A5** with **B4**), the non-porous material will be formed finally (Fig. 4.27).

It has been described in 2003 by Tattershall and co-workers for the earliest synthesis of a nanoporous network polymer incorporating 5,6,11,12,17,18-hexaazatrinapthylene (HATN) rigid functional units through the efficient dibenzodioxane forming reaction [254]. The described HATN-network-PIM, derived from the spiro-monomer **A1** and HATN **B2**, exhibited high surface areas in the range of 750–850 $m^2\ g^{-1}$ and was suitable as catalytic support which provided a high loading of accessible active sites. It also indicated a potential application as adsorbents for the removal of toxic organic compounds such as phenols from water or gas streams.

Of particular interest is the potential to tune the microporous structure by choosing different monomer precursors, and one of the examples is the utilization of monomers that contain preformed cavities to provide sites of an appropriate small size for hydrogen adsorption. In 2007, a novel triptycene-based PIM (Trip-PIM)

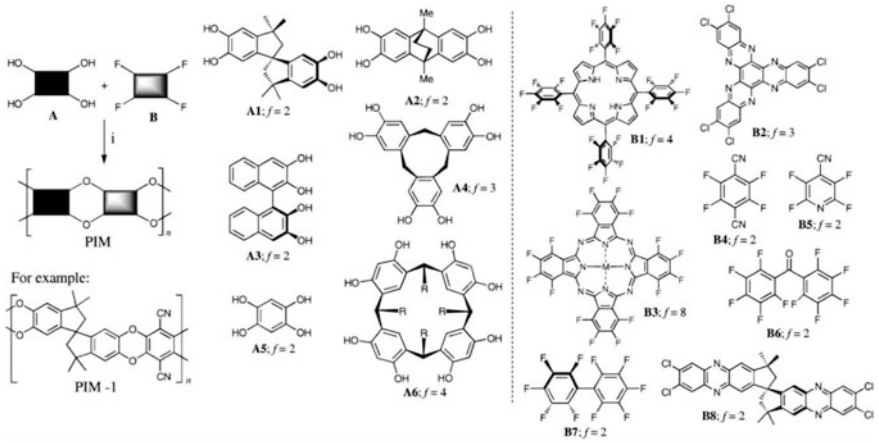

Fig. 4.27 Synthesis and properties of PIMs. Reproduced from Ref. [33] with kind permission of © 2006 Royal Society of Chemistry

was developed and displayed enhanced surface area of 1065 $m^2\ g^{-1}$, and reversibly adsorbed 2.71% hydrogen by mass at 10 bar/77 K [255]. The effective blocking of close, face-to-face association between these fused-ring struts may be helpful to further frustrate space-efficient packing of the macromolecules leading to larger microporosity. Following this work, in 2010, Mckeown et al. reported the synthesis of network-PIMs derived from triptycene monomers containing alkyl groups attached to their bridgehead positions [256]. Gas adsorption can be controlled by varying the alkyl chains, and the apparent BET surface area of the materials was within the range of 618–1760 $m^2\ g^{-1}$. Shorter alkyl chains or chains with branched structure provided the materials with larger microporosity, while longer alkyl chains appear to block the microporosity created by the rigid organic framework.

Since some of network-PIMs displayed swelling property in the presence of an adsorbate, researchers have sorted for new types of intrinsic microporosity which could be obtained from a linear polymer without a network structure. As can be seen from the previous results, insoluble network-PIMs possess both high surface areas and hydrogen storage which may be attributed to highly covalent connected network structure resulting in larger microporous volume. The microporosity within network-PIMs is maintained by a robust network of covalent bonds. It is reasonable to anticipate that above a certain amount of free volume, the voids would be interconnected, and therefore, the polymer will behave as a conventional microporous material despite the lack of a network structure. Such a material could be soluble and would facilitate solution-based processing, which provides advantages over other microporous materials.

In 2004, Budd et al. demonstrated that a network of covalent bonds is not an essential aspect for microporous organic materials. A family of non-network polymers was described which formed microporous solids simply because their highly rigid and contorted molecular structure cannot fill space efficiently. Under this guidance, they successfully synthesized the first soluble PIM using the same dioxane-forming polymerization reaction between the aromatic tetrol monomers **A1–A3** with the appropriate fluorine-containing compounds **B1–B3**, in which microporosity arises simply from a polymer whose molecular structure is highly rigid and contorted so that space-efficient packing in the solid state is frustrated [16]. The lack of rotation freedom along the polymer backbone ensures that the macromolecules cannot rearrange their conformation to collapse the open structure of the material. Consequently, the polymer molecular structure remains intact which maintains the microporosity. PIM-1 showed highest surface area among PIM 1–6 up to 850 $m^2\ g^{-1}$. Nitrogen sorption analysis indicated a significant proportion of micropores with dimensions in the range of 0.4–0.8 nm. There was also evidence of some mesoporosity that the marked hysteresis at low pressures may be attributed to pore network effects.

For the purpose of enhancing hydrogen adsorption, Mckeown et al. incorporated the bowl-shaped receptor monomer, cyclotricatechylene (CTC), within a network-PIM by using benzodioxane-forming reaction via CTC and tetra-flurotere-phthalonitrile [257]. The hydrogen adsorption property of CTC-network-PIM (0.56 wt%) is much higher than that of PIM-1 (0.5 wt%) and

HATN-network-PIM (0.43 wt%), which suggests that the greater predominance of ultramicropores resulting from the bowl-shaped CTC subunits enhances hydrogen adsorption.

In 2007, Thomas and co-workers expanded the concept of dibenzodioxane-based, soluble, ladder-type polymers to more common polymers of higher commercial interest, such as polyamides (PA) or polyimides (PI) [18]. They used 9,9′-spirobifluorene as the structure-directing motif since it can be easily modified to give 2,2′-dicarboxy-9,9′-spirobifluorene or 2,2′-diamino-9,9′-spirobifluorene compounds, and formed aromatic polyamides, polyimides, or poly(benzimidazole)s (PBI) PIM-P4. They showed intrinsic microporosity and consequently high surface areas of 550 $m^2\ g^{-1}$. Before this work, the synthesis of polyimides based on a spirobifluorene monomer has already been reported, but no attention was paid to the investigation of microporosity. Compared to linear PI, these polymers showed superior properties in terms of solubility and processability.

In the later 2008, Ghanem et al. prepared novel PIMs via bis(phenazyl) monomers derived from readily available bis(catechol)s [17]. They described the simple synthesis of suitable reactive tetrachloride monomers 4 and 5 based on phenazine units. PIMs 7–9 are soluble in several organic solvents (especially $CHCl_3$), but PIM-10 is soluble only in m-cresol and concentrated H_2SO_4, and the films from PIM-7 are particularly flexible and robust. Nitrogen sorption analysis provides an apparent surface area of 680 $m^2\ g^{-1}$ for PIM-7. The promising gas permeability data for PIM-7 confirms that PIMs are excellent for designing highly rigid but solution-processible polymers, which combine high selectivity with high permeability as required for the fabrication of efficient gas separation membranes.

In 2009, Yampolskii et al. reported a series of PIM-PIs prepared by reacting with various aromatic diamines of bis(carboxylic anhydride) containing spirocenters [258]. Membranes were directly prepared by casting from chloroform solution. In comparison with other polyimides, these novel groups of PIM-PIs showed especially good results for the separation of the mixtures CO_2/CH_4 and CO_2/N_2. The gas separation properties exceeded most of the permeable conventional polyimides.

In 2011, Mckeown et al. introduced a rigid and propeller-like shape unit, hexaphenylbenzene (HPB) into polymers, resulting in HPB-PIM-1 and HPB-PIM-2 derived from 1,2- and 1,4-di(3′,4′-dihydroxyphenyl)tetraphenylbenzene monomers, respectively [259]. The inefficient molecular packing of benzene rings led to intrinsic microporosity. HPB-PIM-2 showed significantly lower permeability similar to PIM-1 but enhanced selectivity ($CO_2/N_2 = 26$), which can be attributed both to lower diffusivity due to lower intrinsic microporosity and lower solubility due to a smaller concentration of polar groups such as ether and nitrile. Owing to the advantages of these aspects, HPB-PIM-2 was still attractive for gas separation.

In general, improving carbon dioxide capture by introducing functional groups often results in the loss of the accessible pores and surface area. While in the year 2012, Yavuz and co-workers reported the first noninvasive functionalization of the

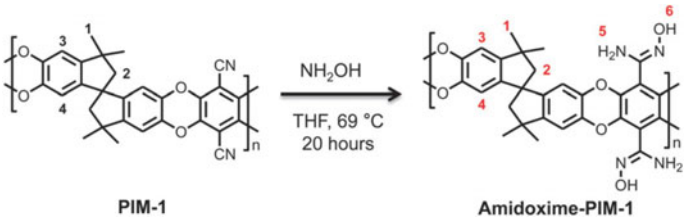

Fig. 4.28 Synthetic pathway of amidoxime-PIM-1. Reproduced from Ref. [260] with kind permission of © 2012 Royal Society of Chemistry

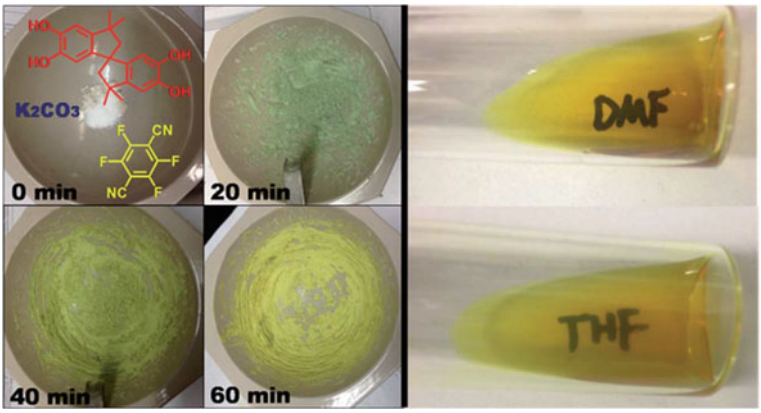

Fig. 4.29 Preparation of PIM-1-MS and 1 wt% solution in different solvents. The big difference between PIMs and common polymers arouses great interest of researchers. Reproduced from Ref. [261] with kind permission of © 2015 Royal Society of Chemistry

PIMs by introducing the amidoxime groups in PIM-1 (Fig. 4.28) without adversely affecting physicochemical properties [260]. Incorporating amidoxime group increased a carbon dioxide adsorption capacity up to 17 wt%, and the amidoxime-based PIM-1 still exhibited good processability without losing the film-forming ability.

In 2015, Dai et al. reported a solvent-free mechanochemical approach to construct PIM-1-MS and PIM-4-MS polymers with high molecular weight and low polydispersity by solid grinding [261]. Both the number average molar mass (M_n) and weight average molar mass (M_w) were much higher than PIM-1 and PIM-4 polymers, while the value of M_n/M_w and surface area was much lower (Fig. 4.29).

4.5.2 Applications

4.5.2.1 Gas Permeability and Separations

Due to the wide applications for commercial, it has been a hot topic to explore polymeric membranes with both high gas permeability and separation. Before the appearance of PIMs, polymers with high permeability, like poly[1-(trimethylsilyl)-1-propyne] (PTMSP), often revealed low selectivity [262]. As well, polymers with high selectivity usually met with low permeability. As to microporous polymer materials, membranes made from PIM-1 and PIM-7 show higher selectivity compared with polymers which have similar permeability [263]. At the same time, the selectivity of CO_2/CH_4, H_2/N_2, and H_2/CH_4 is all relatively high, which indicates the superior performance of PIMs.

In terms of the separation of O_2 and N_2, the key factor is the mobility selectivity. PIMs are more likely to adsorb smaller oxygen molecule (diameter = 0.346 nm), rather than the larger nitrogen molecule (diameter = 0.364 nm). For microporous polymers, it initially depended on the micropores size distribution, while PIM-1 and PIM-7 have rather smaller pore size.

Regarding how to improve the performance of gas permeability and selectivity of PIMs membranes, researchers have also carried out a large amount of researches and achieved some progress. In 2013, Mckeown et al. used the Tröger's base (TB) polymerization reaction to prepare ethanoanthracene-based TB polymer and spirobisindane-based TB polymer, which extended the polymerization types of PIMs (Fig. 4.30) [264]. BET surface areas of 1028 $m^2\ g^{-1}$ for PIM-EA-TB and 745 $m^2\ g^{-1}$ for PIM-SBI-TB are obtained, respectively, and theses PIMs were proved to be highly soluble in chloroform and can be prepared into thin films readily.

In 2014, Jansen and co-workers used borane complexes to reduce nitrile groups in PIM-1 forming the amine-PIM-1 [265]. The incorporation of primary amine decreased the CO_2 diffusion coefficient and permeability, while enhanced the

Fig. 4.30 Synthesis and molecular structures of PIM-EA-TB and PIM-SBI-TB (*left*). A solvent cast film (10 cm in diameter) of PIM-EA-TB (*right*). Reproduced from Ref. [264] with kind permission of © 2013 The American Association for the Advancement of Science

banding affinity for CO_2 and the sorption selectivity of CO_2/N_2 and CO_2/CH_4. Colina et al. reported a functionalized PIM with carboxylate backbone [266]. It was found that the enthalpy of CO_2 adsorption and adsorption capacity increased, which can be attributed to the increasing concentration of ions. Meanwhile, the selectivity of CO_2/N_2 and CO_2/N_2 enhanced in accordance with the increasing ion content.

Shamsipur and co-workers prepared a hydroxyl-functionalized polyimides using 2,2-bis(3-amino-4-hydroxyphenyl)hexafluoropropane and 4,6-diamino-resorcinol monomers, which was followed by a thermal treatment at 450 °C under N_2 for 1 h yielding the polybenzoxazole polymers (Fig. 4.31) [267]. This conversion increased membrane gas permeability and CO_2/N_2 selectivity, and also enhanced solvent resistance. Although the microporous structure and chemical functionalities enable PIMs with high gas uptake, permeability and selectivity, and solvent-resistant nanofiltration properties [268–271]. One major obstacle to the commercialization of glassy amorphous PIMs for membrane application is physical aging and the ensuing instability of their permeation property over time. In 2015, Pinnau et al. investigated the effect that relatively extreme intra-chain rigidity and high ultramicroporosity in some of the most permeable and selective PIMs potentially alleviate long-term physical aging and plasticization [272]. Through this work, they found this physical aging occurs in all PIMs despite their high interchain rigidity. Meanwhile, the inherent chain architecture plays an important role in physical aging. And finally, higher interchain rigidity does not prevent plasticization.

Various approaches have been made to avoid physical aging including copolymerization [273], crosslinking [274], and surface plasma treatment [275]. In 2014, Sivaniah and co-workers reported thermo-oxidative crosslinking of PIM-1 by heating in a suitable temperature window (350–450 °C) in the presence of trace amount of oxygen [276]. The pore size distribution, structure of channel and pore can be successfully tailored and subsequently increase the selectivity. The thermal-oxidative crosslinked PIM-1 (termed as TOX-PIM-1) polymer exhibited

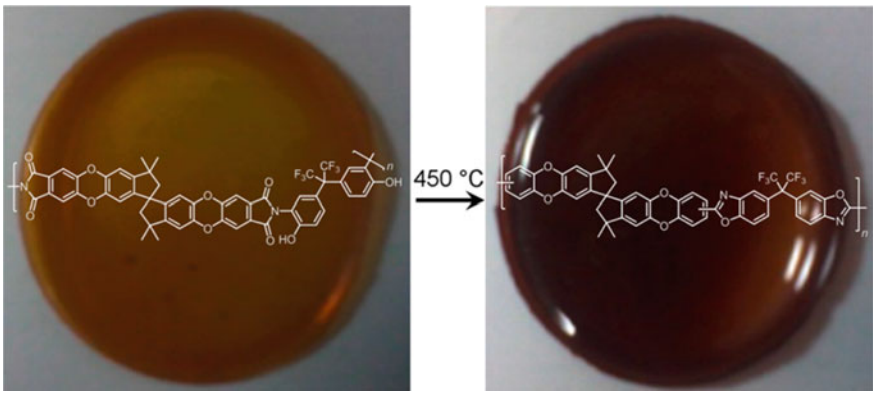

Fig. 4.31 PIM-PBO membrane derived from PIM-PI-OH membrane. Reproduced from Ref. [267] with kind permission of © 2014 American Chemical Society

decreased solubility compared with PIM-1 (Fig. 4.32). After crosslinking at 385 °C, the CO_2/CH_4 selectivity of TOX-PIM-1 membrane increased up to 70, along with a high CO_2 permeability of 1100 barrer. In 2015, the Sivaniah and co-workers incorporated nanofillers into TOX-PIM-1 polymer which combined the covalent crosslinking of microporous polymers [277]. This thermal oxidative crosslinking of the PIM-1 polymer improved the gas selectivity of nanocomposites; meanwhile, the gas permeability remained at a remarkably high level. After aging for two years, they tested the gas separation properties again and demonstrated a higher selectivity.

Although these methods can successfully reduce aging, there still exists a big challenge for the performance loss in permeability. One efficient method to overcome this challenge is incorporating a secondary phase to form a mixed matrix membrane. In 2016, Casiraghi and co-workers combined PIMs with graphene, and formed PIM-1/graphene (PIM-1/Gr) composites [278]. The presence of PIM-1 enhanced the direct exfoliation of graphene in chloroform, and the graphene concentration played an important role in the efficiency of the process and stability of the resulting dispersion. It has been proved that there is strong re-stacking of initially exfoliated graphene in solution when forming the composites, which is expected to produce strong promotion in mechanical properties and physical aging of the membranes.

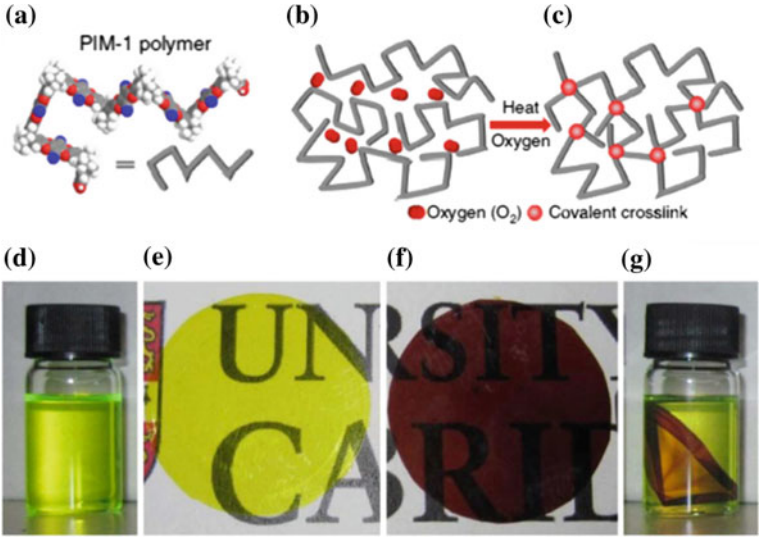

Fig. 4.32 **a** An ideal molecular model of PIM-1 polymer chain segment. **b**, **c** Two-dimensional schematic illustration of thermal oxidative crosslinking. **d** Photograph of PIM-1 polymer solution in chloroform. **e** Photograph of as-prepared PIM-1 membrane. **f** Photograph of TOX-PIM-1 membrane. **g** Solubility test of TOX-PIM-1 membrane in chloroform. Reproduced from Ref. [276] with kind permission of © 2014 Macmillan Publishers Limited

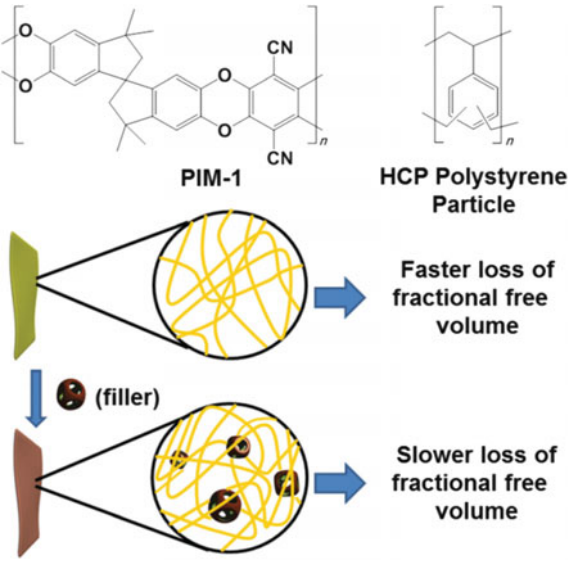

Fig. 4.33 Molecular structure of PIM-1 and the hypercrosslinked polymer used as the filler (*top*). Schematic illustration of effect of filler on the performance of MMMs. Reproduced from Ref. [279] with kind permission of © 2016 Royal Society of Chemistry

The free volume in PIMs will diminish over time, thus limiting the real application. Besides the nanofillers mentioned above, other new types of fillers are also selected to enhance the properties of PIMs. Cooper et al. reported a mixed matrix membrane by adding hypercrosslinked polystyrene as a filler into PIM-1 [279]. Since hypercrosslinked polymers possess water- and acid-tolerant properties, these mixed matrix membranes not only resulted in higher permeability but also alleviated polymer aging and permeability loss (Fig. 4.33).

4.5.2.2 Heterogeneous Catalysis

Usually, PIMs network containing porphyrin, phthalocyanine, or hexaazatrinaphthylene subunits could be used for catalysis by incorporating appropriate transition metal ions. For example, PcCo-network-PIM could be used for the degradation of hydrogen peroxide and showed a great enhanced rate compared to a non-porous microcrystalline model compound. In addition, this network-PIM is efficient for the catalysis of the oxidation of cyclohexene to 2-cyclohexene-1-one (78% yield after 48 h) which was comparable to the cobalt phthalocyanine-based homogeneous catalysts. The HATN subunits are well-established ligands capable of forming a complex with up to three transition metal ions. By exposing the orange HATN-network-PIM to a chloroform solution containing bis(benzonitrile) palladium(Π) dichloride, the resulting material catalyzed a model Suzuki aryl-aryl coupling reaction with high efficiency, however that around 20% of the metal leached from the PIMs.

Similar palladium-containing materials with even higher specific surface area can be derived from PIM-7 by exploiting the ability of its phenazine subunits which act as ligands for metal ion coordination. This material contained over 20% by mass Pd^{2+} and showed a surface area of 650 $m^2\ g^{-1}$. It can be deduced that the Pd^{2+} ions act as bridges between the PIM macromolecules to result in a network. Of great interest, a solvent cast film of PIM-7, swollen in methanol, can also be linked by Pd^{2+} to give an insoluble network.

In 2014, Mckeown and co-workers synthesized PIM-TB-Trip microporous polymer networks, which were assembled from triamino-triptycene monomers using Tröger's base forming polymerization reaction [280]. BET surface areas up to 1035 $m^2\ g^{-1}$ for PIM-TB-Trip-1 and 752 $m^2\ g^{-1}$ for PIM-TB-Trip-2 can be obtained, respectively. These materials possess high catalytic efficiency for Knoevenagel condensation reaction between benzaldehyde and malononitrile compounds.

In 2016, Marken and co-workers developed a composite film electrode by incorporating traditional carbon microparticles into PIM-EA-TB with a BET surface area of 1027 $m^2\ g^{-1}$, then immobilized the free radical 4-benzoyloxy-2,2,6,6-tetramethyl-piperidine-1-oxyl (4B-TEMPO) on the surface of electrode [281]. Good access of solvent, substrate to catalyst site through rigid pores, and stabilization toward corrosion allow the porous PIM-EA-TB polymer to act as a host matrix for embedding free radical catalyst, thus improving the catalytic process for primary alcohols oxidation in a carbonate buffer at pH 10.3 (Fig. 4.34).

4.5.2.3 Hydrogen Storage

Under the condition of 77 K/1 bar, three PIMs (PIM-1, HATN-network, and CTC-network) are measured for their hydrogen adsorption properties with efficient H_2 uptake of 0.56 wt% for CTC-network, 0.43 wt% for HATN-network, and

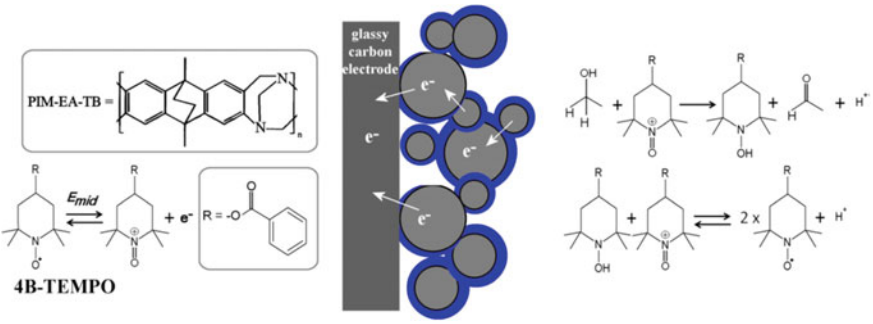

Fig. 4.34 Structure of the PIM-EA-TB polymer and 4B-TEMPO (*left*). Scheme showing the composite film with electrocatalyst embedded in PIM-EA-TB on carbon microparticles (*right*). Reproduced from Ref. [281] with kind permission of © 2016 Springer

0.5 wt% for PIM-1, respectively [257]. The bowl-shaped CTC subunits showed enhanced H_2 adsorption due to the greater predominance of ultramicropores. These results indicate that PIMs adsorb comparable amounts of H_2 to that of the best examples for zeolites and MOFs. Moreover, unlike all other types of microporous materials, the structures of PIMs are not necessarily constrained by a fixed network structure and may be dissolved in suitable solvents and swollen by several non-solvents. In order to achieve practical hydrogen storage materials from PIMs, it will be necessary to explore examples with higher surface areas (>2000 $m^2\ g^{-1}$) while maintain the predominately ultramicroporous structure which is necessary to retain the beneficial multiwall interactions with H_2 molecules.

4.5.2.4 Other Applications

Except for the wide applications in gas separation and adsorption, heterogeneous catalysis, and hydrogen storage, PIMs have been employed in some of the unexplored fields. In 2015, chiral PIMs have been developed for selective membrane permeation of enantiomers by Shea and co-workers [282]. They reported the synthesis of chiral ladder polymers, (+)-PIM-CN and (+)-PIM-COOH, by using 5,5′,6,6′-tetrahydroxy-3,3,3′,3′-tetramethyl-1,1′-spirobisindan building blocks. The as-prepared chiral polymers were found to be strongly effective in the selection of a range of enantiomers. Marken et al. discussed the vacuum carbonization of PIM-EA-TB in generating a novel type of microporous heterocarbon materials in 2015 [283]. Compared to traditional organic precursors which usually causes tremendous structural damage and vanish of morphology under vacuum carbonization, the rigid molecular backbone of PIM-EA-TB was retained even carbonized under 500 °C in vacuum. Although the BET surface area decreased drastically from 1027 to 242 $m^2\ g^{-1}$, microporosity increased considerably. Further study showed an interesting switch of electrochemical properties to higher pH-dependent capacitance from ca. 33 Fg^{-1} (oxidized) to ca. 147 Fg^{-1} (reduced), without significant electron transfer reactivity toward oxygen and toward hydrogen peroxide, and conductivity of approximately 40 MΩ/square for a ca. 1–2-μm-thick film.

4.5.3 Limitation and Challenge of Development

Compared with other MOPs materials, PIMs have advantages which can be listed as follows: Linear PIMs can be easily dissolved in suitable organic solvents, which makes it possible to test molecular weight by using gel permeation chromatography (GPC). This parameter provides information for controlling the reaction conditions. Furthermore, membranes with microporous structure can be obtained by casting, and then applied to gas separation and adsorption, and even the selectivity of CO_2, H_2, CH_4, and so on. Moreover, PIMs show great potential in hydrogen storage and gas adsorption. The main problem for the development of PIMs is that surface areas

cannot achieve very high value as well as the limited contorted structure and toneless types of polymerization. In addition, how to enhance the gas permeability and separation property also needs further discussion.

4.6 Macroporous Polymers

Porous polymers which are normally quiet low in density and very high in porosity have gained considerable attention and research. And when there are interconnected pore canals in polymer framework, high permeability and large effective surface area can be achieved [284, 285]. The different kinds of porous polymers with appropriate pore structure show potential applications in catalysts [102, 286–288], waste oil and wastewater treatment [14, 289–291], tissue engineering scaffolds [292–296], and separation [276, 297]. To satisfy the various application requirements, macroporous polymers are always designed with an adjustable pore structure and a high porosity. Compared to the microporous and mesoporous materials, macroporous materials have obvious advantages of fast mass transfer and simple separation [14, 293, 294]. The complex macrostructures can be achieved either by the incorporation of a functional comonomer into the HIPE [289, 298], or via a post-polymerization functionalization approach [14, 299] as well as the use of 3D printing [300, 301]. At present, macroporous materials prepared by feasible HIPE templates exhibit advantages in controllable pore size as well as inherent high porosity by varying the volume ratio of dispersed phase and continue phase.

HIPEs are defined as the untraditional emulsions which are highly viscous, paste-like emulsions with the internal volume ratio above 74% [285]. At present, polyHIPEs from water-in-oil (W/O) HIPEs and oil-in-water (O/W) HIPEs are becoming more and more common. The investigation range of HIPEs has been expanded a lot including supercritical CO_2-in-water (CO_2/W) HIPEs, non-aqueous oil-in-oil (O/O) HIPEs, and oil-in-ionic liquid (O/IL) HIPEs. In addition, the use of ionic liquids can extend the range of synthesis temperatures, which has been limited by the presence of water, to above 100 °C [302]. In recent work, the ionic liquid-in-oil (IL/O) HIPEs have been synthesized of which the external phase (20%) was lauryl methacrylateand and the internal phase (80%) was a 1.15 wt% solution of bis(trifluoromethane) sulfonimide lithium salt in 1-ethyl-3-methylimidazolium bis(trifluoromethylsulfonyl)imide. The ability to synthesize water-free polyHIPEs could have a major impact upon polyHIPEs development, expanding the types of polymerization reactions that are sensitive to the presence of water (step growth polymerizations, anionic, cationic, or metathesis chain growth polymerizations) [303].

A typical polyHIPEs porous structure with voids and interconnecting holes can be achieved once the appropriate surfactant concentration is determined. Internal phase contents of over 74% can be reached for monodispersed droplets through their deformation into polyhedral. Meanwhile, the internal phase can also be obtained through the formation of a polydisperse droplet size distribution.

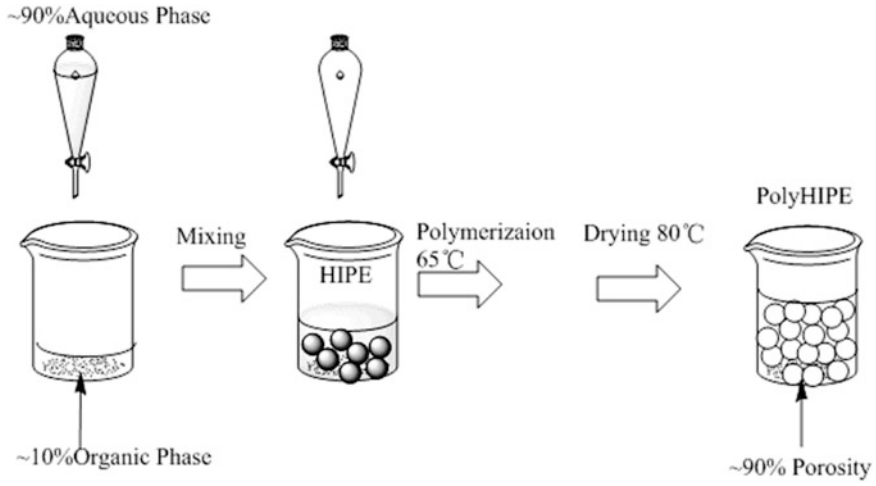

Fig. 4.35 Schematic illustration of HIPE formation and polyHIPEs synthesis in a W/O HIPE that contains an aqueous internal phase dispersed in a hydrophobic monomer external phase. Reproduced from Ref. [285] with kind permission of © 2014 Elsevier

Theoretical analysis has shown that the formation of polyhedral from monodispersed droplets should be favored over the formation of a polydisperse droplet size distribution [284, 285]. The conventional HIPEs are based on amphiphilic surfactants, such as sorbitan monooleate (Span 80), cetyltrimethylammonium bromide (CTAB), amphiphilic block polymers, and amphiphilic solid particles. Upon adding surfactants with the amount up to 5–50% into the continuous phase, a stable HIPE can be achieved. In a traditional polyHIPEs, the monomers are only dissolved in a continuous external phase, which surround the dispersed droplets of the internal phase. The formation of a typical W/O HIPEs (an aqueous internal phase dispersed within the hydrophobic monomers in the external phase) and the synthesis of a typical polyHIPE are illustrated schematically in Fig. 4.35.

A "typical" polyHIPE porous structure with voids and interconnecting holes is seen. In the traditional thermally initiated free radical polymerization process, droplet coalescence, volume shrinkage of monomer, and Ostwald ripening occur during polymerization, especially when the elevated temperatures are used for polymerization which enhance diffusion and interfacial destabilization. The widespread formation of such holes transforms the discrete droplets of the HIPE's internal phase into a continuous interconnected phase in the polyHIPEs. Removal of the internal phase, which now becomes continuous, yields voids in place of the internal phase droplets and results in a highly interconnected, open-cell, emulsion-templated porous structure [285, 304, 305]. Recent work on polyHIPEs with tunable void sizes and narrow void size distributions has been carried out for developing theoretical models to describe the relationships between the void size and the mechanical behavior. The formation of open pores can be contributed to

several factors, such as partial coalescence between neighboring droplets, phase separation at surfactant rich phase and polymer rich phase, and volume contraction in the process of conversion from monomer to polymer [305].

The types of polyHIPEs systems developed including copolymers, interpenetrating polymer networks, biodegradable polymers, bicontinuous polymers, organic–inorganic hybrids, porous inorganics, and nanocomposites. PolyHIPEs have also been developed for applications such as chemical synthesis, chromatography, ion exchange, separation, sensing, tissue engineering, and controlled drug delivery. The recent surge in publications on polyHIPE systems mirrors that for porous polymers, the results of a relatively restrictive literature search for articles that contain "polyHIPEs." This part is a brief review and survey of recent advances made in macroporous materials synthesis, structure, and application by polyHIPEs.

4.6.1 Macroporous Polymer Synthesis in PolyHIPEs of W/O

Traditionally, the polymeric surfactants suitable for HIPE preparation have been limited to several kinds of polyethylene oxide (PEO)-based copolymers, such as Pluronic and Hypermer. Recently, more and more efforts have been directed for the design of amphiphilic block copolymers that can be used for the stabilization of HIPEs, which can provide a one-step route for the surface functionalization of the 3D matrix [306]. Wang et al. disclosed a facile and rapid route for tailoring the polymer amphiphilicity, which can enable systematic investigation of the influence of polymer amphiphilicity on the phase behaviors of high internal phase emulsions [307]. A commercial polystyrene-b-polyvinylpyridine (PS-b-P4VP; Mn = 8800 Da; PDI = 1.15) was applied as the surfactant with a water contact angle of 95° which can be obtained by recombining trifluoroacetic acid (CF_3COOH) to adjust the hydrophilization of the P4VP segment. So, it is worth mentioning that this method for tailoring the amphiphilicity of PS-b-P4VP is rather facile and controllable by quaternization reaction. The surfactant with a molar ratio of 1:0.2 of the pyridine rings to carboxyl groups possessed a more extraordinary gel-like property of thixotropic non-Newtonian fluids even if the vial was placed upside down for two weeks and the highest internal phase volume of 95% was achieved with adding 40 mg mL^{-1} of the amphiphilic mixture [307]. Due to its relative low specific surface area, the adsorption capacity of macroporous materials is much smaller that limits their practical applications in treatment of water contamination. Thus, assembling the macroporous materials with nanoscale mesoporous particles could be an ideal solution to overcome these drawbacks, because hierarchical macro- and mesoporous adsorbents will have both of their advantages [14]. Pan et al. [308] fabricated a new hierarchical porous foam with macroporous and mesoporous structure. The macroporous (glycidylmethacrylate) (MPGMA) foams were synthesized by W/O HIPEs template. Then, carboxylated mesoporous silica nanoparticles (CMSNs) were grafted onto the interface of macroporous foams via the chemical bond (Fig. 4.36). Large amounts of carboxyl groups which were

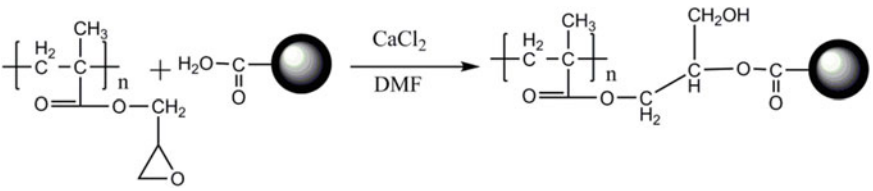

Fig. 4.36 Schematic illustration for the reaction of the MPGMA's epoxy groups with CMSN's carboxyl groups. Reproduced from Ref. [308] with kind permission of © 2016 Elsevier

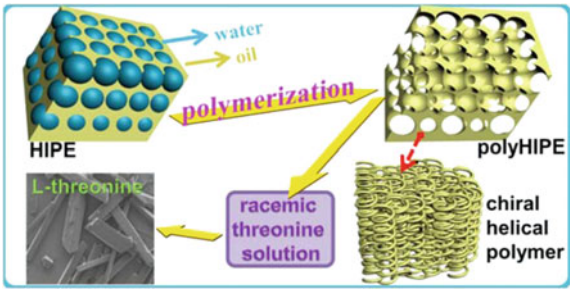

Fig. 4.37 Schematic illustration for the preparation and application of chiral helical macroporous materials. Reproduced from Ref. [298] with kind permission of © 2015 American Chemical Society

introduced into the as-prepared hierarchical porous foams could be benefited for the rapid capture of pollutants. The maximum adsorption capacity of HPFs for λ-cyhalothrin and Cu(II) was 80.11 and 21.79 mg g^{-1} at 288 K, respectively. And the excellent adsorption ability provides more potential opportunities for the HIPEs to be applied in the field of simultaneous removal of λ-cyhalothrin and Cu (II) [308].

A variety of achiral advanced materials have been fabricated through HIPEs and exhibit potential applications such as biomaterials and separation materials. Chiral porous materials combine two special properties, chirality and porosity, which can render the material with smartness by certain stimulation, e.g., optical, PH, and force. However, for chiral porous organic polymers, there have been only a few reports [309]. Meanwhile, the open pore structure in polyHIPEs has a positive effect on the sufficient contact between racemates and polyHIPEs and the bulk polyHIPEs are extremely easily recyclable compared with the other types of induced crystal. Deng group combined the HIPEs approach with chiral acetylenic monomers for preparing a novel, unique type of chiral porous material. The novel macroporous materials consisting of chiral helical polymer by coordination polymerization or free radical polymerization (Fig. 4.37) demonstrated their significant applications as chiral inducers for enantioselective crystallization. The high *cis* content with the max ratio of 90% by measuring the UV–Vis absorption and Raman spectra endowed the polyHIPEs to possess optical activity and exhibited promising application in chiral resolution. Enantioselective L-threonine and L-alanine were successfully induced to crystals from respective racemic solution. For a series of crystallization of racemic threonine, the max enantiomeric excess (ee) was about 74% [298].

4.6.2 HIPE of O/W

Conventional O/W HIPEs are stabilized by surfactants, such as polyethylene glycol tert-octylphenyl ether (Triton X-405), polyethylene glycol dodecyl ether (Brij 35), and poly(ethylene glycol)-block-poly(propylene glycol)-block-poly(ethylene glycol) (Pluronic F68). However, large amounts of expensive surfactants are required to stabilize HIPEs at the concentration of 5–50% with respect to the continuous phase [284, 285]. In recent work, macroporous materials have been used as biomaterials and tissue engineering materials. Pores with size in the range of 25–300 μm in macroporous polymer are required so as to be larger than the dimensions of mammalian cells, which are typically around 20–30 μm. And it is desirable for scaffolds to possess high surface areas (>500 m^2 g^{-1}), high porosities (>90%), and a high degree of pore interconnectivity to facilitate transport of nutrients and oxygen as well as cell migration and cell attachment [310]. Nevertheless, it has been found that the optimal pore size for tissue engineering scaffolds is in the range of 50–300 μm depending on the cell type. Cells are mostly shown to be spreading on the outer surface of the scaffold and have rather limited cell penetration into the scaffolds due to small pore throat in the range of 5–20 μm of hydrophilic polyHIPEs [295]. Then this system allows the injection of cell-laden hydrogel scaffold, which offers significant advantages over other types of rigid scaffolds that require open surgery for their implantation by eliminating possible complications that may accompany invasive surgery or a potential misfit of the scaffold in the defect site because of its ability to construct into a potential defect site.

Bismarck group designed a biocompatible amphiphilic copolymer, specifically gelatin-graft-poly (N-isopropylacrylamide) (GN) (Fig. 4.38a), as surfactant to construct high internal phase emulsion templates, thus proposing an effective and versatile route to create remarkably high porosity and interconnected macroporous foams, which are also biocompatible and suitable as cell carriers. The amphiphilic copolymer without any cytotoxic can stabilize oil phase (p-xylene) in water phase (Fig. 4.38b), which can produce the resultant hydrogel scaffold as biocompatibility

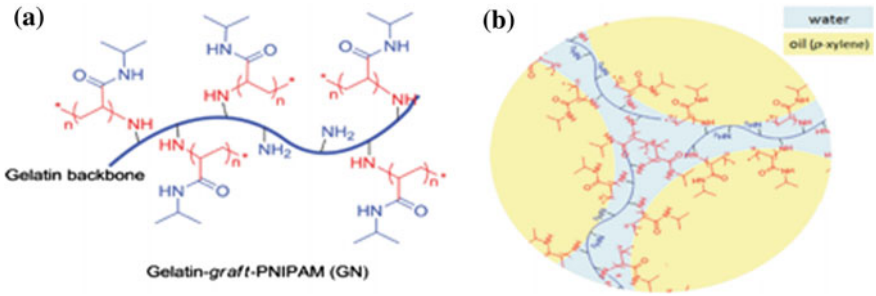

Fig. 4.38 **a** Molecular structure of gelatin-graft-PNIPAM; **b** schematic of the oil (p-xylene)/water interface of HIPE stabilized by GN. Reproduced from Ref. [311] with kind permission of © 2015 Wiley-VCH

materials. In this work, human skin fibroblast cells with large amount of proliferation colonized the bulk surface of the foams, spreading extensively and extending into the scaffold along the pore throats [311]. Due to the dual temperature sensitivity of polyHIPE hydrogel, the cells break the associations between gelatin chains, widen the pores, and loosen the hydrogel network for the cells to penetrate deeper into the scaffold in warm culture medium.

4.6.3 HIPE of CO_2/Water

In order to facilitate the template removal and to avoid the contamination of the porous structure by residual traces of organic solvents, the high internal phase CO_2/W emulsion templating technique was developed [285]. Supercritical carbon dioxide ($ScCO_2$) is a nontoxic, nonflammable, non-expensive, natural solvent and can be used as an alternative to conventional organic solvents for the preparation of high internal phase CO_2/W emulsions [312]. Above 70 bar, the decrease in surface tension (γ) was smaller as CO_2 is less compressible at higher pressures. In this range of higher pressures, the value of the W/CO_2 interfacial tension was close to 20 mNm^{-1}. The requirements for surfactants for lowering the interfacial tension are less stringent than for microemulsions. A potential solution to this problem is to prepare CO_2/W emulsion templates. These are composed of an ionic or neutral hydrophilic head associated with a CO_2-philic tail consisting of fluorinated or branched aliphatic sequences, polysiloxanes or polyvinyl esters [313]. With the exception of fluorinated and silicone-based polymers, CO_2 lacks the solvent power to solvate macromolecules easily. Although these fluorinated or silicone-based materials have been studied as steric stabilizers in dispersion polymerization and as surfactants in preparing CO_2/W or water-in-CO_2 (W/CO_2) emulsions or microemulsions, the associated cost and poor environmental degradability may prohibit their industrial-scale applications. CO_2 is a naturally abundant alternative to the organic solvents, which can be readily removed from a polyHIPEs scaffold simply by depressuring the system as shown in Fig. 4.39. The materials with well-defined porous structures without using any volatile organic solvents, only water and CO_2, are used [314].

In earlier work, Butler et al. used perfluoropolyether (PFPE) surfactants and poly (vinyl alcohol) (PVA) as a co-surfactant to stabilize CO_2/W emulsions of acrylamide polymers [315]. Palocci et al. reported the preparation of dextran-based macroporous materials using supercritical CO_2 as the internal phase and ammonium salt of perfluoropolyether (PFPE, Mw = 550 g/mol) carboxylic acid as the surfactant [316]. Debuigne et al. used sugar-based fluorinated compound as emulsifiers and PVA as co-stabilizer (5% w/v based on water) at 60 °C and 250 bar to prepare highly interconnected macroporous poly(acrylamide) and poly(vinylimidazolium) porous monoliths [314]. Macroporous PAM was a brittle porous sample with the size of large pores (18 μm and cells 30–100 μm). The better performance of the fluorinated surfactant **40b** over the aliphatic **40a** for the polyHIPE synthesis is in agreement with the higher CO_2/W surface activity recorded for **b** compared to **a** as

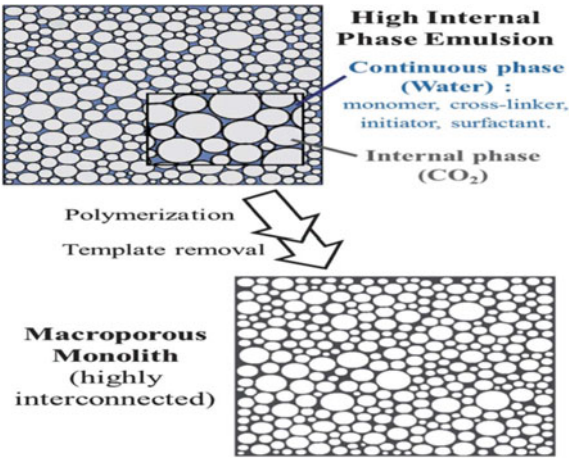

Fig. 4.39 Schematic representation for the fabrication of polyHIPEs. Reproduced from Ref. [314] with kind permission of © 2013 Royal Society of Chemistry

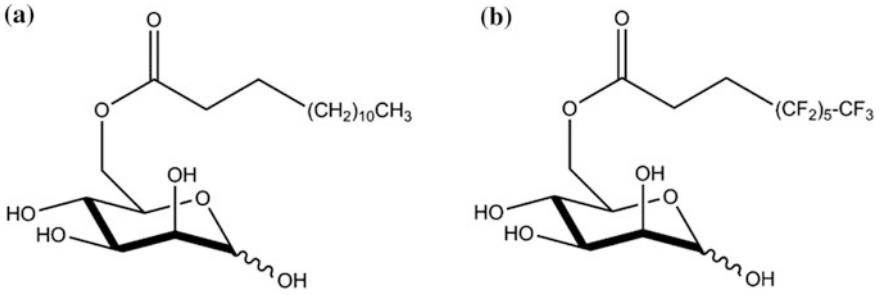

Fig. 4.40 Chemo-enzymatic syntheses of the sugar-based surfactants considered in this study. Reproduced from Ref. [314] with kind permission of © 2013 Royal Society of Chemistry

shown in Fig. 4.40. The beneficial effect of the fluorinated tail on the stabilization of the CO_2/W emulsion and the preparation of PAM polyHIPE was further confirmed when using a surfactant with a longer fluorinated chain.

However, synthesis of these fluorinate polymers and siloxane-based polymers which cannot be degraded in the nature will lead to big environment problems. Considering the principles of green chemistry, the non-fluorous and non-siloxane hydrocarbon is necessary in the $ScCO_2$ application. HIPEs prepared with non-fluorinated surfactants at lower pressures (<120 bar) can also be accessed [312]. In previous work, Da Rocha et al. studied the behavior of poly(propylene oxide)-b-poly(ethylene oxide)-b-poly(propylene oxide) (Fig. 4.41a) at the W/CO_2 interface as a function of their Mw and hydrophilic/CO_2-philic balance (HCB) [317]. A symmetric triblock copolymer comprising 30 propylene oxide units and 26 ethylene oxide has the lowest γ with a slightly turbid W/CO_2 emulsion for

over 10 min using 0.1 wt% of surfactant/CO_2 and less than 1 w/w% of water. Sarbu et al. [312] designed the new non-fluorous $(CHOCO_2)_n$–$(EO)_m$–$(CHOCO_2)_m$ poly(ether-carbonate) (Fig. 4.41b) that can be dissolved in CO_2 by optimizing the balance between enthalpy and entropy of solute–copolymer and copolymer–copolymer interaction. CHO–$CO_2)_{25}$–$(EO)_7$–(CHO–$CO_2)_{25}$ is soluble in CO_2 at lower pressures than 15 MPa, and when added 1.8 mM polymer to a mixture of water and CO_2, it forms an emulsion upon stirring which is stable for hours. Meanwhile, the emulsion is more stable at pressures between 170 and 350 bar than at pressures above 400 bar.

However, these CO_2-soluble hydrocarbon surfactants are applied in high internal water-CO_2 emulsion. Later on, stable CO_2/W HIPEs were formulated with amphiphilic poly(vinyl acetate)/poly(ethylene glycol) (PVAc-b-PEO, Fig. 4.41c1) block copolymers and cured for polymerization of acrylamide. Then, Tan et al. [318] prepared the diblock copolymer oligo (vinyl acetate) as surfactant to synthesize the porous, crosslinked poly(acrylamide) (PAM) materials (bulk density

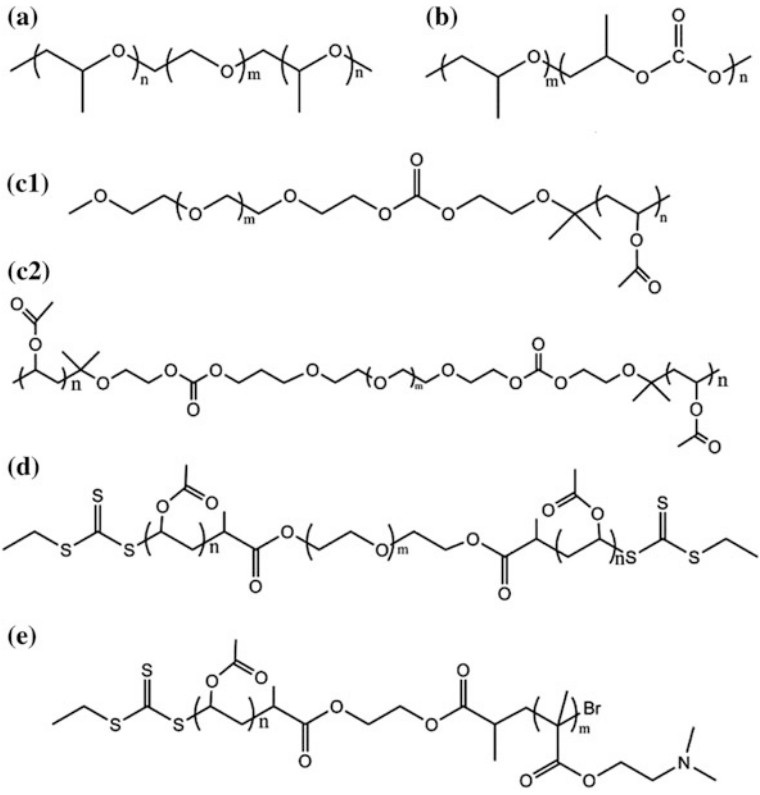

Fig. 4.41 Molecular structures of **a** PPO-b-PEO-b-PPO, **b** poly(ether-carbonate) $(CHO–CO_2)_n$–$(EO)_m$–$(CHO–CO_2)_n$, **c1** PVAc-b-PEO, **c2** PVAc-b-PEO-b-PVAc, **d** X-OVAc-b-PEG-b-OVAc-X, **e** PVAc-b-PDMAEMA [294, 312, 317–319]

0.057 g/cm^3, median pore diameter 10.85 μm) by emulsion-templated material via polymerization of a CO_2/W emulsion (90% v/v CO_2). And the triblock polymer PVAc-b-PEG-b-PVAc surfactant (Fig. 4.41c2, $m = 60$, $n = 30$) was found to emulsify up to 97% v/v CO_2 in water and form a uniform, opaque emulsion which can be stable for at least 48 h.

Following, Tan group adjusted the hydrophic-CO_2 philic balance of X-OVAc-b-PEG-b-OVAc-X (Fig. 4.41d) copolymer surfactants in the water-CO_2 emulsion to prepare the macroporous materials (pore size in the range of 3.2–10.0 μm, the intrusion volume in the range of 4.66–7.82 cm^3/g) under lower pressures which were achieved using a low-temperature redox-initiated polymerization of acrylamide-based HIPEs [319]. The influence of the surfactant concentration and molecular weight of OVAc block on the morphology of the porous structures was also investigated.

Then, Zhang et al. [294] designed and grafted the ionic component polydimethyl-aminoethyl methacrylate (PDMAEMA) to PVAc-b-PDMAEMA (Fig. 4.41e) which contains pendant tertiary amines that are easily protonated below their pKa (7.5) and demonstrate a strong hydrophilic character. By adjusting the appropriate hydrophilic/CO_2-philic ratio of PVAc-b-PDMAEMA, the $(PVAc)_{16}$-b-$(PDMAEMA)_{17}$ with best hydrophilic/CO_2-philic balance ratio can stable the emulsion for 12 h under static conditions. Moreover, the HIPE is still formed when the concentration of surfactant decreases to 0.16% (w/v), and remains stable for at least 1.5 h. When the concentration of $(PVAc)_{16}$-b-$(PDMAEMA)_{17}$ is 1.0%, the pore size of the PAM materials is mostly below 10 μm (taking up 81% volume), and the percentage of macropores (>19 μm) is very low (<4%) (Fig. 4.42) [294].

Compared with other high internal phase emulsions, CO_2/W adopts different stabilizers. Tan et al. [292] reported a method to stable CO_2/W emulsions using only partially hydrolyzed PVA solutions without the addition of any surfactants PVA (25% w/v solution in H_2O) and crosslinker (glutaraldehyde 20% w/w based on PVA) which formed the milky white CO_2/W emulsions under 8 °C and proved to be stable for at least 12 h without the phenomenon of phase separation

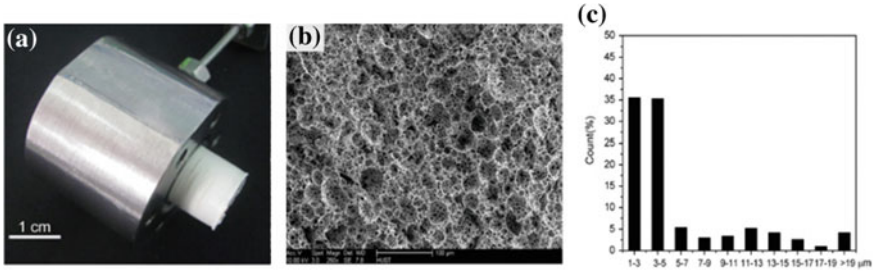

Fig. 4.42 **a** Photographs of low-density C/W emulsion-templated PAM-based materials. **b** SEM analysis of PAM-based macroporous materials and their pore size distributions prepared by C/W emulsion templating polymerization with various concentrations of the $(PVAc)_{16}$-b-$(PDMAEMA)_{17}$ surfactant (w/v) 1.0%. Reproduced from Ref. [294] with kind permission of © 2014 American Chemical Society

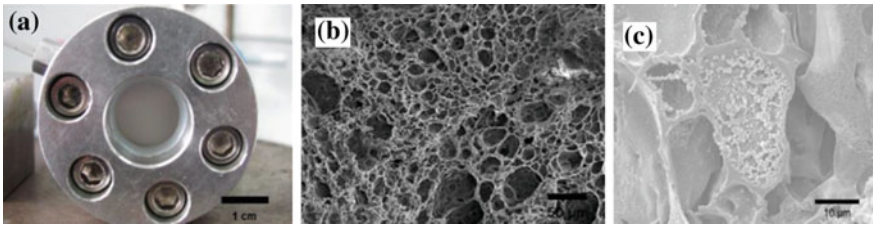

Fig. 4.43 **a** Photographs of a PVA hydrogel formed by gelation of a C/W emulsion, **b** SEM image of hydrogels at a constant ratio of V_{CO2}/V_{H2O} (8/2), 16.8% w/v PVA (88% hydrolyzed, Mw: 22,000 g/mol) based on aqueous phase, **c** SEM images of fibroblast cells attached to PVA hydrogels. Reproduced from Ref. [292] with kind permission of © 2015 Elsevier

(Fig. 4.43a). In this work, it is mentioned that PVA solution with a high viscosity can increase the stable concentrated CO_2/W emulsions owing to the high viscosity of PVA solution and higher solubility of PVA in CO_2 under lower temperature.

As shown in Fig. 4.43b, the hydrogels have an open porous structure (the average pore size of PVA (10.18 ± 3.28 μm), cavities of which are interconnected by a series of channels enable rapid nutrient and oxygen transfer through a polyHIPE material, which is important for cell culture. Due to using biodegradable surfactants, human embryonic lung diploid fibroblast cells' cellular growth and proliferation in PVA hydrogels were examined by SEM in Fig. 4.43c to demonstrate the feasibility of using the processed PVA hydrogels for tissue engineering applications. And the commercial partially hydrolyzed PVA (80% hydrolyzed, Mw 10,000) as surfactant was used to prepare the macroporous PAM (the size range of 13.18–26.67 μm) in high internal emulsion CO_2/W. The H9c2 cardiac muscle cells can grow and proliferate on the surface of these porous PAM scaffolds demonstrating their applications to produce organs by 3D printing technology [292].

4.6.4 HIPE of Pickering Emulsion

The relative large amounts of surfactant are needed for HIPE stabilization reflecting the instability inherent in dispersing the major internal phase within the minor external phase. Residual surfactants can affect the structure, properties, and applications of the resulting polyHIPEs materials. And some short-chain surfactants are leachable contaminants especially in biotechnology application. These surfactants can be difficult and expensive to remove. Some organic–inorganic hybrid polyHIPEs materials synthesized by the post-process of polymer would waste large amount of solvent which cause serious environmental problem. Unlike short-chain surfactants, particles can irreversibly adsorb on the interface of emulsions because of their appropriate wettability and high energy of attachment, which makes them good emulsifiers (Fig. 4.44) [327].

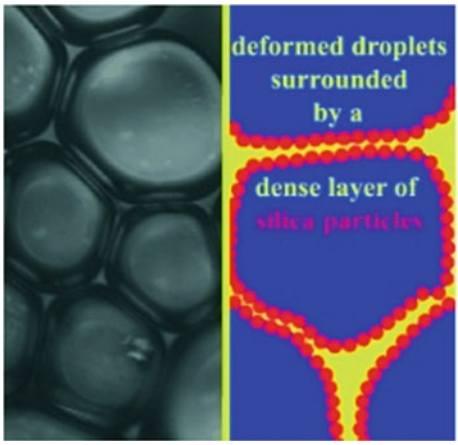

Fig. 4.44 Schematic illustration of Pickering emulsion. Reproduced from Ref. [327] with kind permission of © 2008 Wiley-VCH

It has been proved that many solid particles, such as silica particles, titania particles [320], iron oxide nanoparticles [321], polymer, and graphene oxide flakes [322], can also be used to stabilize HIPEs, which is named as the Pickering HIPEs. Some specific approaches have also been developed to open pores of poly-Pickering HIPEs, including the use of a particular poly(urethane urea) stabilizer, an amphiphilic monomer to costabilize HIPEs, or a reactive lignin stabilizer [323]. The larger droplets of Pickering emulsions lead to thicker monomer layer between droplets. The particle geometry and dimension should also be well regulated in order to avoid the instability caused by gravity and Brownian motion. Meanwhile, these nanoparticles, quasi-irreversibly anchored at the oil–water interface, form dense interfacial barriers that resist coalescence. These solid shells could protect the emulsion droplets against any structural imperfection during polymerization, including coalescence and film rupture. Therefore, closed pores solid particles adsorbed firmly on the oil–water interface can act as steric barriers to hinder the formation of pore throats. The excellent barrier effect of solid particles is dominant in most cases unfortunately, leading to a closed-cell structure [324].

PolyHIPEs synthesized from Pickering HIPEs can be stabilized by relatively low loadings (compared to typical surfactant contents) of nanoparticles specially carbon nanotubes. For example, Noa et al. [325] prepared the organic–inorganic hybrid macroporous material by PS-based CNT-filled HIPEs. The CNTs which migrated from the HIPE's aqueous phase droplets into the HIPE's organic phase formed interconnected bundles within the polyHIPEs walls, act as "bridges," that enhanced the connection between existing conductive pathways. The surfaces of the polyHIPEs are covered with spherical particles whose diameters range from around 300 to 1000 nm. There are no changes to the nanoparticles or to the porous structure on sulfonation that could be discerned using SEM (Fig. 4.45).

Furthermore, the incorporation of inorganic solid particles into the organic framework in poly-Pickering HIPEs can endow porous polymers with functional particles decorated pore walls exhibiting additional properties, such as magnetism,

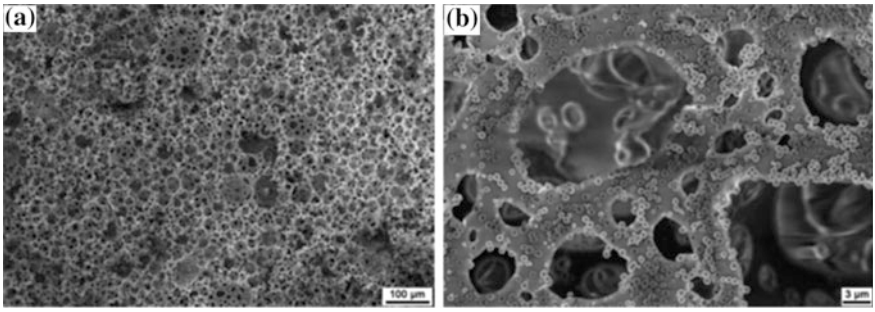

Fig. 4.45 Polymer-nanoparticles-covered polyHIPEs from W/O HIPEs containing surfactant-stabilized CNTs in the aqueous internal phase (SEM). A **a**, **b** typical porous polyHIPE structure with polymer nanoparticles on the void surfaces (SEM). Reproduced from Ref. [325] with kind permission of © 2013 Royal Society of Chemistry

electrical, or thermal conductivity. The use of magnetic, electrical, or thermal conductive particles can also introduce corresponding properties to materials. For example, Mert et al. [326] prepared the macroporous polymers with magnetic response by the removal of the internal phase after the curing of emulsions at 80 °C. The porosity and pore morphology of the macroporous polymers were characterized by nitrogen sorption analysis, the specific surface area and average pore size of the magnetic polyHIPEs with 5 wt% Fe_3O_4@ Humic acid is 36.48 $m^2\ g^{-1}$ and 2.7 nm responsively. The M–H curves of all samples display no hysteresis. Meanwhile, the value of magnetization sharply increases with the applied magnetic field even if it does not attain saturation in the presence of a relatively strong magnetic field of even 20 kOe for the sample MP3.

4.6.5 Conclusions

This review has focused upon recent advances in macroporous polymer by different high internal emulsion polymerization types (O/W, W/O, CO_2/W, and Pickering emulsion). The traditional W/O HIPEs will focus on more new composite materials with more applications (photoelectricity, heterogeneous catalysis, high strength modulus materials, and tissue engineering). A large fraction of contemporary polyHIPEs research and development has focused on expanding the library of novel monomers that can be used for polyHIPEs synthesis. And the synthesis of macroporous materials by HIPEs will become more and more environmental benign and low cost by CO_2/W and IL/W. This way will make the tissue engineering become reality due to the rapid expansion of green chemistry. Then, the hybrid of inorganic and organic, or organic and organic macroporous material by high internal phase Pickering emulsion can endow one composite material with

multifunctional materials for various applications. In a word, the development of polyHIPEs with new synthesis chemistries, material component, and porous structures has clearly established their potential for numerous applications and this is now driving the continuing expansion and intensification of polyHIPEs research.

4.7 Outlook and Perspective

The introduction of porous architecture into traditional non-porous polymers has been a successful innovation in materials science and showed dramatic expansion over the last decades. Owing to the fast development of modern organic synthesis and polymer chemistry, a wide range of optional building blocks as well as numerous synthetic strategies are available for the design and construction of MOPs with well-controlled porous structures. Moreover, diverse chemical functionalities can be easily incorporated into the polymer networks with functional monomers or by post-modification methods which are hardly to be achieved for inorganic porous materials. These remarkable advantages ensure MOPs with additional interesting properties, thus creating more advanced application fields in energy, environment, and health. For example,

Gas storage—HCPs as absorbents for hydrogen, for methane storage and for CO_2 capture and storage; COFs for ammonia storage
Separation—PIM membranes for CO_2 separation; hierarchical porous monoliths for liquid chromatography separation of small molecules and as absorbents for oil spill cleaning
Catalysis—MOPs as platform for heterogeneous catalysis; BT-Ph_2-based knitting polymers as photocatalysts
Sensors—CMPs as fluorescence probes for TNT, Fe^{3+}, and benzene sensing; lithium-modified knitting polymers as humidity-sensitive materials; COFs as repetitive on–off photocurrent switcher
Energy devices—CMPs as electrode materials for energy storage devices and supercapacitors
Drug delivery—HMOCs as drug nanocarriers for controlled release; COFs for drug release
Thermal therapy—CMPs capsules with tunable NIR absorption ability for thermal ablation of HeLa cells

In spite of these outstanding achievements, a number of challenges are also needed to be addressed. For instance, COFs are usually synthesized with consuming period and difficult to scale up; the cost of CMPs is extremely high due to their noble metal catalysis and special monomers; HCPs are highly irregular networks which limit the real applications in advanced fields such as photoelectric devices; PIMs can be soluble in organic solvents while thier surface areas are relatively low. These challenges, which are also generated along with the evolution

of MOPs, will always inspire scientists and researchers to develop new routes for novel materials' invention as a result of encouraging collaboration with researchers in related disciplines and creating new applications.

Acknowledgements This work was financially supported by the program for New Century Excellent Talents in University (NCET-10-0389), Program for Changjiang Scholars and Innovative Research Team in University (PCSIRT) and National Natural Science Foundation of China (Nos. 51173058/51273074/21474033).

References

1. Wu D, Xu F, Sun B et al (2012) Design and preparation of porous polymers. Chem Rev 112 (7):3959–4015
2. Ben T, Ren H, Ma S et al (2009) Targeted synthesis of a porous aromatic framework with high stability and exceptionally high surface area. Angew Chem Int Ed 48(50):9457–9460
3. El-Kaderi HM, Hunt JR, Mendoza-Cortés JL et al (2007) Designed synthesis of 3d covalent organic frameworks. Science 316(5822):268–272
4. Jiang J-X, Trewin A, Su F et al (2009) Microporous poly(tri(4-ethynylphenyl)amine) networks: synthesis, properties, and atomistic simulation. Macromolecules 42(7):2658–2666
5. Shi S, Chen C, Wang M et al (2014) Designing a yolk-shell type porous organic network using a phenyl modified template. Chem Commun 50(65):9079–9082
6. Yang X, Song K, Tan L et al (2014) Hollow microporous organic capsules loaded with highly dispersed Pt nanoparticles for catalytic applications. Macromol Chem Phys 215 (12):1257–1263
7. Li B, Yang X, Xia L et al (2013) Hollow microporous organic capsules. Sci Rep 3:2128
8. Chinnappan A, Chung W-J, Kim H (2015) Hypercross-linked microporous polymeric ionic liquid membranes: synthesis, properties and their application in H_2 generation. J Mater Chem A 3(45):22960–22968
9. Qiao Z, Chai S, Nelson K et al (2014) Polymeric molecular sieve membranes via in situ crosslinking of non-porous polymer membrane templates. Nat Commun 5:3705
10. Kim JK, Yang SY, Lee Y et al (2010) Functional nanomaterials based on block copolymer self-assembly. Prog Polym Sci 35(11):1325–1349
11. Beiler B, Vincze Á, Svec F et al (2007) Poly(2-hydroxyethyl acrylate-co-ethyleneglycol dimethacrylate) monoliths synthesized by radiation polymerization in a mold. Polymer 48 (11):3033–3040
12. Svec F (2010) Porous polymer monoliths: amazingly wide variety of techniques enabling their preparation. J Chromatogr A 1217(6):902–924
13. Wood CD, Tan B, Trewin A et al (2008) Microporous organic polymers for methane storage. Adv Mater 20(10):1916–1921
14. Yang X, Tan L, Xia L et al (2015) Hierarchical porous polystyrene monoliths from polyHIPE. Macromol Rapid Commun 36(17):1553–1558
15. Maya F, Svec F (2014) A new approach to the preparation of large surface area poly (styrene-co-divinylbenzene) monoliths via knitting of loose chains using external crosslinkers and application of these monolithic columns for separation of small molecules. Polymer 55(1):340–346
16. Budd PM, Ghanem BS, Makhseed S et al (2004) Polymers of intrinsic microporosity (PIMs): robust, solution-processable, organic nanoporous materials. Chem Commun 2:230–231
17. Ghanem BS, McKeown NB, Budd PM et al (2008) Polymers of intrinsic microporosity derived from bis(phenazyl) monomers. Macromolecules 41(5):1640–1646

18. Weber J, Su Q, Antonietti M et al (2007) Exploring polymers of intrinsic microporosity—microporous, soluble polyamide and polyimide. Macromol Rapid Commun 28(18–19):1871–1876
19. Du N, Robertson GP, Song J et al (2008) Polymers of intrinsic microporosity containing trifluoromethyl and phenylsulfone groups as materials for membrane gas separation. Macromolecules 41(24):9656–9662
20. Yao S, Yang X, Yu M et al (2014) High surface area hypercrosslinked microporous organic polymer networks based on tetraphenylethylene for CO_2 capture. J Mater Chem A 2 (21):8054–8059
21. Li B, Guan Z, Yang X et al (2014) Multifunctional microporous organic polymers. J Mater Chem A 2(30):11930–11939
22. Zhu X, Mahurin SM, An S-H et al (2014) Efficient CO_2 capture by a task-specific porous organic polymer bifunctionalized with carbazole and triazine groups. Chem Commun 50 (59):7933–7936
23. Sing KSW, Everett DH, Haul RAW et al (1985) Reporting physisorption data for gas/solid systems with special reference to the determination of surface area and porosity (recommendations 1984). Pure Appl Chem 57(4):603–619
24. Germain J, Fréchet JMJ, Svec F (2009) Nanoporous polymers for hydrogen storage. Small 5 (10):1098–1111
25. Jiang J-X, Su F, Trewin A et al (2007) Conjugated microporous poly (aryleneethynylene) networks. Angew Chem Int Ed 46(45):8574–8578
26. Dawson R, Su F, Niu H et al (2008) Mesoporous poly(phenylenevinylene) networks. Macromolecules 41(5):1591–1593
27. Dawson R, Cooper AI, Adams DJ (2012) Nanoporous organic polymer networks. Prog Polym Sci 37(4):530–563
28. Côté AP, Benin AI, Ockwig NW et al (2005) Porous, crystalline, covalent organic frameworks. Science 310(5751):1166–1170
29. Xu S, Luo Y, Tan B (2013) Recent development of hypercrosslinked microporous organic polymers. Macromol Rapid Commun 34(6):471–484
30. Tan L, Tan B (2015) Research progress in hypercrosslinked microporous organic polymers. Acta Chim Sinica 73(6):530–540
31. Cooper AI (2009) Conjugated microporous polymers. Adv Mater 21(12):1291–1295
32. Xu Y, Jin S, Xu H et al (2013) Conjugated microporous polymers: design, synthesis and application. Chem Soc Rev 42(20):8012–8031
33. McKeown NB, Budd PM (2006) Polymers of intrinsic microporosity (PIMs): organic materials for membrane separations, heterogeneous catalysis and hydrogen storage. Chem Soc Rev 35(8):675–683
34. McKeown NB, Budd PM (2010) Exploitation of intrinsic microporosity in polymer-based materials. Macromolecules 43(12):5163–5176
35. Ren S, Bojdys MJ, Dawson R et al (2012) Porous, fluorescent, covalent triazine-based frameworks via room-temperature and microwave-assisted synthesis. Adv Mater 24 (17):2357–2361
36. Kuhn P, Antonietti M, Thomas A (2008) Porous, covalent triazine-based frameworks prepared by ionothermal synthesis. Angew Chem Int Ed 47(18):3450–3453
37. Ben T, Qiu S (2013) Porous aromatic frameworks: synthesis, structure and functions. Cryst Eng Comm 15(1):17–26
38. Stockel E, Wu X, Trewin A et al (2009) High surface area amorphous microporous poly (aryleneethynylene) networks using tetrahedral carbon- and silicon-centred monomers. Chem Commun 2:212–214
39. Rowan SJ, Cantrill SJ, Cousins GRL et al (2002) Dynamic covalent chemistry. Angew Chem Int Ed 41(6):898–952
40. O'Keeffe M (2009) Design of MOFs and intellectual content in reticular chemistry: a personal view. Chem Soc Rev 38(5):1215–1217

41. O'Keeffe M, Yaghi OM (2012) Deconstructing the crystal structures of metal-organic frameworks and related materials into their underlying nets. Chem Rev 112(2):675–702
42. D'Alessandro DM, Smit B, Long JR (2010) Carbon dioxide capture: prospects for new materials. Angew Chem Int Ed 49(35):6058–6082
43. Banerjee R, Furukawa H, Britt D et al (2009) Control of pore size and functionality in isoreticular zeolitic imidazolate frameworks and their carbon dioxide selective capture properties. J Am Chem Soc 131(11):3875–3877
44. Tranchemontagne DJ, Mendoza-Cortes JL, O'Keeffe M et al (2009) Secondary building units, nets and bonding in the chemistry of metal-organic frameworks. Chem Soc Rev 38 (5):1257–1283
45. Waller PJ, Gandara F, Yaghi OM (2015) Chemistry of covalent organic frameworks. Acc Chem Res 48(12):3053–3063
46. Feng X, Liu L, Honsho Y et al (2012) High-rate charge-carrier transport in porphyrin covalent organic frameworks: switching from hole to electron to ambipolar conduction. Angew Chem Int Ed 51(11):2618–2622
47. Beletskaya I, Tyurin VS, Tsivadze AY et al (2009) Supramolecular chemistry of metalloporphyrins. Chem Rev 109(5):1659–1713
48. Spitler EL, Dichtel WR (2010) Lewis acid-catalysed formation of two-dimensional phthalocyanine covalent organic frameworks. Nat Chem 2(8):672–677
49. Bojdys MJ, Jeromenok J, Thomas A et al (2010) Rational extension of the family of layered, covalent, triazine-based frameworks with regular porosity. Adv Mater 22(19):2202–2205
50. Ding X, Guo J, Feng X et al (2011) Synthesis of metallophthalocyanine covalent organic frameworks that exhibit high carrier mobility and photoconductivity. Angew Chem Int Ed 50(6):1289–1293
51. Ding X, Chen L, Honsho Y et al (2011) An n-channel two-dimensional covalent organic framework. J Am Chem Soc 133(37):14510–14513
52. Kappe CO (2004) Controlled microwave heating in modern organic synthesis. Angew Chem Int Ed 43(46):6250–6284
53. Kappe CO, Dallinger D (2009) Controlled microwave heating in modern organic synthesis: highlights from the 2004–2008 literature. Mol Divers 13(2):71–193
54. Makhseed S, Samuel J (2008) Hydrogen adsorption in microporous organic framework polymer. Chem Commun 36:4342–4344
55. Ritchie LK, Trewin A, Reguera-Galan A et al (2010) Synthesis of COF-5 using microwave irradiation and conventional solvothermal routes. Microporous Mesoporous Mater 132(1–2):132–136
56. Zwaneveld NAA, Pawlak R, Abel M et al (2008) Organized formation of 2D extended covalent organic frameworks at surfaces. J Am Chem Soc 130(21):6678–6679
57. Guan CZ, Wang D, Wan LJ (2012) Construction and repair of highly ordered 2D covalent networks by chemical equilibrium regulation. Chem Commun 48(24):2943–2945
58. Colson JW, Woll AR, Mukherjee A et al (2011) Oriented 2D covalent organic framework thin films on single-layer graphene. Science 332(6026):228–231
59. Spitler EL, Colson JW, Uribe-Romo FJ et al (2012) Lattice expansion of highly oriented 2D phthalocyanine covalent organic framework films. Angew Chem Int Ed 51(11):2623–2627
60. Spitler EL, Koo BT, Novotney JL et al (2011) A 2D covalent organic framework with 47-nm pores and insight into its interlayer stacking. J Am Chem Soc 133(48):19416–19421
61. Dienstmaier JF, Medina DD, Dogru M et al (2012) Isoreticular two-dimensional covalent organic frameworks synthesized by on-surface condensation of diboronic acids. ACS Nano 6(8):7234–7242
62. Kalidindi SB, Wiktor C, Ramakrishnan A et al (2013) Lewis base mediated efficient synthesis and solvation-like host-guest chemistry of covalent organic framework-1. Chem Commun 49(5):463–465
63. Smith BJ, Dichtel WR (2014) Mechanistic studies of two-dimensional covalent organic frameworks rapidly polymerized from initially homogenous conditions. J Am Chem Soc 136 (24):8783–8789

64. Wan S, Guo J, Kim J et al (2008) A belt-shaped, blue luminescent, and semiconducting covalent organic framework. Angew Chem Int Ed 47(46):8826–8830
65. Chen L, Furukawa K, Gao J et al (2014) Photoelectric covalent organic frameworks: converting open lattices into ordered donor-acceptor heterojunctions. J Am Chem Soc 136 (28):9806–9809
66. Xu F, Jin S, Zhong H et al (2015) Electrochemically active, crystalline, mesoporous covalent organic frameworks on carbon nanotubes for synergistic lithium-ion battery energy storage. Sci Rep 5:8225
67. Huang N, Ding X, Kim J et al (2015) A photoresponsive smart covalent organic framework. Angew Chem Int Ed 54(30):8704–8707
68. Yang H, Du Y, Wan S et al (2015) Mesoporous 2D covalent organic frameworks based on shape-persistent arylene-ethynylene macrocycles. Chem Sci 6(7):4049–4053
69. Feng X, Dong Y, Jiang D (2013) Star-shaped two-dimensional covalent organic frameworks. Cryst Eng Comm 15(8):1508–1511
70. Uribe-Romo FJ, Hunt JR, Furukawa H et al (2009) A crystalline imine-linked 3-D porous covalent organic framework. J Am Chem Soc 131(13):4570–4571
71. Chen X, Addicoat M, Irle S et al (2013) Control of crystallinity and porosity of covalent organic frameworks by managing interlayer interactions based on self-complementary pi-electronic force. J Am Chem Soc 135(2):546–549
72. Xu H, Jiang D (2014) Covalent organic frameworks: crossing the channel. Nat Chem 6 (7):564–566
73. Chen X, Addicoat M, Jin E et al (2015) Locking covalent organic frameworks with hydrogen bonds: general and remarkable effects on crystalline structure, physical properties, and photochemical activity. J Am Chem Soc 137(9):3241–3247
74. Dalapati S, Addicoat M, Jin S et al (2015) Rational design of crystalline supermicroporous covalent organic frameworks with triangular topologies. Nat Commun 6:7786
75. Xu H, Gao J, Jiang D (2015) Stable, crystalline, porous, covalent organic frameworks as a platform for chiral organocatalysts. Nat Chem 7(11):905–912
76. Huang N, Krishna R, Jiang D (2015) Tailor-made pore surface engineering in covalent organic frameworks: systematic functionalization for performance screening. J Am Chem Soc 137(22):7079–7082
77. Kandambeth S, Mallick A, Lukose B et al (2012) Construction of crystalline 2D covalent organic frameworks with remarkable chemical (acid/base) stability via a combined reversible and irreversible route. J Am Chem Soc 134(48):19524–19527
78. Biswal BP, Chandra S, Kandambeth S et al (2013) Mechanochemical synthesis of chemically stable isoreticular covalent organic frameworks. J Am Chem Soc 135(14): 5328–5331
79. Chandra S, Kandambeth S, Biswal BP et al (2013) Chemically stable multilayered covalent organic nanosheets from covalent organic frameworks via mechanical delamination. J Am Chem Soc 135(47):17853–17861
80. Chandra S, Kundu T, Kandambeth S et al (2014) Phosphoric acid loaded azo (–N horizontal line N–) based covalent organic framework for proton conduction. J Am Chem Soc 136 (18):6570–6573
81. Das G, Biswal BP, Kandambeth S et al (2015) Chemical sensing in two dimensional porous covalent organic nanosheets. Chem Sci 6(7):3931–3939
82. Chen X, Huang N, Gao J et al (2014) Towards covalent organic frameworks with predesignable and aligned open docking sites. Chem Commun 50(46):6161–6163
83. Das G, Balaji Shinde D, Kandambeth S et al (2014) Mechanosynthesis of imine, beta-ketoenamine, and hydrogen-bonded imine-linked covalent organic frameworks using liquid-assisted grinding. Chem Commun 50(84):12615–12618
84. Fang Q, Gu S, Zheng J et al (2014) 3D microporous base-functionalized covalent organic frameworks for size-selective catalysis. Angew Chem Int Ed 53(11):2878–2882
85. Zhou TY, Xu SQ, Wen Q et al (2014) One-step construction of two different kinds of pores in a 2D covalent organic framework. J Am Chem Soc 136(45):15885–15888

86. Zhu Y, Wan S, Jin Y et al (2015) Desymmetrized vertex design for the synthesis of covalent organic frameworks with periodically heterogeneous pore structures. J Am Chem Soc 137 (43):13772–13775
87. Uribe-Romo FJ, Doonan CJ, Furukawa H et al (2011) Crystalline covalent organic frameworks with hydrazone linkages. J Am Chem Soc 133(30):11478–11481
88. Ding SY, Dong M, Wang YW et al (2016) Thioether-based fluorescent covalent organic framework for selective detection and facile removal of mercury(II). J Am Chem Soc 138 (9):3031–3037
89. Fang Q, Zhuang Z, Gu S et al (2014) Designed synthesis of large-pore crystalline polyimide covalent organic frameworks. Nat Commun 5:4503
90. Fang Q, Wang J, Gu S et al (2015) 3D porous crystalline polyimide covalent organic frameworks for drug delivery. J Am Chem Soc 137(26):8352–8355
91. Zeng Y, Zou R, Luo Z et al (2015) Covalent organic frameworks formed with two types of covalent bonds based on orthogonal reactions. J Am Chem Soc 137(3):1020–1023
92. Zuttel A (2004) Hydrogen storage methods. Naturwissenschaften 91(4):157–172
93. Fichtner M (2005) Nanotechnological aspects in materials for hydrogen storage. Adv Eng Mater 7(6):443–455
94. Furukawa H, Yaghi OM (2009) Storage of hydrogen, methane, and carbon dioxide in highly porous covalent organic frameworks for clean energy applications. J Am Chem Soc 131 (25):8875–8883
95. Furukawa H, Miller MA, Yaghi OM (2007) Independent verification of the saturation hydrogen uptake in MOF-177 and establishment of a benchmark for hydrogen adsorption in metal-organic frameworks. J Mater Chem 17(30):3197–3204
96. Kaye SS, Dailly A, Yaghi OM et al (2007) Impact of preparation and handling on the hydrogen storage properties of Zn_4O(1,4-benzenedicarboxylate)$_3$ (MOF-5). J Am Chem Soc 129(46):14176–14177
97. Haszeldine RS (2009) Carbon capture and storage: how green can black be? Science 325 (5948):1647–1652
98. Xu X, Song C, Andrésen JM et al (2003) Preparation and characterization of novel CO_2 "molecular basket" adsorbents based on polymer-modified mesoporous molecular sieve MCM-41. Microporous Mesoporous Mater 62(1–2):29–45
99. Phan A, Doonan CJ, Uribe-Romo FJ et al (2010) Synthesis, structure, and carbon dioxide capture properties of zeolitic imidazolate frameworks. Acc Chem Res 43(1):58–67
100. Doonan CJ, Tranchemontagne DJ, Glover TG et al (2010) Exceptional ammonia uptake by a covalent organic framework. Nat Chem 2(3):235–238
101. MacMillan DW (2008) The advent and development of organocatalysis. Nature 455 (7211):304–308
102. Yoon M, Srirambalaji R, Kim K (2012) Homochiral metal-organic frameworks for asymmetric heterogeneous catalysis. Chem Rev 112(2):1196–1231
103. Lee J, Farha OK, Roberts J et al (2009) Metal-organic framework materials as catalysts. Chem Soc Rev 38(5):1450–1459
104. Ding SY, Gao J, Wang Q et al (2011) Construction of covalent organic framework for catalysis: Pd/COF-LZU1 in Suzuki-Miyaura coupling reaction. J Am Chem Soc 133 (49):19816–19822
105. Mullangi D, Nandi S, Shalini S et al (2015) Pd loaded amphiphilic COF as catalyst for multi-fold Heck reactions, C–C couplings and CO oxidation. Sci Rep 5:10876
106. Wan S, Guo J, Kim J et al (2009) A photoconductive covalent organic framework: self-condensed arene cubes composed of eclipsed 2D polypyrene sheets for photocurrent generation. Angew Chem Int Ed 48(30):5439–5442
107. Shultz AM, Farha OK, Hupp JT et al (2009) A catalytically active, permanently microporous MOF with metalloporphyrin struts. J Am Chem Soc 131(12):4204–4205
108. Drain CM, Varotto A, Radivojevic I (2009) Self-organized porphyrinic materials. Chem Rev 109(5):1630–1658

109. Chen L, Yang Y, Jiang D (2010) CMPs as scaffolds for constructing porous catalytic frameworks: a built-in heterogeneous catalyst with high activity and selectivity based on nanoporous metalloporphyrin polymers. J Am Chem Soc 132(26):9138–9143
110. Tsyurupa MP, Davankov VA (2002) Hypercrosslinked polymers: basic principle of preparing the new class of polymeric materials. React Funct Polym 53(2–3):193–203
111. Davankov VA, Rogozhin SV, Tsyurupa MP (1971) US Patent 3729457
112. Tsyurupa MP, Davankov VA (2006) Porous structure of hypercrosslinked polystyrene: State-of-the-art mini-review. React Funct Polym 66(7):768–779
113. Germain J, Fréchet JMJ, Svec F (2007) Hypercrosslinked polyanilines with nanoporous structure and high surface area: potential adsorbents for hydrogen storage. J Mater Chem 17 (47):4989
114. Davankov VA, Ilyin MM, Tsyurupa MP et al (1996) From a dissolved polystyrene coil to an intramolecularly-hyper-cross-linked "nanosponge". Macromolecules 29(26):8398–8403
115. Davankov V, Tsyurupa M, Ilyin M et al (2002) Hypercross-linked polystyrene and its potentials for liquid chromatography: a mini-review. J Chromatogr A 965(1–2):65–73
116. Tsyurupa MP, Blinnikova ZK, Borisov YA et al (2014) Physicochemical and adsorption properties of hypercross-linked polystyrene with ultimate crosslinking density. J Sep Sci 37 (7):803–810
117. Hradil J, Králová E (1998) Styrene-divinylbenzene copolymers post-crosslinked with tetrachloromethane. Polymer 39(24):6041–6048
118. Veverka P, Jeřábek K (1999) Mechanism of hypercrosslinking of chloromethylated styrene-divinylbenzene copolymers. React Funct Polym 41(1–3):21–25
119. Ahn J-H, Jang J-E, Oh C-G et al (2006) Rapid generation and control of microporosity, bimodal pore size distribution, and surface area in davankov-type hyper-cross-linked resins. Macromolecules 39(2):627–632
120. Li B, Gong R, Luo Y et al (2011) Tailoring the pore size of hypercrosslinked polymers. Soft Matter 7(22):10910–10916
121. Seo M, Kim S, Oh J et al (2015) Hierarchically porous polymers from hyper-cross-linked block polymer precursors. J Am Chem Soc 137(2):600–603
122. Li Z, Wu D, Huang X et al (2014) Fabrication of novel polymeric and carbonaceous nanoscale networks by the union of self-assembly and hypercrosslinking. Energy Environ Sci 7(9):3006–3012
123. Wood CD, Tan B, Trewin A et al (2007) Hydrogen storage in microporous hypercrosslinked organic polymer networks. Chem Mater 19(8):2034–2048
124. Martín CF, Stöckel E, Clowes R et al (2011) Hypercrosslinked organic polymer networks as potential adsorbents for pre-combustion CO_2 capture. J Mater Chem 21(14):5475–5483
125. Yang Y, Zhang Q, Zhang S et al (2013) Synthesis and characterization of triphenylamine-containing microporous organic copolymers for carbon dioxide uptake. Polymer 54(21):5698–5702
126. Yang Y, Zhang Q, Zhang S et al (2014) Triphenylamine-containing microporous organic copolymers for hydrocarbons/water separation. RSC Adv 4(11):5568–5574
127. Luo Y, Zhang S, Ma Y et al (2013) Microporous organic polymers synthesized by self-condensation of aromatic hydroxymethyl monomers. Polym Chem 4(4):1126–1131
128. Grzybowski M, Skonieczny K, Butenschön H et al (2013) Comparison of oxidative aromatic coupling and the scholl reaction. Angew Chem Int Ed 52(38):9900–9930
129. Li L, Ren H, Yuan Y et al (2014) Construction and adsorption properties of porous aromatic frameworks via $AlCl_3$-triggered coupling polymerization. J Mater Chem A 2(29): 11091–11098
130. Li B, Gong R, Wang W et al (2011) A new strategy to microporous polymers: knitting rigid aromatic building blocks by external cross-linker. Macromolecules 44(8):2410–2414
131. Dawson R, Stoeckel E, Holst JR et al (2011) Microporous organic polymers for carbon dioxide capture. Energy Environ Sci 4(10):4239–4245
132. Nielsen CJ, Herrmann H, Weller C (2012) Atmospheric chemistry and environmental impact of the use of amines in carbon capture and storage (CCS). Chem Soc Rev 41(19):6684–6704

133. Chen S, Zhang J, Wu T et al (2009) Multiroute synthesis of porous anionic frameworks and size-tunable extraframework organic cation-controlled gas sorption properties. J Am Chem Soc 131(44):16027–16029
134. Couck S, Denayer JFM, Baron GV et al (2009) An Amine-Functionalized MIL-53 metal-organic framework with large separation power for CO_2 and CH_4. J Am Chem Soc 131(18):6326–6327
135. Farha OK, Spokoyny AM, Hauser BG et al (2009) Synthesis, properties, and gas separation studies of a robust diimide-based microporous organic polymer. Chem Mater 21(14): 3033–3035
136. Woodward RT, Stevens LA, Dawson R et al (2014) Swellable, water- and acid-tolerant polymer sponges for chemoselective carbon dioxide capture. J Am Chem Soc 136 (25):9028–9035
137. Dawson R, Ratvijitvech T, Corker M et al (2012) Microporous copolymers for increased gas selectivity. Polym Chem 3(8):2034–2038
138. Dawson R, Stevens LA, Drage TC et al (2012) Impact of water coadsorption for carbon dioxide capture in microporous polymer sorbents. J Am Chem Soc 134(26):10741–10744
139. Jing X, Zou D, Cui P et al (2013) Facile synthesis of cost-effective porous aromatic materials with enhanced carbon dioxide uptake. J Mater Chem A 1(44):13926–13931
140. Li H, Meng B, Mahurin SM et al (2015) Carbohydrate based hyper-crosslinked organic polymers with –OH functional groups for CO_2 separation. J Mater Chem A 3(42): 20913–20918
141. Zhu J-H, Chen Q, Sui Z-Y et al (2014) Preparation and adsorption performance of cross-linked porous polycarbazoles. J Mater Chem A 2(38):16181–16189
142. Yang X, Yu M, Zhao Y et al (2014) Hypercrosslinked microporous polymers based on carbazole for gas storage and separation. RSC Adv 4(105):61051–61055
143. Zhang Y, Li Y, Wang F et al (2014) Hypercrosslinked microporous organic polymer networks derived from silole-containing building blocks. Polymer 55(22):5746–5750
144. Yang X, Yu M, Zhao Y et al (2014) Remarkable gas adsorption by carbonized nitrogen-rich hypercrosslinked porous organic polymers. J Mater Chem A 2(36):15139–15145
145. Zhai T-L, Tan L, Luo Y et al (2016) Microporous polymers from a carbazole-based triptycene monomer: synthesis and their applications for gas uptake. Chem-Asian J 11 (2):294–298
146. Zhang C, Zhu P-C, Tan L et al (2016) Synthesis and properties of organic microporous polymers from the monomer of hexaphenylbenzene based triptycene. Polymer 82:100–104
147. Zhang C, Zhu P-C, Tan L et al (2015) Triptycene-based hyper-cross-linked polymer sponge for gas storage and water treatment. Macromolecules 48(23):8509–8514
148. Luo Y, Li B, Wang W et al (2012) Hypercrosslinked aromatic heterocyclic microporous polymers: a new class of highly selective CO_2 capturing materials. Adv Mater 24(42): 5703–5707
149. Saleh M, Lee HM, Kemp KC et al (2014) Highly stable CO_2/N_2 and CO_2/CH_4 selectivity in hyper-cross-linked heterocyclic porous polymers. ACS Appl Mater Interfaces 6(10): 7325–7333
150. Wang J, Yang JGW, Yi G et al (2015) Phosphonium salt incorporated hypercrosslinked porous polymers for CO_2 capture and conversion. Chem Commun 51(86):15708–15711
151. Guan Z, Li B, Hai G et al (2014) A highly efficient catalyst for Suzuki-Miyaura coupling reaction of benzyl chloride under mild conditions. RSC Adv 4(69):36437–36443
152. Song K, Liu P, Wang J et al (2015) Controlled synthesis of uniform palladium nanoparticles on novel micro-porous carbon as a recyclable heterogeneous catalyst for the Heck reaction. Dalton Trans 44(31):13906–13913
153. Song K, Zou Z, Wang D et al (2016) Microporous organic polymers derived microporous carbon supported pd catalysts for oxygen reduction reaction: impact of framework and heteroatom. J Phys Chem C 120(4):2187–2197

154. Li B, Guan Z, Wang W et al (2012) Highly dispersed Pd catalyst locked in knitting aryl network polymers for Suzuki-Miyaura coupling reactions of aryl chlorides in aqueous media. Adv Mater 24(25):3390–3395
155. Xu S, Song K, Li T et al (2015) Palladium catalyst coordinated in knitting N-heterocyclic carbene porous polymers for efficient Suzuki-Miyaura coupling reactions. J Mater Chem A 3 (3):1272–1278
156. Li R, Wang ZJ, Wang L et al (2016) Photocatalytic selective bromination of electron-rich aromatic compounds using microporous organic polymers with visible light. ACS Catal 6 (2):1113–1121
157. Jiang K, Fei T, Zhang T (2014) Humidity sensing properties of LiCl-loaded porous polymers with good stability and rapid response and recovery. Sens Actuators, B 199:1–6
158. Jiang K, Kuang D, Fei T et al (2014) Preparation of lithium-modified porous polymer for enhanced humidity sensitive properties. Sens Actuators, B 203:752–758
159. Yang X, Li B, Majeed I et al (2013) Magnetic microporous polymer nanoparticles. Polym Chem 4(5):1425–1429
160. Chinnappan A, Tamboli AH, Chung W-J et al (2016) Green synthesis, characterization and catalytic efficiency of hypercross-linked porous polymeric ionic liquid networks towards 4-nitrophenol reduction. Chem Eng J 285:554–561
161. Ji G, Yang Z, Zhao Y et al (2015) Synthesis of metalloporphyrin-based conjugated microporous polymer spheres directed by bipyridine-type ligands. Chem Commun 51 (34):7352–7355
162. Xu Y, Nagai A, Jiang D (2013) Core-shell conjugated microporous polymers: a new strategy for exploring color-tunable and -controllable light emissions. Chem Commun 49(16): 1591–1593
163. Liu X, Xu Y, Jiang D (2012) Conjugated microporous polymers as molecular sensing devices: microporous architecture enables rapid response and enhances sensitivity in fluorescence-on and fluorescence-off sensing. J Am Chem Soc 134(21):8738–8741
164. Zhang Y, Sigen A, Zou Y et al (2014) Gas uptake, molecular sensing and organocatalytic performances of a multifunctional carbazole-based conjugated microporous polymer. J Mater Chem A 2(33):13422–13430
165. Ding X, Han BH (2015) Copper phthalocyanine-based CMPs with various internal structures and functionalities. Chem Commun 51(64):12783–12786
166. Chun J, Park JH, Kim J et al (2012) Tubular-shape evolution of microporous organic networks. Chem Mater 24(17):3458–3463
167. Senkovskyy V, Senkovska I, Kiriy A (2012) Surface-initiated synthesis of conjugated microporous polymers: chain-growth Kumada catalyst-transfer polycondensation at work. ACS Macro Lett 1(4):494–498
168. Yang RX, Wang TT, Deng WQ (2015) Extraordinary capability for water treatment achieved by a perfluorous conjugated microporous polymer. Sci Rep 5:10155
169. Cheng G, Hasell T, Trewin A et al (2012) Soluble conjugated microporous polymers. Angew Chem Int Ed 51(51):12727–12731
170. Chen Q, Luo M, Hammershoj P et al (2012) Microporous polycarbazole with high specific surface area for gas storage and separation. J Am Chem Soc 134(14):6084–6087
171. Cho HC, Lee HS, Chun J et al (2011) Tubular microporous organic networks bearing imidazolium salts and their catalytic CO_2 conversion to cyclic carbonates. Chem Commun 47(3):917–919
172. Kang N, Park JH, Choi J et al (2012) Nanoparticulate iron oxide tubes from microporous organic nanotubes as stable anode materials for lithium ion batteries. Angew Chem Int Ed 51(27):6626–6630
173. Laybourn A, Dawson R, Clowes R et al (2014) Network formation mechanisms in conjugated microporous polymers. Polym Chem 5(21):6325–6333
174. Xu Y, Jiang D (2014) Structural insights into the functional origin of conjugated microporous polymers: geometry-management of porosity and electronic properties. Chem Commun 50(21):2781–2783

175. Dawson R, Laybourn A, Khimyak YZ et al (2010) High surface area conjugated microporous polymers: the importance of reaction solvent choice. Macromolecules 43(20):8524–8530
176. Tan D, Fan W, Xiong W et al (2012) Study on the morphologies of covalent organic microporous polymers: the role of reaction solvents. Macromol Chem Phys 213(14): 1435–1440
177. Schmidt J, Weber J, Epping JD et al (2009) Microporous conjugated poly(thienylene arylene) networks. Adv Mater 21(6):702–705
178. Schmidt J, Werner M, Thomas A (2009) Conjugated microporous polymer networks via yamamoto polymerization. Macromolecules 42(13):4426–4429
179. Jiang J-X, Su F, Niu H et al (2008) Conjugated microporous poly(phenylene butadiynylene) s. Chem Commun 4:486–488
180. Schwab MG, Fassbender B, Spiess HW et al (2009) Catalyst-free preparation of melamine-based microporous polymer networks through schiff base chemistry. J Am Chem Soc 131(21):7216–7217
181. Gu C, Chen Y, Zhang Z et al (2013) Electrochemical route to fabricate film-like conjugated microporous polymers and application for organic electronics. Adv Mater 25(25):3443–3448
182. Wang X, Zhao Y, Wei L et al (2015) Nitrogen-rich conjugated microporous polymers: impact of building blocks on porosity and gas adsorption. J Mater Chem A 3(42): 21185–21193
183. Jiang J-X, Su F, Trewin A et al (2008) Synthetic control of the pore dimension and surface area in conjugated microporous polymer and copolymer networks. J Am Chem Soc 130 (24):7710–7720
184. Feng L-J, Chen Q, Zhu J-H et al (2014) Adsorption performance and catalytic activity of porous conjugated polyporphyrins via carbazole-based oxidative coupling polymerization. Polym Chem 5(8):3081–3088
185. Liao Y, Weber J, Faul CFJ (2014) Conjugated microporous polytriphenylamine networks. Chem Commun 50(59):8002–8005
186. Hayashi S, Togawa Y, Ashida J et al (2016) Synthesis of π-conjugated porous polymers via direct arylation of fluoroarenes with three-arm triazine. Polymer 90:187–192
187. Yoo J, Park N, Park JH et al (2015) Magnetically separable microporous fe-porphyrin networks for catalytic carbene insertion into N–H bonds. ACS Catal 5(1):350–355
188. Xiao Z, Zhou Y, Xin X et al (2015) Iron(III) Porphyrin-based porous material as photocatalyst for highly efficient and selective degradation of congo red. Macromol Chem Phys 217(4):599–604
189. Lu G, Yang H, Zhu Y et al (2015) Synthesis of a conjugated porous Co(ii) porphyrinylene-ethynylene framework through alkyne metathesis and its catalytic activity study. J Mater Chem A 3(9):4954–4959
190. Chun J, Kang S, Kang N et al (2013) Microporous organic networks bearing metal-salen species for mild CO_2 fixation to cyclic carbonates. J Mater Chem A 1(18):5517–5523
191. Zhang H, Zhang Y, Gu C et al (2015) Electropolymerized conjugated microporous poly (zinc-porphyrin) films as potential electrode materials in supercapacitors. Adv Energy Mater 5(10):1402175
192. Ding X, Han BH (2015) Metallophthalocyanine-based conjugated microporous polymers as highly efficient photosensitizers for singlet oxygen generation. Angew Chem Int Ed 54 (22):6536–6539
193. Sheng X, Guo H, Qin Y et al (2015) A novel metalloporphyrin-based conjugated microporous polymer for capture and conversion of CO_2. RSC Adv 5(40):31664–31669
194. Jiang J-X, Wang C, Laybourn A et al (2011) Metal-organic conjugated microporous polymers. Angew Chem Int Ed 123(5):1104–1107
195. Fischer S, Schmidt J, Strauch P et al (2013) An anionic microporous polymer network prepared by the polymerization of weakly coordinating anions. Angew Chem Int Ed 52 (46):12174–12178

196. Xie Y, Wang TT, Liu XH et al (2013) Capture and conversion of CO_2 at ambient conditions by a conjugated microporous polymer. Nat Commun 4:1960
197. Gu C, Huang N, Chen Y et al (2015) Pi-conjugated microporous polymer films: designed synthesis, conducting properties, and photoenergy conversions. Angew Chem Int Ed 54 (46):13594–13598
198. Lee HS, Choi J, Jin J et al (2012) An organometallic approach for microporous organic network (MON)–Co_3O_4 composites: enhanced stability as anode materials for lithium ion batteries. Chem Commun 48(1):94–96
199. Lindemann P, Schade A, Monnereau L et al (2016) Surface functionalization of conjugated microporous polymer thin films and nanomembranes using orthogonal chemistries. J Mater Chem A 4(18):6815–6818
200. Liu J, Tobin JM, Xu Z et al (2015) Facile synthesis of a conjugated microporous polymeric monolith via copper-free Sonogashira-Hagihara cross-coupling in water under aerobic conditions. Polym Chem 6(41):7251–7255
201. Urakami H, Zhang K, Vilela F (2013) Modification of conjugated microporous poly-benzothiadiazole for photosensitized singlet oxygen generation in water. Chem Commun 49(23):2353–2355
202. Ratvijitvech T, Dawson R, Laybourn A et al (2014) Post-synthetic modification of conjugated microporous polymers. Polymer 55(1):321–325
203. Zhuang X, Zhang F, Wu D et al (2013) Two-dimensional sandwich-type, graphene-based conjugated microporous polymers. Angew Chem Int Ed 52(37):9668–9672
204. Zhuang X, Gehrig D, Forler N et al (2015) Conjugated microporous polymers with dimensionality-controlled heterostructures for green energy devices. Adv Mater 27(25):3789–3796
205. Kang N, Park JH, Jin M et al (2013) Microporous organic network hollow spheres: useful templates for nanoparticulate CO_3O_4 hollow oxidation catalysts. J Am Chem Soc 135(51):19115–19118
206. Ko JH, Kang N, Park N et al (2015) Hollow microporous organic networks bearing triphenylamines and anthraquinones: diffusion pathway effect in visible light-driven oxidative coupling of benzylamines. ACS Macro Lett 4(7):669–672
207. Lim B, Jin J, Yoo J et al (2014) Fe_3O_4 nanosphere@microporous organic networks: enhanced anode performances in lithium ion batteries through carbonization. Chem Commun 50(57):7723–7726
208. Kang S, Chun J, Park N et al (2015) Hydrophobic zeolites coated with microporous organic polymers: adsorption behavior of ammonia under humid conditions. Chem Commun 51(59):11814–11817
209. Chun J, Kang S, Park N et al (2014) Metal-organic framework@microporous organic network: hydrophobic adsorbents with a crystalline inner porosity. J Am Chem Soc 136(19):6786–6789
210. Tan J, Wan J, Guo J et al (2015) Self-sacrificial template-induced modulation of conjugated microporous polymer microcapsules and shape-dependent enhanced photothermal efficiency for ablation of cancer cells. Chem Commun 51(98):17394–17397
211. Zhang SC, Luo YL, Yang HW et al (2013) Functional oligo(vinyl acetate) bearing bipyridine moieties by RAFT polymerization and extraction of metal ions in supercritical carbon dioxide. Polym Chem 4(12):3507–3513
212. Ma BC, Ghasimi S, Landfester K et al (2015) Conjugated microporous polymer nanoparticles with enhanced dispersibility and water compatibility for photocatalytic applications. J Mater Chem A 3(31):16064–16071
213. Kim M, Byeon M, Bae J-S et al (2011) Preparation of ultrathin films of molecular networks through layer-by-layer crosslinking polymerization of tetrafunctional monomers. Macromolecules 44(18):7092–7095
214. Lindemann P, Tsotsalas M, Shishatskiy S et al (2014) Preparation of freestanding conjugated microporous polymer nanomembranes for gas separation. Chem Mater 26(24):7189–7193

215. Wu X, Li H, Xu Y et al (2014) Thin film fabricated from solution-dispersible porous hyperbranched conjugated polymer nanoparticles without surfactants. Nanoscale 6(4): 2375–2380
216. Gu C, Chen Y, Zhang Z et al (2014) Achieving high efficiency of PTB7-based polymer solar cells via integrated optimization of both anode and cathode interlayers. Adv Energy Mater 4(8):1301771
217. Gu C, Huang N, Gao J et al (2014) Controlled synthesis of conjugated microporous polymer films: versatile platforms for highly sensitive and label-free chemo- and biosensing. Angew Chem Int Ed 53(19):4850–4855
218. Deng S, Zhi J, Zhang X et al (2014) Size-controlled synthesis of conjugated polymer nanoparticles in confined nanoreactors. Angew Chem Int Ed 53(51):14144–14148
219. Huang B, Zhao P, Dai Y et al (2016) Size-controlled synthesis of soluble-conjugated microporous polymer nanoparticles through sonogashira polycondensation in confined nanoreactors. J Polym Sci Pol Chem 54(15):2285–2290
220. Du R, Zhang N, Xu H et al (2014) CMP aerogels: ultrahigh-surface-area carbon-based monolithic materials with superb sorption performance. Adv Mater 26(47):8053–8058
221. Wang ZJ, Landfester K, Zhang KAI (2014) Hierarchically porous π-conjugated polyHIPE as a heterogeneous photoinitiator for free radical polymerization under visible light. Polym Chem 5(11):3559–3562
222. Liu X, Xu Y, Guo Z et al (2013) Super absorbent conjugated microporous polymers: a synergistic structural effect on the exceptional uptake of amines. Chem Commun 49(31):3233–3235
223. Chen Y, Sun H, Yang R et al (2015) Synthesis of conjugated microporous polymer nanotubes with large surface areas as absorbents for iodine and CO_2 uptake. J Mater Chem A 3(1):87–91
224. Wang J, Wang G, Wang W et al (2014) Hydrophobic conjugated microporous polymer as a novel adsorbent for removal of volatile organic compounds. J Mater Chem A 2(34): 14028–14037
225. Du R, Zheng Z, Mao N et al (2015) Fluorosurfactants-directed preparation of homogeneous and hierarchical-porosity CMP aerogels for gas sorption and oil cleanup. Adv Sci 2(1–2):1400006
226. Chen Q, Liu DP, Luo M et al (2014) Nitrogen-containing microporous conjugated polymers via carbazole-based oxidative coupling polymerization: preparation, porosity, and gas uptake. Small 10(2):308–315
227. Wang J, Senkovska I, Oschatz M et al (2013) Highly porous nitrogen-doped polyimine-based carbons with adjustable microstructures for CO_2 capture. J Mater Chem A 1(36):10951–10961
228. Song W-C, Xu X-K, Chen Q et al (2013) Nitrogen-rich diaminotriazine-based porous organic polymers for small gas storage and selective uptake. Polym Chem 4(17):4690–4696
229. Qiao S, Wang T, Huang W et al (2016) Dendrimer-like conjugated microporous polymers. Polym Chem 7(6):1281–1289
230. Fischer S, Schimanowitz A, Dawson R et al (2014) Cationic microporous polymer networks by polymerisation of weakly coordinating cations with CO_2-storage ability. J Mater Chem A 2(30):11825–11829
231. Zhang S, Huang W, Hu P et al (2015) Conjugated microporous polymers with excellent electrochemical performance for lithium and sodium storage. J Mater Chem A 3(5): 1896–1901
232. Xu F, Chen X, Tang Z et al (2014) Redox-active conjugated microporous polymers: a new organic platform for highly efficient energy storage. Chem Commun 50(37):4788–4790
233. Yuan K, Guo-Wang P, Hu T et al (2015) Nanofibrous and graphene-templated conjugated microporous polymer materials for flexible chemosensors and supercapacitors. Chem Mater 27(21):7403–7411
234. To JWF, Chen Z, Yao H et al (2015) Ultrahigh surface area three-dimensional porous graphitic carbon from conjugated polymeric molecular framework. ACS Cent Sci 1(2):68–76

235. Zhang K, Kopetzki D, Seeberger PH et al (2013) Surface area control and photocatalytic activity of conjugated microporous poly(benzothiadiazole) networks. Angew Chem Int Ed 52(5):1432–1436
236. Wang ZJ, Ghasimi S, Landfester K et al (2015) Molecular structural design of conjugated microporous poly(benzooxadiazole) networks for enhanced photocatalytic activity with visible light. Adv Mater 27(40):6265–6270
237. Wang ZJ, Ghasimi S, Landfester K et al (2014) Highly porous conjugated polymers for selective oxidation of organic sulfides under visible light. Chem Commun 50(60): 8177–8180
238. Luo J, Zhang X, Zhang J (2015) Carbazolic porous organic framework as an efficient, metal-free visible-light photocatalyst for organic synthesis. ACS Catal 5(4):2250–2254
239. Wang ZJ, Ghasimi S, Landfester K et al (2015) Photocatalytic suzuki coupling reaction using conjugated microporous polymer with immobilized palladium nanoparticles under visible light. Chem Mater 27(6):1921–1924
240. Wang X, S-m Lu, Li J et al (2015) Conjugated microporous polymers with chiral BINAP ligand built-in as efficient catalysts for asymmetric hydrogenation. Catal Sci Technol 5 (5):2585–2589
241. Wu X, Li H, Xu B et al (2014) Solution-dispersed porous hyperbranched conjugated polymer nanoparticles for fluorescent sensing of TNT with enhanced sensitivity. Polym Chem 5(15):4521–4525
242. Bonillo B, Sprick RS, Cooper AI (2016) Tuning photophysical properties in conjugated microporous polymers by co-monomer doping strategies. Chem Mater 28(10):3469–3480
243. Jiang J-X, Trewin A, Adams DJ et al (2011) Band gap engineering in fluorescent conjugated microporous polymers. Chem Sci 2(9):1777–1781
244. Ma H, Li F, Li P et al (2016) A dendrimer-based electropolymerized microporous film: multifunctional, reversible, and highly sensitive fluorescent probe. Adv Funct Mater 26 (12):2025–2031
245. Jin J, Kim B, Park N et al (2014) Porphyrin entrapment and release behavior of microporous organic hollow spheres: fluorescent alerting systems for existence of organic solvents in water. Chem Commun 50(94):14885–14888
246. Okay O (2000) Macroporous copolymer networks. Prog Polym Sci 25(6):711–779
247. Cameron NR, Sherrington DC (1996) High internal phase emulsions (HIPEs)-structure, properties and use in polymer preparation. Biopolymers liquid crystalline polymers phase emulsion. Springer Berlin Heidelberg, pp 163–214
248. McKeown NB, Budd PM, Msayib KJ et al (2005) Polymers of intrinsic microporosity (PIMs): bridging the void between microporous and polymeric materials. Chem Eur J 11(9):2610–2620
249. Patrick J, Walker A (eds) (1995) Porosity in carbons. Edward Arnold, London
250. Kaneko K, Ishii C, Ruike M et al (1992) Origin of superhigh surface area and microcrystalline graphitic structures of activated carbons. Carbon 30(7):1075–1088
251. McKeown NB (2000) Phthalocyanine-containing polymers. J Mater Chem 10(9):1979–1995
252. McKeown NB, Makhseed S, Budd PM (2002) Phthalocyanine-based nanoporous network polymers. Chem Commun 23:2780–2781
253. McKeown NB, Hanif S, Msayib K et al (2002) Porphyrin-based nanoporous network polymers. Chem Commun 23:2782–2783
254. Budd PM, Ghanem B, Msayib K et al (2003) A nanoporous network polymer derived from hexaazatrinaphthylene with potential as an adsorbent and catalyst support. J Mater Chem 13(11):2721–2726
255. Ghanem BS, Msayib KJ, McKeown NB et al (2007) A triptycene-based polymer of intrinsic microposity that displays enhanced surface area and hydrogen adsorption. Chem Commun 1:67–69
256. Ghanem BS, Hashem M, Harris KDM et al (2010) Triptycene-based polymers of intrinsic microporosity: organic materials that can be tailored for gas adsorption. Macromolecules 43(12):5287–5294

257. McKeown NB, Gahnem B, Msayib KJ et al (2006) Towards polymer-based hydrogen storage materials: engineering ultramicroporous cavities within polymers of intrinsic microporosity. Angew Chem Int Ed 45(11):1804–1807
258. Ghanem BS, McKeown NB, Budd PM et al (2009) Synthesis, characterization, and gas permeation properties of a novel group of polymers with intrinsic microporosity: PIM-polyimides. Macromolecules 42(20):7881–7888
259. Short R, Carta M, Bezzu CG et al (2011) Hexaphenylbenzene-based polymers of intrinsic microporosity. Chem Commun 47(24):6822–6824
260. Patel HA, Yavuz CT (2012) Noninvasive functionalization of polymers of intrinsic microporosity for enhanced CO_2 capture. Chem Commun 48(80):9989–9991
261. Zhang P, Jiang X, Wan S et al (2015) Advancing polymers of intrinsic microporosity by mechanochemistry. J Mater Chem A 3(13):6739–6741
262. Nagai K, Masuda T, Nakagawa T et al (2001) Poly[1-(trimethylsilyl)-1-propyne] and related polymers: synthesis, properties and functions. Prog Polym Sci 26(5):721–798
263. Budd PM, McKeown NB, Fritsch D (2005) Free volume and intrinsic microporosity in polymers. J Mater Chem 15(20):1977–1986
264. Carta M, Malpass-Evans R, Croad M et al (2013) An efficient polymer molecular sieve for membrane gas separations. Science 339(6117):303–307
265. Mason CR, Maynard-Atem L, Heard KWJ et al (2014) Enhancement of CO_2 affinity in a polymer of intrinsic microporosity by amine modification. Macromolecules 47(3): 1021–1029
266. Hart KE, Colina CM (2014) Ionomers of intrinsic microporosity: in silico development of ionic-functionalized gas-separation membranes. Langmuir 30(40):12039–12048
267. Shamsipur H, Dawood BA, Budd PM et al (2014) Thermally rearrangeable PIM-polyimides for gas separation membranes. Macromolecules 47(16):5595–5606
268. Bernardo P, Drioli E, Golemme G (2009) Membrane gas separation: a review/state of the art. Ind Eng Chem Res 48(10):4638–4663
269. Fang W, Zhang L, Jiang J (2010) Polymers of intrinsic microporosity for gas permeation: a molecular simulation study. Mol Simul 36(12):992–1003
270. Fritsch D, Merten P, Heinrich K et al (2012) High performance organic solvent nanofiltration membranes: Development and thorough testing of thin film composite membranes made of polymers of intrinsic microporosity (PIMs). J Membr Sci 401:222–231
271. Anokhina T, Yushkin A, Budd P et al (2015) Application of PIM-1 for solvent swing adsorption and solvent recovery by nanofiltration. Sep Purif Technol 156:683–690
272. Swaidan R, Ghanem B, Litwiller E et al (2015) Physical aging, plasticization and their effects on gas permeation in "rigid" polymers of intrinsic microporosity. Macromolecules 48(18):6553–6561
273. Kelman SD, Rowe BW, Bielawski CW et al (2008) Crosslinking poly[1-(trimethylsilyl)-1-propyne] and its effect on physical stability. J Membr Sci 320(1–2):123–134
274. Li FY, Xiao Y, Chung T-S et al (2012) High-performance thermally self-cross-linked polymer of intrinsic microporosity (PIM-1) membranes for energy development. Macromolecules 45(3):1427–1437
275. Shao L, Samseth J, Hägg MB (2007) Effect of plasma treatment on the gas permeability of poly (4-methyl-2-pentyne) membranes. Plasma Processes Polym 4(9):823–831
276. Song Q, Cao S, Pritchard RH et al (2014) Controlled thermal oxidative crosslinking of polymers of intrinsic microporosity towards tunable molecular sieve membranes. Nat Commun 5:4813
277. Song Q, Cao S, Pritchard RH et al (2016) Nanofiller-tuned microporous polymer molecular sieves for energy and environmental processes. J Mater Chem A 4(1):270–279
278. Shin Y, Prestat E, Zhou K-G et al (2016) Synthesis and characterization of composite membranes made of graphene and polymers of intrinsic microporosity. Carbon 102:357–366
279. Mitra T, Bhavsar RS, Adams DJ et al (2016) PIM-1 mixed matrix membranes for gas separations using cost-effective hypercrosslinked nanoparticle fillers. Chem Commun 52(32):5581–5584

280. Carta M, Croad M, Bugler K et al (2014) Heterogeneous organocatalysts composed of microporous polymer networks assembled by Troger's base formation. Polym Chem 5(18):5262–5266
281. Ahn SD, Kolodziej A, Malpass-Evans R et al (2016) Polymer of intrinsic microporosity induces host-guest substrate selectivity in heterogeneous 4-benzoyloxy-TEMPO-catalysed alcohol oxidations. Electrocatalysis 7(1):70–78
282. Weng X, Baez JE, Khiterer M et al (2015) Chiral polymers of intrinsic microporosity: selective membrane permeation of enantiomers. Angew Chem Int Ed 54(38):11214–11218
283. Rong Y, He D, Sanchez-Fernandez A et al (2015) Intrinsically microporous polymer retains porosity in vacuum thermolysis to electroactive heterocarbon. Langmuir 31(44): 12300–12306
284. Silverstein MS (2014) Emulsion-templated porous polymers: a retrospective perspective. Polymer 55(1):304–320
285. Silverstein MS (2014) PolyHIPEs: recent advances in emulsion-templated porous polymers. Prog Polym Sci 39(1):199–234
286. Herbst A, Khutia A, Janiak C (2014) Brønsted instead of lewis acidity in functionalized MIL-101Cr MOFs for efficient heterogeneous (nano-MOF) catalysis in the condensation reaction of aldehydes with alcohols. Inorg Chem 53(14):7319–7333
287. Wickenheisser M, Janiak C (2015) Hierarchical embedding of micro-mesoporous MIL-101 (Cr) in macroporous poly(2-hydroxyethyl methacrylate) high internal phase emulsions with monolithic shape for vapor adsorption applications. Microporous Mesoporous Mater 204:242–250
288. Zhu Y, Hua Y, Zhang S et al (2015) Open-cell macroporous bead: a novel polymeric support for heterogeneous photocatalytic reactions. J Polym Res 22(4):1–6
289. Wickenheisser M, Paul T, Janiak C (2016) Prospects of monolithic MIL-MOF@poly (NIPAM)HIPE composites as water sorption materials. Microporous Mesoporous Mater 220:258–269
290. Yu S, Tan H, Wang J et al (2015) High porosity supermacroporous polystyrene materials with excellent oil-water separation and gas permeability properties. ACS Appl Mater Interfaces 7(12):6745–6753
291. Tebboth M, Kogelbauer A, Bismarck A (2015) Liquid-liquid extraction within emulsion templated macroporous polymers. Ind Eng Chem Res 54(29):7284–7291
292. Luo W, Zhang S, Li P et al (2015) Surfactant-free CO_2-in-water emulsion-templated poly (vinyl alcohol) (PVA) hydrogels. Polymer 61:183–191
293. Luo W, Xu R, Liu Y et al (2015) Emulsion-templated poly(acrylamide)s by using polyvinyl alcohol (PVA) stabilized CO_2-in-water emulsions and their applications in tissue engineering scaffolds. RSC Adv 5(112):92017–92024
294. Zhang S, Luo W, Yan W et al (2014) Synthesis of a CO_2-philic poly(vinyl acetate)-based cationic amphiphilic surfactant by RAFT/ATRP and its application in preparing monolithic materials. Green Chem 16(9):4408–4416
295. Hayward AS, Sano N, Przyborski SA et al (2013) Acrylic-acid-functionalized polyHIPE scaffolds for use in 3D cell culture. Macromol Rapid Commun 34(23–24):1844–1849
296. Prieto EM, Page JM, Harmata AJ et al (2014) Injectable foams for regenerative medicine. Wiley Interdiscip Rev Nanomed Nanobiotechnol 6(2):136–154
297. Qu Q, Pan J, Yin Y et al (2015) Synthesis of macroporous polymer foams via pickering high internal phase emulsions for highly efficient 2,4,5-trichlorophenol removal. J Appl Polym Sci 132(6):41430
298. Liang J, Wu Y, Deng X et al (2015) Optically active porous materials constructed by chirally helical substituted polyacetylene through a high internal phase emulsion approach and the application in enantioselective crystallization. ACS Macro Lett 4(10):1179–1183
299. Sevsek U, Brus J, Jerabek K et al (2014) Post polymerisation hypercrosslinking of styrene/divinylbenzene poly(HIPE)s: Creating micropores within macroporous polymer. Polymer 55(1):410–415

300. Liliang O, Rui Y, Xi C et al (2015) 3D printing of HEK 293FT cell-laden hydrogel into macroporous constructs with high cell viability and normal biological functions. Biofabrication 7(1):015010
301. Wu Z, Su X, Xu Y et al (2016) Bioprinting three-dimensional cell-laden tissue constructs with controllable degradation. Sci Rep 6:24474
302. Perez-Garcia MG, Carranza A, Puig JE et al (2015) Porous monoliths synthesized via polymerization of styrene and divinyl benzene in nonaqueous deep-eutectic solvent-based HIPEs. RSC Adv 5(30):23255–23260
303. Carranza A, Pojman JA, Mota-Morales JD (2014) Deep-eutectic solvents as a support in the nonaqueous synthesis of macroporous poly(HIPEs). RSC Adv 4(78):41584–41587
304. Tebboth M, Kogelbauer A, Bismarck A (2015) Highly permeable macroporous polymers via controlled agitation of emulsion templates. Chem Eng Sci 137:786–795
305. Menner A, Bismarck A (2006) New evidence for the Mechanism of the pore formation in polymerising high internal phase emulsions or why polyHIPEs have an interconnected pore network structure. Macromol Symp 242(1):19–24
306. Mathieu K, Jerome C, Debuigne A (2015) Influence of the macromolecular surfactant features and reactivity on morphology and surface properties of emulsion-templated porous polymers. Macromolecules 48(18):6489–6498
307. Huang X, Yang Y, Shi J et al (2015) High-internal-phase emulsion tailoring polymer amphiphilicity towards an efficient NIR-sensitive bacteria filter. Small 11(37):4876–4883
308. Pan J, Zeng J, Cao Q et al (2016) Hierarchical macro and mesoporous foams synthesized by HIPEs template and interface grafted route for simultaneous removal of lambda-cyhalothrin and copper ions. Chem Eng J 284:1361–1372
309. Qiu H, Che S (2011) Chiral mesoporous silica: chiral construction and imprinting via cooperative self-assembly of amphiphiles and silica precursors. Chem Soc Rev 40(3): 1259–1268
310. Hayward AS, Eissa AM, Maltman DJ et al (2013) Galactose-functionalized polyHIPE scaffolds for use in routine three dimensional culture of mammalian hepatocytes. Biomacromol 14(12):4271–4277
311. Oh BHL, Bismarck A, Chan-Park MB (2015) Injectable, interconnected, high-porosity macroporous biocompatible gelatin scaffolds made by surfactant-free emulsion templating. Macromol Rapid Commun 36(4):364–372
312. Sarbu T, Styranec T, Beckman EJ (2000) Non-fluorous polymers with very high solubility in supercritical CO_2 down to low pressures. Nature 405(6783):165–168
313. Eastoe J, Paul A, Nave S et al (2001) Micellization of hydrocarbon surfactants in supercritical carbon dioxide. J Am Chem Soc 123(5):988–989
314. Boyère C, Favrelle A, Léonard AF et al (2013) Macroporous poly (ionic liquid) and poly (acrylamide) monoliths from CO_2-in-water emulsion templates stabilized by sugar-based surfactants. J Mater Chem A 1(29):8479–8487
315. Butler R, Davies CM, Cooper AI (2001) Emulsion templating using high internal phase supercritical fluid emulsions. Adv Mater 13(19):1459–1463
316. Palocci C, Barbetta A, La Grotta A et al (2007) Porous biomaterials obtained using supercritical CO_2-water emulsions. Langmuir 23(15):8243–8251
317. da Rocha SRP, Harrison KL, Johnston KP (1999) Effect of surfactants on the interfacial tension and emulsion formation between water and carbon dioxide. Langmuir 15(2): 419–428
318. Tan B, Cooper AI (2005) Functional Oligo(vinyl acetate) CO_2-philes for solubilization and emulsification. J Am Chem Soc 127(25):8938–8939
319. Chen K, Grant N, Liang L et al (2010) Synthesis of CO_2-philic Xanthate-Oligo(vinyl acetate)-based hydrocarbon surfactants by RAFT polymerization and their applications on preparation of emulsion-templated materials. Macromolecules 43(22):9355–9364
320. Li X, Sun G, Li Y et al (2014) Porous TiO_2 materials through pickering high-internal phase emulsion templating. Langmuir 30(10):2676–2683

321. Kovacic S, Matsko NB, Ferk G et al (2013) Macroporous poly(dicyclopentadiene) gamma Fe_2O_3/Fe_3O_4 nanocomposite foams by high internal phase emulsion templating. J Mater Chem A 1(27):7971–7978
322. Yi W, Wu H, Wang H et al (2016) Interconnectivity of macroporous hydrogels prepared via graphene oxide-stabilized pickering high internal phase emulsions. Langmuir 32(4):982–990
323. Yang Y, Wei Z, Wang C et al (2013) Lignin-based pickering HIPEs for macroporous foams and their enhanced adsorption of copper(II) ions. Chem Commun 49(64):7144–7146
324. Horozov TS, Binks BP (2006) Particle-stabilized emulsions: a bilayer or a bridging monolayer? Angew Chem Int Ed 45(5):773–776
325. Cohen N, Samoocha DC, David D et al (2013) Carbon nanotubes in emulsion-templated porous polymers: polymer nanoparticles, sulfonation, and conductivity. J Polym Sci Pol Chem 51(20):4369–4377
326. Mert EH, Yildirim H, Uzumcu AT et al (2013) Synthesis and characterization of magnetic polyHIPEs with humic acid surface modified magnetic iron oxide nanoparticles. React Funct Polym 73(1):175–181
327. Ikem VO, Menner A, Bismarck A (2008) High internal phase emulsions stabilized solely by functionalized silica particles. Angew Chem Int Ed 47(43):8277–8279